Development of ternary multilayer systems from polysaccharides and metal ions for tissue engineering applications

Dissertation

zur Erlangung des
Doktorgrades der Ingenieurwissenschaften (Dr.-Ing.)

des

Instituts für Pharmazie
Naturwissenschaftliche Fakultät I

der Martin-Luther-Universität
Halle-Wittenberg,

vorgelegt

von M.Eng. Husnia Muftah Kindi

Gutachter: Prof. Dr. rer. nat. habil. Thomas Groth
Prof. Dr. Sonja Keßler
Prof. Dr. Kirsten Peters

Halle (Saale), im 18.12. 2025

To My Family

Contents

List of abbreviations

Alg	Alginic acid / alginate
a.u	Arbitrary units
AFM	Atomic force microscopy
ANOVA	Analysis of variance
ATCC	American Tissue Culture Collection
BCA	Bicinchoninic acid
BODIPY	Fluorescent F-actin stain
BSA	Bovine serum albumin
BMP-2	Bone morphogenic protein 2
CLSM	Confocal laser scanning microscope
COL	collagen
CD44	Cluster of differentiation 44
Chi	Chitosan
Chi/Alg	Chitosan/alginate multilayer films
Chi/HA	Chitosan/ Hyaluronan multilayer films
C3H10T1/2	Embryonic fibroblast
CY2	Polyclonal goat anti-mouse Cy2 conjugated secondary antibody
CY3	Polyclonal goat anti-rabbit CY3-conjugated secondary antibody
DMEM	Dulbecco's modified Eagle's medium.
DEX	Dexamethasone
DSMO	Dimethyl sulfoxide
EDC	1-ethyl-3-(3-dimethylaminopropyl) carbodiimide
ECM	Extra cellular matrix
EBM	Eagle's basal medium
EDTA	Ethylenediaminetetraacetic acid
FA	Focal adhesion
FAK	Focal adhesion kinase
FBS	Fetal bovine serum
FN	Fibronectin
FTIR	Fourier Transformed Infrared spectroscopy
GAG	Glycosaminoglycan
GlcA	D-glucuronic acid

GLUT4	Glucose transporter 4
HA	Hyaluronic acid / Hyaluronan
IF	Immunofluorescence
ICP	Inductively Coupled Plasma Mass Spectrometry
LBL	Layer-by-Layer technique
MUDA	Mercaptoundecanoic acid
MSCs	Mesenchymal stem cells
NaCl	Sodium chloride
PBS	Phosphate buffered saline
Pen/Strep	Penicillin/streptomycin
PEM	Polyelectrolyte multilayer
PEL	Polyelectrolyte
pH	pH value
PFA	Paraformaldehyde
PZC	Point of zero charge
RI	Refractive index
RCA	Radio corporation of America
ROI	Region of interest
RT	Room temperature
Si	Silicon
SPR	Surface plasmon resonance
SEM	Scanning electron microscopy
TE	Tissue engineering
TOP-PRO3	Nucleic acid (nuclear) stain
UV	Ultraviolet
VN	Vitronectin
VEGF	Vascular endothelial growth factor
WCA	Water contact angle
ZEN	Zeiss efficient navigation software
ZP	Zeta potential

Graphical abstract

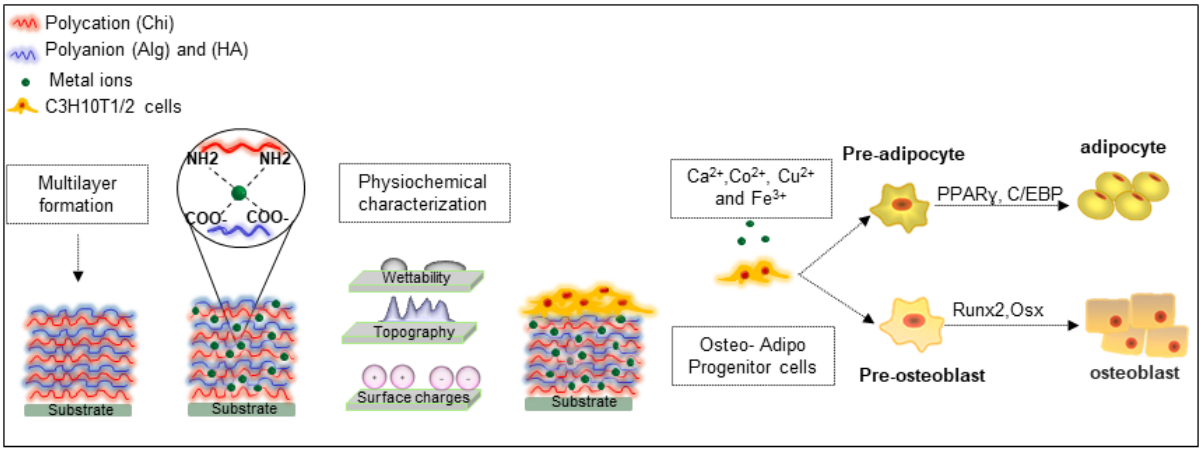

General overview on thesis chapters: Multilayer films were fabricated using layer-by-layer (LbL) technique on cleaned substrates (glass coverslip, gold sensors and silicone) represented as green base. This technique is based on alternating adsorption of the polyanions alginate or hyaluronan (blue layer with a negative charge) and the polycation chitosan (red layer with a positive charge). The multilayers were subsequently exposed to different types and concentrations of metal ions. The primary focus of this work is a thorough evaluation of the effect of doping metal ions on multilayers, particularly in terms of their physicochemical properties, including wettability, surface charge and topography. Additionally, the study determined the quantities of metal ions within the multilayers for both the chitosan/alginate and chitosan/hyaluronan systems. Most importantly, murine embryonic C3H10T1/2 fibroblasts were utilized for biological studies to assess the effect of metal ions on cell adhesion, growth and differentiation without induction medium. These findings are crucial for basic scientific understanding and practical applications in the field biomedical implants and tissue regeneration.

Abstract

The modification of biomaterial surfaces at the micro and nanometre scales offers great potential for the precise control of biological events such as protein adsorption, cell adhesion, proliferation, and differentiation. Among the available surface modification techniques, a simple method called layer-by-layer technique (LbL) is currently widely used in biomedical applications. In this study, we applied the LbL technique, based on the alternating adsorption of oppositely charged polyelectrolytes (PEL) onto charged surfaces to design polyelectrolyte multilayer (PEM) surface coatings that mimic the natural extracellular matrix (ECM) of connective tissue. This was achieved by combining chitosan (Chi) as the polycation and alginate (Alg) or hyaluronic acid (HA) as polyanions on glass, serving as a model substrate. The goal was to gain control over cell adhesion, growth, and adipo and osteogenic differentiation of C3H10T1/2 cells in situ. The polyelectrolyte multilayers (PEM) were exposed to different types of metal ions (Ca^{2+}, Co^{2+}, Cu^{2+} and Fe^{3+}), which were selected due to their distinct chemical properties and roles in biological systems. The metal ions bound to polyelectrolyte multilayers PEMs and form complexes through functional groups present in polysaccharides. This research focuses on the physicochemical characteristics of the resultant PEMs, such as surface zeta potential, thickness, layer growth, wettability, and topography. Fourier-transformed infrared (FTIR) spectroscopy of PEMs comprising Alg and HA shows some small changes in spectra indicating interaction of metal ions with hydroxyl and carboxyl groups in the layers. This study utilized inductively coupled plasma mass spectrometry (ICP-MS) to quantify the metal ions in the [Chi/Alg] and [Chi/HA] multilayers. The analysis revealed elevated highest concentration for Fe^{3}+, followed by Ca^{2+}, Cu^{2+} and then Co^{2+} ions in the PEMs multilayers. The highest concentration of iron and calcium ions, ,resulting in an increased positive surface charge, as demonstrated by higher ζ potential at acidic pH values obtained by streaming potential measurements. Additionally, incorporation of Fe^{3+} ions lead to a decrease in the surface wettability of the films, as indicated by an increase in the water contact angles. Conversely, treatments with Ca^{2+}, Co^{2+}, and Cu^{2+} ions resulted in only slight changes in wettability. Murine C3H10T1/2 embryonic fibroblasts were used in this study, revealing alterations in their adhesion, proliferation, and differentiation behaviour on plain multilayers [Chi/Alg], [Chi/HA] and metal ion-doped PEMs.

This work demonstrates that the Fe^{3+} ions significantly enhance adhesion, spreading and proliferation in both PEMs systems in comparison to plain [Chi/Alg] and [Chi/HA] systems. In contrast, Ca^{2+} and Co^{2+} doping PEMs induces a notable inhibitory effect on cell adhesion and growth. However the [Chi/HA] doped with higher concentration (50Mm) of Co^{2+} supported cell adhesion and growth after 72h. The plain [Chi/Alg] and [Chi/HA] did not promote adipogenic

differentiation. Additionally, Co^{2+} inhibited adipogenic differentiation by suppressing the expression of adipogenic transcription factors. PEMs exposed to Cu^{2+} and Fe^{3+} promoted cell adhesion and spreading, resulting in an increased the cell area. Additionally, these metal ions also stimulated the metabolic activity of cells after 24h and induced cell differentiation towards adipocytes in the absence of additional adipogenic media supplements. Confirmation of adipogenic differentiation was achieved through histochemistry (oil red staining of lipid vacuoles) and immunohistochemistry staining (perilipin and GLUT4) after 21 days. Interestingly, Ca^{2+} doped PEMs show positive histochemical staining for lipid vacuoles as well as the expression of GLUT4 and perilipin in C3H10T1/2. Collectively, metal ions (Co^{2+}, Cu^{2+}, and Fe^{3+}) can be used to induce the osteogenic differentiation of C3H10T1/2 multipotent mouse cell in situ, as indicated by immunohistochemical staining of upregulated genes playing a crucial role in osteogenesis (RunX2, ALP, Osteocalcin (OCN), Noggin) and quantitative Real-time polymerase chain reaction (qRT-PCR) after 21 days. Overall, Chi/Alg and Chi/HA multilayer systems with metal ions (Co^{2+}, Cu^{2+}, and Fe^{3+}) can serve as promising coatings on implants and scaffolds, offering regenerative potential for connective tissues like bone. Additionally, the novel insight that doping multilayer PEMs with metal ions (Ca^{2+}, Cu^{2+}, and Fe^{3+}) has the capacity to significantly enhance adipogenic differentiation holds great promise for various practical applications in tissue regeneration, such as breast augmentation, reconstruction and the acceleration of wound healing.

Zusammenfassung

Die Modifikation von Biomaterialien auf Mikro- und Nanometer Ebene weist ein gutes Potenzial auf, biologische Geschehen, wie Proteinabsorption, Zelladhäsion sowie Proliferation und Differenzierung, präzise zu kontrollieren. So gehört zu den Techniken der Oberflächenmodifikation die Schicht-für-Schicht (layer-by-layer) Methode (LbL), welche einen großen und bemerkenswerten Gebrauch in den biomedizinischen Verfahren genießt. Diese LBL- Methode beruht auf der alternierende Absorption von entgegengesetzt geladenen Polyelektrolyten (PEL) auf geladene Oberflächen und wird genutzt, um mehrschichtige Polyelekeltrolytoberflächen (PEM), welche die natürliche extrazellulär Matrix von Bindegewebe nachahmen, zu bilden. Dabei erfolgt die Durchführung der LbL Methode, indem Chitosan (Chi) als Polykation und Alginate (Alg) oder Hyaluronsäure (HA) als Polyanion auf einem Glas kombiniert werden, sodass die Zelladhäsion, das Wachstum und die adipo- und osteogenetische Differenzierung von C3H10T1/2 Zellen in Situ kontrolliert und verfolgt werden. Während der Ausführung der Layer- by- Layer Technik sind die polyelektrolytischen Multischichten (PEM) verschiedenen Metallionen (Ca^{2+}, Co^{2+}, Cu^{2+} and Fe^{3+}) ausgesetzt. Folglich binden sich die Metallionen an die polyelektrolytischen Multischichten (PEM) und formen Komplexe über die funktionellen Gruppen, welche an den Polysacchariden zu erkennen sind. Diese Forschung fokussiert sich hierbei auf die physikochemischen Charakteristiken der gebildeten PEMs, wie dem Oberflächen-Zetapotential, dem Dicke- und Schichtwachstum, der Benetzbarkeit sowie der Topografie. Zudem wurde infolge dieser Forschung mittels der Fourier-transformierten Infrarot-Spektroskopie (FITR) des mehrschichtigen Systems, welches sowohl Alg als auch HA umfasst, gezeigt, dass es zu Interaktionen zwischen den Metallionen und den Hydroxyl- und Carboxylgruppen innerhalb der großen Schichten kommt. Für die Untersuchung der Quantifizierung von Metallionen in den [Chi/Alg] und [Chi/HA] Multischichten wurde hingegen eine induktiv gekoppelte Plasma-Massenspektrometrie (ICP-MS) genutzt, welche darauf hingedeutet hat, dass die Konzentration von den Fe^{3+} in den mehrschichtigen Systemen (PEM) am höchsten ist, gefolgt von den Konzentrationen der Ca^{2+}, den Cu^{2+} und den Co^{2+} in den PEM-Multischichten. Die höchste Konzentration von Eisen- und Calciumionen führte zu einer erhöhten positiven Oberflächenladung, welche durch ein erhöhtes ζ-Potential bei sauren pH-Werten zu erkennen ist. Darüber hinaus führt der Einbau von Fe^{3+}-Ionen zu einer Verringerung der Oberflächenbenetzbarkeit der Filme, was durch die Vergrößerung des Kontaktwinkels zum Wasser erfasst wird. Kontrastierend dazu verursachten Behandlungen mit Ca^{2+}, Co^{2+}, und Cu^{2+} Ionen kaum bzw. wenige Veränderungen hinsichtlich der Oberflächenbenetzbarkeit. Des Weiteren wurden für die Studie embryonale Fibroblasten der Maus C3H10T1/2 verwendet, die viele Merkmale mit mesenchymalen Stammzellen (MSCs) teilen und daher eine alternative

Zellquelle für Studien zur Entwicklung biomimetischer Oberflächen für die Gewebezüchtung darstellen könnten. Diese wiesen im Zuge der experimentellen Untersuchung Veränderungen in ihrem Adhäsions, Proliferations und Differenzierungsverhalten durch die einfachen Mehrschichten [Chi/Alg], [Chi/HA] auf. Die Metallionen verursachten hingegen Dotierungen der PEMs.

Diese Arbeit zeigt, dass Fe^{3+} Ionen die Adhäsion, Ausbreitung und Proliferation in beiden PEM-Systemen im Vergleich zu den einfachen [Chi/Alg]- und [Chi/HA]-Systemen signifikant verbessern. Im Gegensatz dazu induzierte die Dotierung der PEMs mit Ca^{2+} und Co^{2+} eine deutliche Hemmung der Zelladhäsion und des Wachstums. Allerdings unterstützten die [Chi/HA]-Systeme, die mit einer höheren Konzentration (50mM) von Co^{2+} dotiert waren, die Zelladhäsion und das Wachstum nach 72 Stunden. Das reine [Chi/Alg] und [Chi/HA] förderte die adipogene Differenzierung nicht. Darüber hinaus hemmte Co^{2+} die adipogene Differenzierung, indem es die Expression adipogener Transkriptionsfaktoren unterdrückte. PEMs, die Cu^{2+} und Fe^{3+} ausgesetzt wurden, förderten die Zelladhäsion und -ausbreitung, was zu einer Vergrößerung der Zellfläche führte. Darüber hinaus stimulierten diese Metallionen auch die Stoffwechselaktivität der Zellen nach 24 Stunden und induzierten die Zelldifferenzierung in Richtung Adipozyten bei Abwesenheit zusätzlicher adipogener Medienzusätze. Die Bestätigung für die adipogenen Differenzierung wurde durch histochemische (Ölrotfärbung von Lipidvakuolen) und immunhistochemische Färbung (Perilipin und GLUT4) nach 21 Tagen erreicht. Interessanterweise zeigten Ca^{2+} dotierte PEMs eine positive histochemische Färbung für Lipidvakuolen sowie eine Expression von GLUT4 und Perilipin in C3H10T1/2.

Letztlich zeigt das Resultat dieser Forschung, dass Metallionen (Co^{2+}, Cu^{2+} und Fe^{3+}) verwendet werden können, um die osteogene Differenzierung der multipotenten Mauszelle C3H10T1/2 in situ zu induzieren. Auf diese Erkenntnis deutete vor allem die immunhistochemische Färbung hochregulierter Gene hin, welche eine entscheidende Rolle bei der Osteogenese (RunX2, ALP, Osteocalcin (OCN), Noggin) und quantitative Echtzeit-Polymerase-Kettenreaktion (qRT-PCR) nach 21 Tagen trug. Resümierend konnte infolge der Untersuchung festgestellt werden, dass Chi/Alg- und Chi/HA-Mehrschichtsysteme gemeinsam mit den Metallionen (Co^{2+}, Cu^{2+} und Fe^{3+}) als vielversprechende Beschichtungen auf Implantaten und Gerüsten dienen können und ein regeneratives Potenzial für Bindegewebe wie Knochen bieten. Die wesentliche, und neue Erkenntnis, welche mit dieser Arbeit erforscht wurde, ist jedoch, dass die Dotierung von mehrschichtigen PEMs mit Metallionen (Ca^{2+}, Cu^{2+} und Fe^{3+}) die Fähigkeit besitzt, die adipogene Differenzierung deutlich zu verbessern und somit vielversprechend für verschiedene praktische Anwendungen für die Geweberegeneration, wie Brustvergrößerung, Rekonstruktion und Wundheilung ist.

Chapter 1: Introduction

1.1 Brief survey on biomaterials for implants and tissue engineering scaffolds

Tissue and organ damage caused by illnesses, trauma, or aging often necessitates medical interventions such as transplantation. Common approaches include autografts (transferring tissue within the same patient), allografts (transplantation between a donor and a recipient of the same species), xenografts (using tissue from a different species), and synthetic implants. Although these methods have demonstrated varying degrees of success, they are accompanied by significant limitations. Challenges include donor site morbidity, pain, limited availability and quality of grafts, risks of disease transmission, and immunological complications such as graft rejection, particularly in allografts and xenografts [1, 2].

Consequently, tissue engineering has emerged as a promising alternative to conventional approaches like total hip or knee prostheses, which, despite their role in addressing certain medical challenges, still face limitations such as long-term functionality and complications. Biomaterials, designed to interact with biological systems for diagnostic or therapeutic purposes, are fundamental to replacing damaged tissues, organs, or body functions either temporarily or permanently [3]. These materials are essential in medical applications such as medical devices, implants, drug delivery systems, and tissue engineering scaffolds. To serve as effective implants and scaffolds, biomaterials must meet strict criteria, including biocompatibility to prevent adverse tissue reactions, and mechanical properties that match the characteristics of the target tissue (whether soft or hard). Additionally, these biomaterials should promote cell attachment, support cellular behavior, facilitate proliferation, migration, and differentiation, and enhance cellular functionality [4, 5]. Biomaterials are generally classified into three major classes; the first is bioinert materials, including metals like titanium and ceramics (e.g. alumina and calcium phosphates). The second is bioactive and biodegradable materials consisting of natural (e.g. collagen, alginate, chitosan and glycosaminoglycan) and synthetic polymers (e.g. polyglycolic acid polyethylene and polypropylene). The third class includes specifically designed materials stimulating specific cellular responses [6, 7]. In the context of biomaterials, bioinert materials are chemically stable and designed to provide mechanical support without eliciting significant biological responses, making them ideal for applications like orthopedic and dental implants. On the other hand, bioactive and biodegradable materials actively interact with the biological environment to promote tissue integration, cell attachment, and regeneration.

Natural polymers are often biodegradable and inherently biocompatible, and many of them exhibit natural bioactivity. Natural polymers play a crucial role in the field of tissue engineering, particularly in the creation of scaffolds for delivering therapeutic agents. Novel natural

polymeric materials are being developed with the aim of improving various therapies, leveraging their inherent bioactivity, biocompatibility, and ability to be naturally absorbed by the body [8, 9]. Naturally, derived polymers, such as collagen, chitin, chitosan, gelatin, silk fibroin, soybean, fibrinogen, fibrin, elastin, proteoglycan, hyaluronan, and laminin. These polymers are comprised of elongated chains, encompassing nucleotides, amino acids, or monosaccharides with recurring covalently bonded groups. Within these polymers, biofunctional molecules play a crucial role in ensuring bioactivity, biomimetic characteristics, and natural restructuring. Furthermore, several significant drawbacks limit the use of natural polymers in certain applications, particularly for hard tissue regeneration [10]. These drawbacks include susceptibility to microbial contamination, decreased adjustability, potential for immunogenic reactions, an uncontrollable rate of degradation, and inadequate mechanical strength [10]. For instance, collagen, as a natural protein-based polymer, possesses excellent biological functions that help bind cells, promote proliferation, differentiation, and the secretion of ECM components, making it an ideal substrate for tissue regeneration. While certain applications have achieved remarkable success and are now integrated into clinical treatments, others are still in the early developmental stages, because, collagen has limitations in terms of biomechanical properties, enzymatic degradation, and antigenicity[10].

Collagen-based scaffolds, widely used in tissue engineering, often face challenges related to mechanical strength, stability, and degradation rates. To overcome these limitations, collagen is commonly combined with both natural and synthetic polymers. Natural polymers, such as chitosan, hyaluronic acid, and alginate, enhance collagen's biological properties, promoting cell adhesion, proliferation, and tissue-specific functionality [10, 11]. Synthetic polymers like poly(lactic acid) (PLA), polycaprolactone (PCL), and polyethylene glycol (PEG) improve the mechanical strength, stability, and controlled degradation of collagen scaffolds, making them suitable for a range of tissue engineering applications [10, 11]. These scaffolds offer a balance of mechanical support and bioactivity, providing versatile solutions for soft tissue repair, bone regeneration, and controlled drug delivery [11]. Nevertheless, it remains a valuable and versatile biomaterial in the field of medicine [12]. Collagen type I is the most abundant collagen and is present in connective tissue excluding hyaline cartilage. It constitutes approximately 95% of collagen content in bone [13]. Collagen type I is an appealing medium for the improvement of tissue engineering scaffolds. Furthermore, glycosaminoglycans (GAGs) are linear long-chain polysaccharides composed of repeating disaccharide units. These molecules are highly negatively charged due to the presence of sulfate and carboxyl groups, which contributes to their biological activity. GAGs are primarily found on the surface of cells and are key components of the extracellular matrix (ECM) a complex network of macromolecules such as proteins, glycoproteins, and proteoglycans that provides structural and biochemical support

to surrounding cells. The ECM plays a crucial role in regulating cellular behavior, including processes like cell adhesion growth, differentiation, and migration. GAGs interact with various ECM proteins and growth factors, thereby modulating signaling pathways that influence cell functions. Because of their ability to regulate these critical processes, GAGs are considered excellent candidates for tissue engineering applications, where their incorporation can help create scaffolds that promote tissue regeneration, repair, and functional integration. By mimicking the natural ECM environment, GAG-based scaffolds can enhance cellular responses, such as facilitating cell adhesion and promoting the differentiation of stem cells into specific tissue types. These properties make GAGs valuable for developing biomaterials in tissue engineering, especially in applications that require mimicking or supporting complex cellular behaviors, such as in cartilage, bone, and skin regeneration [14-16]. Natural polymers like (GAGs) undergo enzymatic degradation since the glycosidic bond is relatively stable against chemical hydrolysis [17]. Hyaluronic acid (HA) is a polysaccharide, which belonging to GAG found in many parts of the body in the extracellular tissue. It has great anti-inflammatory potential through interactions with CD44, which translates the signals from HA to down-regulate leukocyte activation, growth, and differentiation [18]. In general, GAG can bind and interact with a wide range of proteins including ECM adhesive proteins (e.g. collagen, fibronectin, laminin), as well as growth factors, cytokines, chemokines and enzymes to modulate biological processes such as migration, homing, growth and differentiation of leukocytes, which are associated with inflammation [19, 20]. This unique combination of factors makes these natural polymers highly effective in promoting biocompatibility and tissue regeneration [21]. The polymer can be divided into two classes: non-biodegradable and degradable polymers. Polymer degradation can occur passively by hydrolysis or actively by enzymatic reaction [22]. Synthetic polymers, such as polyester, can be produced with repeating units and high purity, considered a degradable polymer in medical applications and degraded by chemical hydrolysis [23]. On the other hand, non-degradable polymers such as poly (methyl methacrylate) (PMMA) are used in application where a long-lasting biomaterial is required. For instance, PMMA is commonly used in intraocular lenses due to its durability and optical properties [24, 25]. The specific advantage of synthetic polymers is that their mechanical properties can be tuned to suit specific applications. Additionally, synthetic polymers can be modified to control their degradation rate and surface properties, which can be important for improving their biocompatibility and reducing the risk of adverse reactions in the body. Synthetic biomaterials often lack the natural cell adhesion sites found in native tissues and extracellular matrices. To enhance cell adhesion and bioactivity in synthetic biomaterials, chemical modifications are frequently required. Consequently, one common approach is to functionalize the biomaterial surface with the arginylglycylaspartic Acid (RGD) sequence, which is widely employed to enhance cell interactions with synthetic biomaterial

surfaces. However, certain limitations persist, including a potential reduction in biological activity or receptor specificity when using synthetic peptides [26-28]. Much research is going on to develop surface-functionalized biomaterials (metals alloys, ceramics, and polymers) to render them with new functional biological cues to improve biocompatibility and bioactivity [29, 30]. However, after implantation of these artificial constructs, protein adsorption occurs before any contact of cells with the biomaterials due to the presence of proteins in the surrounding body fluids. Protein adsorption on the implanted biomaterials is mostly unpredictable regarding film composition and protein structure [31]. The physicochemical properties of the material surface, depending on presence of different chemical functional groups (e.g. carbon, amino hydroxyl or methyl groups), determining surface charge and wettability that affect protein adsorption and subsequent cellular response as (it is lined out in more detail later on section 1.2) [32, 33]. The surface properties of implants topography, mechanical characteristics, and chemical composition are crucial as they govern the interface between the material and host tissue, directly influencing protein adsorption and key cellular responses, including adhesion, proliferation, differentiation, and inflammation [34, 35]. Additionally, the bulk properties such as mechanical strength and viscoelastic properties play an important role in implant materials. The adsorption of proteins onto biomaterial surfaces such as coagulation proteins like fibrinogen (FBG) and extracellular matrix (ECM) like fibronectin (FN) and vitronectin (VN), serves as a critical intermediary step that profoundly influences cell behaviour. This interaction acts as a bridge between the biomaterial and surrounding cells and play a pivotal role in achieving constructive cellular responses, which are essential for processes like wound healing and tissue integration [36, 37]. Many proteins, including collagen, contain binding sites that can interact with leukocytes and platelets [38]. Both of these cell types play critical roles in the interaction between biomaterials, especially in the context of implants and blood-contacting devices [39]. After implantation, host serum proteins such as albumin, fibrinogen, fibronectin, immune globulins, vitronectin, and others adsorb immediately onto the surface of the biomaterial [40]. The composition of the adsorbed protein layer, along with any changes in its conformation, has been observed to be linked to the activation of coagulation and the complement cascade, as well as the recruitment of leukocytes and platelets. These events can collectively lead to inflammatory responses [41-43]. In addition, various of ECM proteins, including collagen, gelatin, fibrinogen, and others, have been employed to modify biomaterial surfaces through adsorptive or covalent binding methods, because they provide a conducive microenvironment for cells to adhere to and differentiate, owing to ligation of integrins [44]. Also, bioactive peptides, such as the tripeptide sequence arginyl-glycyl-aspartic (RGD) sequence found in ECM proteins like collagen, fibronectin, laminin and others as ligands to various integrins, have been used for grafting to biogenic and synthetic polyelectrolytes to mimic the native ECM structure and function. The functionalization of biomaterial surfaces with

ECM proteins plays a pivotal role in advancing the fields of tissue engineering, regenerative medicine, and medical device design. It enables the creation of biomaterials and devices that can effectively control cell fate, promoting the regeneration and replacement of tissues and organs.

1.2 Effect of surface properties of materials on cell response, including protein adsorption, cell adhesion, growth and differentiation.

The material surface properties such as wettability, roughness, surface charge and chemical (e.g. carbonyl, amino or hydroxyl group), stiffness, protein adsorption, and cellular phenotypic responses are all considered to be interrelated and ultimately determine the biocompatibility of the material [32, 33, 45, 46]. As explained in the previous section, material surface properties such as topography and hydrophilicity influence protein adsorption in quantity adsorbed and conformation, which further affects cellular responses like adhesion and proliferation. In this regard, surface properties are considered critical for biomedical applications. The physicochemical interactions between biomaterial surfaces and biological systems, including protein adsorption, cell adhesion and differentiation, are interrelated and cannot be considered independent variables. The wetting properties of a biomaterial are important parameters for biomedical applications since they determine the adsorption of proteins and, subsequently, the adhesion of cells. The polar region on the material surface is characterized by a hydrophilic feature, which results in tight binding of highly dense water. In contrast, hydrophobic biomaterials lead to non-water adsorbent surfaces [47] and tend to adsorb higher amounts of proteins due to hydrophobic interactions, which may cause fibrinogen adsorption and other proteins, enhancing adhesion and blood platelet activation but also causing inflammation and fibrosis [48, 49]. Surface chemical groups like polar functional groups (-OH), enhance wettable surfaces by interacting with water molecules (**Figure 1.1**). In contrast, less polar functional groups like -CH3 contribute to hydrophobicity, making surfaces less wettable. Nano and microscale roughness with low surface energy results in non-wettable surfaces [50]. A moderately wettable surface with water contact angles (WCA) around 40° to 70° is considered the most effective for protein adsorption in terms of amount and conformation, leading to an optimal environment that promotes cell adhesion and proliferation, as opposed to hydrophilic or hydrophobic surfaces [33, 47, 51]. Attractive interaction forces for cell adhesion and surfaces depend on the material's physiochemical properties, like surface energy, surface potential, and the presence of functional groups. Long-range forces are represented by coulomb or electrostatic interactions that are dependent on the charges of both cell surface and substrate [52], further can be either attractive or repulsive due to the

presence of charged functional groups with protein structure. Cell adhesion studies found that the surface charge strongly influences the adhesion of cells, where positively charged surfaces enhance adhesion while negative ones reduce cell adhesion [53, 54]. Besides the surface properties of materials, roughness and topography can significantly affect the cell's behaviour, such as proliferation and differentiation. Rough surfaces provide more site cells to adhere to, which promotes cell attachment and spreading [55]. Niepel et al. modified multilayers of HA and PLL with variable nano topographies and surface viscoelasticity to regulate cell behaviour specifically adhesion and differentiation of hADSC. The cells behaviour was significantly influenced by the distance between the anchorage points, which were precisely engineered using laser interference lithography. This modification affected cell behaviour by altering the mechanical, chemical, and topographical cues that regulate cell adhesion, spreading, and differentiation pathways [56]. Several studies have attempted to increase cell adhesion of multilayers by using different proteins such as fibronectin (FN), vitronectin (VN), and COL, which are known to attract specific cell receptors [57, 58]. These studies showed that proteins are adsorbed strongly by interaction with PEM film regardless of the sign for both the multilayer surface and the proteins. When the charge of multilayer and protein are similar, a monolayer of proteins was adsorbed due to hydrogen bonding and hydrophobic interactions. When the charge on the protein and multilayer surface were opposite, the electrostatic interaction became dominant and led to adsorption of thicker layer of proteins. Wittmer et al. added a final fibronectin (FN) layer to Poly(L-lysine) / dextran sulfate PLL/ (DS) films and found that a higher amount of FN was adsorbed on positively charged PLL ending films [59]. Collagen is a natural ligand for several cell receptors of the integrin family such as (α1β1, α2β1, α10β1, and α11β1) [60]. Zhao et al. studied the osteogenic differentiation of adhering human adipose-derived stem cells (hADSCs) by multilayers of GAG/ collagen I [61]. The cell attachment to the layer surface was mediated by electrostatic interactions and indirectly by the adsorption of serum proteins. Cells were exposed to multilayers of ECM protein, GAG and polysaccharides. Hence was observed that cellular responses were dependent on cell type and physicochemical properties of PEM.

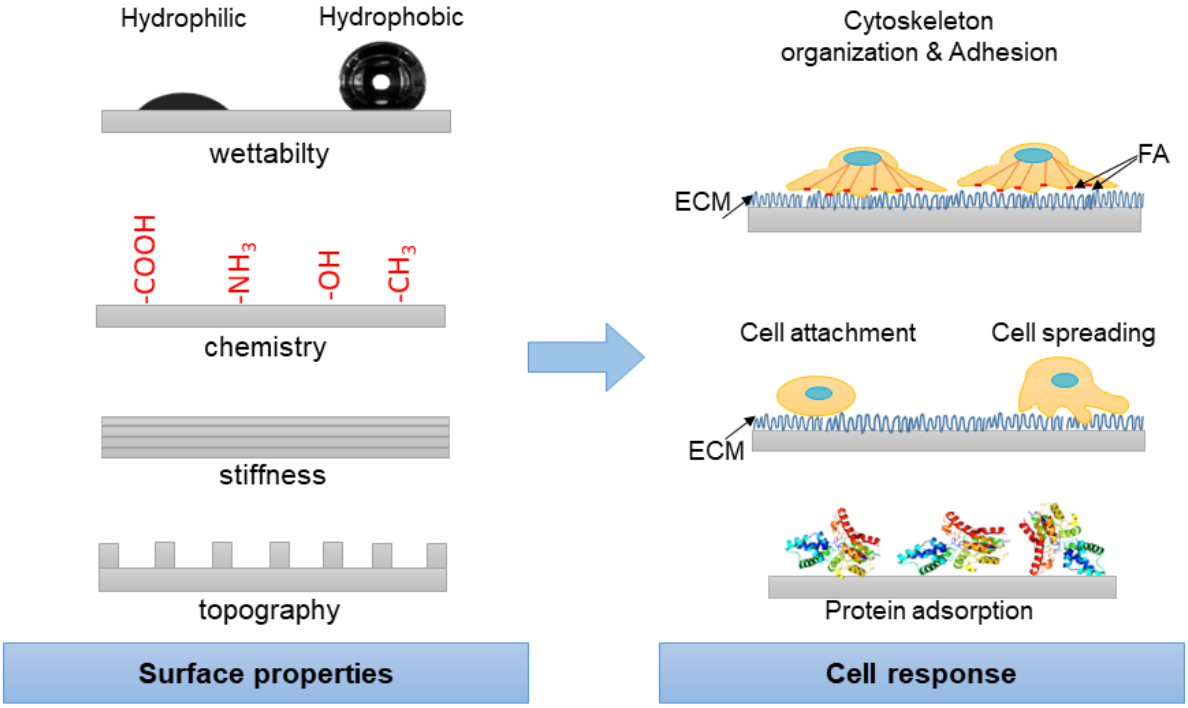

Figure 1.1: Schematic illustration of the surface properties influencing cell behaviour.

1.3 Surface modification of biomaterials

As mentioned earlier, biomaterials are indispensable for application as implants and tissue engineering because they possess numerous properties. These properties can be categorized into physical properties, including (topography, mechanics, etc.) and chemical properties (type and amount of functional groups, etc.) that make them attractive for such applications [62]. However, conventional materials likely include traditional biomaterials or implants that may have been used in the past, such as metals (e.g., titanium), ceramics, and polymers. These materials, while useful in medical applications, do not necessarily meet the advanced criteria required for optimized surface and bulk properties that modern tissue engineering demands, such as facilitating cell adhesion, proliferation, and differentiation [63, 64]. Uncontrolled protein adsorption on the biomaterial surface can lead to adverse effect on cellular behaviour and inflammation [42, 65, 66]. Despite contemporary materials showing promise, challenges arise in clinical use, primarily due to undesirable side effects stemming from uncontrolled protein adsorption. Addressing these issues at the nano to micrometer scale is crucial, as material surface properties directly impact in vitro biological performance and are integral for tissue remodelling [67]. The objective is to establish a biological model for surface science that can effectively mimic the intricate and interactive conditions found in an in vivo biological environment. As a result, substantial efforts are being devoted to the development of novel biomimetic surfaces by employing a combination of cells, surface engineering, and materials

in addition to the appropriate biochemical and biophysical variables [68]. Until now, a wide range of surface modification techniques has been developed to enhance the biocompatibility of (biodegradable) polymers and other biomaterials. Modifications often involve either physical or chemical changes to the atoms, compounds, or molecules that are already present on the surface. Typically, surface modifications techniques can be categorized into two main approaches: chemical and physical modifications. Physical techniques including coating techniques, surface self-assembly [69], vapour deposition [70] and surface coating [71, 72]. The techniques involve physical interaction such as electrostatic interactions, van der Waals forces, hydrogen bonding, hydrophobic interactions, etc., and other similar phenomena, are often simple and do not require extensive or expensive equipment. Chemical techniques play a role in binding molecules to or generating functional groups on material surfaces, for which several methods have been developed [73]. For example, surface grafting is a critical technique for modifying surfaces of biomaterial. It can be accomplished by either “grafting to” or “grafting from” the materials [74]. Biologically modified surfaces can be achieved by immobilizing biomolecules (e.g. cell receptor ligands, antibodies, enzymes, pharmacological agents, lipids and nucleic acids) onto and within biomaterials, supporting numerous therapeutic, diagnostic and bioprocess applications [75]. The biological modification can be achieved through either adsorption or covalent binding of various biomolecules to biomaterial surfaces, including oligopeptides, proteins, glycans [76]. For example, proteins or oligopeptides derived from the extracellular matrix can be covalently immobilized on the surface to target specific adhesion receptors or other molecules present on cells surface. The adsorption process plays a critical role in shaping cellular responses and interactions with the biomaterial. Establishing co-cultures of cells can further enhance these interactions by simulating more physiologically relevant environments, promoting cell-to-cell communication, and influencing how cells respond to the biomaterial. Additionally, immobilizing cell-cell adhesion receptors, such as Cadherins, can improve cellular attachment and coordination, fostering a more integrated and functional cellular response. These approaches are employed to mimic the native microenvironment of cells, facilitating interactions between cells and their surroundings in a manner that resembles native biological conditions [77, 78]. Hence, designing thin films with controlled properties while maintaining the bioactivity of the embedded molecules and adjusting their delivery is thus a great challenge. Hence, various techniques have been used to develop functionalized surfaces to make them biocompatible and bioactive. Decher et al. introduced one of these techniques, called the layer-by-layer method, in 1992 [56]. This method utilized to create thin films with desired properties to induce biological response.

1.4. Introduction to Layer-by-Layer (LbL) technique

Iler first described a principle of the LbL technique in 1966, where he defined a thin film fabrication based on alternating adsorption of oppositely charged species [79]. Decher and co-workers introduced the principle of alternating adsorption of polyelectrolytes (PEL) to create the multilayers. [80]. The LbL technique is a highly flexible and cost-effective method for generating polyelectrolyte multilayers (PEMs) on virtually any material of any shape, such as medical implants, tissue engineering scaffolds but also nanoparticles, cells, and even biological tissues (see **Figure 1.2**) [81, 82]. Basically, PEL multilayer (PEM) formation is based on electrostatic interaction and ion pairing, can lead to material coatings with unique properties [83, 84]. Beside electrostatic forces, other forces such as, such as van der Waals forces, hydrogen bonding, charge transfer, covalent binding, and specific or hydrophobic interactions, might contribute PEMs assembly and stability since the intrinsic net charge of PEL depends on surrounding aqueous environment conditions [85]. Schlenoff et al. modified the concept of electrostatic interaction in formation of polyelectrolyte multilayers (PEMs) by considering the interplay between intrinsic (i.e. PEL of opposite charge) and extrinsic (i.e. counter ions) factors [83, 86]. Further, it has been reported that one of the main driving forces behind the PEM formation is the increase in entropy due to the release of counter ions [87]. This makes it possible to create functionalized surfaces and structures that are robust in physiological environments and can be used in various biomedical applications, such as drug delivery [88] (**see Figure. 1.2**). The pH of the solution can affect the charge density of weak polyelectrolytes, which in turn can affect the electrostatic interactions between the polyelectrolytes. For instance at pH values close to the pKa of the weak polyelectrolyte, the electrostatic interactions between the polyelectrolytes will be weaker due to the lower charge density of the polyelectrolyte. Conversely, at pH values far from the pKa of the weak polyelectrolyte, the electrostatic interactions between the polyelectrolytes will be stronger due to the higher charge density of the polyelectrolyte [89]. Hence, weak polycations tend to adsorb as a thicker layer with coiled conformation at alkaline pH (less charge), while acidic pH values (highly protonated) lead to a thin layer formation with a flat chain conformation [90]. The increase in film thickness was observed when the pH value of the adsorbing PEL was close to its pKa value or if the ionic strength increased only within a narrow range [89, 91]. In addition, the ionic strength greatly affects PEL conformation and charge density [92]. At higher salt concentrations, intramolecular repulsion force screens the charges. It leads to the coiled conformation of PEL, resulting in a thicker film and appears softer [93]. Moreover, a temperature increase could also overcome electrostatic intramolecular repulsion, enhancing the entanglement of the molecule and leading to thicker film formation [94].

PEMs films can incorporate metal ions through ionic and coordinative bonds with functional groups of PEL such as amino, carboxylic, and hydroxyl groups [95-97]. The amount of metal ions that can be incorporated can be tuned by adjusting the conditions during the LbL assembly process, such as the concentration and pH of the metal ion solution and the deposition time of each layer. The change in pH and concentration of metal ions can affect PEM thickness. For example, the amount of Cu^{2+} leads to a decrease in charge density of complex solution, resulting in thinner PEM at alkaline pH. Additionally, by incorporating metal ions, PEM films can exhibit interesting properties such as the release of the metal ions over time. This can be useful for a variety of applications such as drug delivery, catalysis, and sensing. The release of the metal ions can be controlled by adjusting the properties of the PEM film, such as its thickness, charge density, and composition [98]. One of key advantage of the LbL technique is its ability to modify the properties of multilayers films simply by choice of different polyelectrolytes without, requiring any chemical activity of biomaterials. Overall, the LbL technique is a versatile method for building up thin films; this technique has been widely used in the biomedical field due to its ability to control film thickness, surface charge, and functionality.

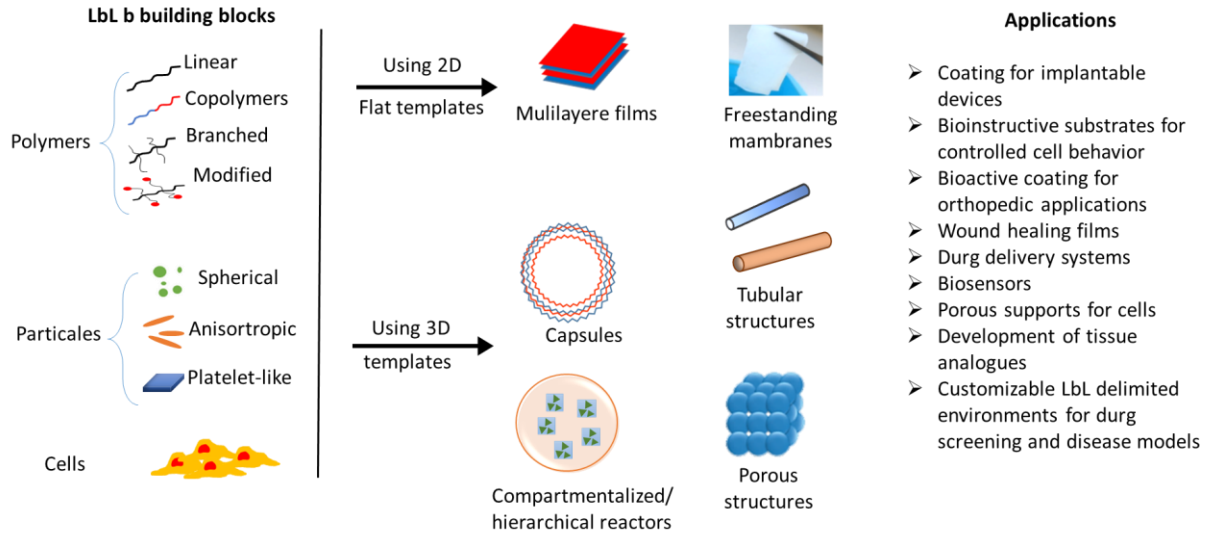

Figure 1.2: Graphical representation of building blocks used in LbL technique and the various multilayered devices conceived from their assembly onto 2D and 3D templates (adapted from [99].

1.4.1 Use of the LbL technique to make bioactive surface coatings

Since the 1990s, layer-by-layer (LbL) self-assembly of the film has been used in fields of biomedical implants such as drug delivery, where it can be used to create multilayered coatings that can release drugs in a controlled manner. By modifying the properties of the

polyelectrolytes used in the LbL assembly, it becomes possible to finely tune the release kinetics and specificity of the drug. Furthermore, LbL has been employed to create tissue analogues, where cells are encapsulated in a polymer matrix to mimic the structure and function of natural tissues. In this application, the LbL technique is used to build up thin films around the cells, creating a protective and supportive environment for cell growth and differentiation [100, 101]. Also, LbL has been utilized to coat implantable devices such as stents and prosthetic joints, thereby reducing the risk of implant rejection and improving their biocompatibility [99]. The multilayered coatings created by LbL can provide a barrier between the implant surface and the surrounding tissue, reducing inflammation and promoting tissue integration. LbL multilayer assembly can be achieved by various methods such as dip, spin and spraying coating. Yang and coworkers highlighted the development of LbL nanocoating to deliver multiple biomolecules, including proteins, polypeptides and DNA [102]. This technique offers precise control over the composition and thickness of the coating, which can be tailored to optimize the release kinetics of the biomolecules, protect them from degradation, and enhance their stability and bioactivity. LbL multilayer coatings mimic some of the properties of the ECM, including providing a platform for cell adhesion, migration, and proliferation; this makes LbL layers an attractive option for developing implantable devices with improved biocompatibility, functionality, biorecognition and integration with surrounding tissues. Materials like metallic alloys, inorganic materials such as glass and ceramics and also many polymers are negatively charged can assist in the formation of multilayers by alternating adsorption of a polycation layer [103]. Zankovych and co-workers evaluated the effect of PEM coating of Chi/ Gel and Chi/HA on titanium alloy implants, studying their anchorage in an animal model in vivo [104]. It was shown that PEMs coating had a beneficial impact on enhancing the osseointegration of the implant when compared to the uncoated titanium alloy. Many types of charge species including (GAG), DNA and ECM proteins like collagens, fibronectin, and elastin also represent polyelectrolytes and can be applied to generate biomimetic multilayers on biomaterial surfaces with biological information [93, 103, 105]. Hence, several scientists have focused their research on using different biopolymers for making multilayer coatings, e.g. hyaluronan, chondroitin sulfate (CS), heparin (HEP), (Chi) etc. [37, 106-108]. Multilayers created from natural polymers offer unique compositions, triggering specific cellular responses while providing both mechanical and biochemical signals. These polymers, characterized by biocompatibility, bioactivity, degradability, and abundance, hold significant value [109]. COL I, a major protein in fibrous connective tissues, is a natural ligand for integrin family cell receptors, offering mechanical support [110]. Collagen finds extensive use in implant coatings, three-dimensional scaffolds, and hydrogels due to its general bioactivity, biodegradability, and weak antigenicity [111, 112]. Glycosaminoglycans are a class of complex carbohydrates (also called glycans) found in animals, play crucial roles

in cell signalling by interacting with cellular receptors, matrix proteins, and growth factors. Heparin, a GAG, exhibits high affinity towards a variety of proteins like fibronectin and growth factors, including bone morphogenic proteins (BMPs) [76, 113]. Heparin interacts with these molecules via specific HEP-binding domains, regions on the proteins that recognize and bind to heparin [114]. Since matrix components like proteins and (GAGs) represent PEL, their application for formation of bioactive multilayer surface coatings by the LbL technique has gained increasing interest.

These coatings can be formed using ECM proteins, polysaccharides, and other bioactive molecules to stimulate cell adhesion and proliferation [69]. In this context, the ECM functions as a reservoir for storage and release of growth factors (GFs), such as bone morphogenetic protein-2 (BMP-2) [115, 116], which induces the differentiation of mesenchymal stem cells (MSCs) and non-osteogenic cells [117]. One limitation of BMP-2 is its short half-life [118]. The osteoinductive effects of BMPs are highly dependent on their concentration, and clinical trials have shown that growth factors like BMPs often require administration at doses significantly higher than physiological levels to effectively induce osteogenesis. Furthermore, combining BMPs with collagen and hydroxyapatite has been demonstrated to enhance bone formation[119]. This raises concerns about the practicality and potential side effects of using such high concentrations of growth factors. One approach to obtaining these growth factors is by synthesizing them through recombinant DNA in organisms like E. coli [120]. However, these recombinant growth factors are often sensitive and can degrade or lose their bioactivity, stability, and efficiency easily, especially when combined with drug delivery systems. Other disadvantages include the high cost associated with recombinant growth factor production and the need to use large quantities [120]. These factors drive the exploration of new and alternative methods to induce and enhance the efficacy of osteogenesis and bone regeneration. The advantage of metal ions is that they may represent a cheap, safe, and "bioactive" solution or alternative approach. On the other hand, techniques of cross-linking multilayers, including the use of coordination-based chemistry, are considered promising for engineering the artificial ECM. Cross-linking the films can address this, improving mechanical properties like stiffness and roughness of the films, which in turn affects intrinsic biological properties such as its adhesion and differentiation of cells [107, 121]. Hence, different physical and chemical crosslinking strategies have been used to tune such films' structural and mechanical stability (see **Figure 1.3**). Chemical cross-linking involves forming covalent bonds between polymer chains or within a single polymer chain, enhancing structural rigidity and stability. It relies on reactions between functional groups on polymer chains and a crosslinking agent with reactive groups. Polymer functional groups such as carboxylic acid (-COOH), hydroxyl (-OH), and amino (-NH2) participate in these cross-linking reactions. Cross-linking

agents commonly used in this process include aldehydes, such as glutaraldehyde and formaldehyde, and carbodiimides, such as N, N'-dicyclohexylcarbodiimide (DCC). For instance, 1-ethyl-3-(-3-dimethylaminopropyl) carbodiimide (EDC) within N-hydroxysuccinimide (NHS) was used to crosslink multilayers from chitosan and - hyaluronic acid. Carbodiimide EDC stimulates the amide bond formation between carboxylic and amine groups of HA and PLL (poly-L-lysine), respectively, where cross-linking led to an increase in the rigidity of the film (Young's modulus) which improved the cell adhesion and spreading [122]. Moreover, genipin was used as a crosslinker due to its lower cytotoxicity and proven efficiency in protein cross-linking [123-125]. The ester group of genipin reacts with amine groups of biomolecules forming an amide bond. Groth and co-workers demonstrated that, using genipin as an extrinsic cross-linker led to increase in the elastic modulus of chitosan/alginate free-standing films while maintaining their biocompatibility for use in wound dressings [124]. Moreover, genipin has been used to cross-link thin multilayers made of Alg and Chi [126], Chi/ HA [127] and Col /Alg [125]. Other polysaccharides like alginate is extracted from cell walls of brown algae and consist and consist of alternating blocks of mannuronic and guluronic acid and possesses polyanionic character but lacks specific bioactivity in mammals. Alginate contains pendant carboxylic groups on the guluronate blocks that can be cross-linked with various divalent or trivalent cations, including calcium (Ca^{2+}), magnesium (Mg^{2+}), and iron (Fe^{3+}), where calcium ions cross-linked alginate to form a gel-like structure through ionic cross-linking. The formation of "quasi-crystalline" segments in the cross-linked alginate can be sued for formation of microcapsules, particles, and hydrogels, which have been used in various applications, such as drug delivery and tissue engineering [128]. Metal ions such as Ca^{2+} induce cross-linking of Chi/Alg multilayers [124, 129], interacting with polyelectrolytes through forming metal-ligand coordination bonds and electrostatic interactions with opposite charges. The Fe^{3+} ions can form stronger and more stable cross-links with alginate than calcium ions, making it a potentially efficient material for use as scaffold, allowing good cell adhesion and proliferation [130]. In addition, Fe^{3+} ions have been shown to promote the secretion of extracellular matrix components by cells, which enhances cell adhesion and proliferation [131]. The metal ions Cu^{2+} and Zn^{2+} were doped into (PAA/PEI) film during the LbL process through interaction with the carboxylic acid groups of PAA. Hence metal ions coordinate strongly with COO- groups of PAA and bind with amine groups of PEI through electron transfer to get optimized capture of ions in the film [132, 133].

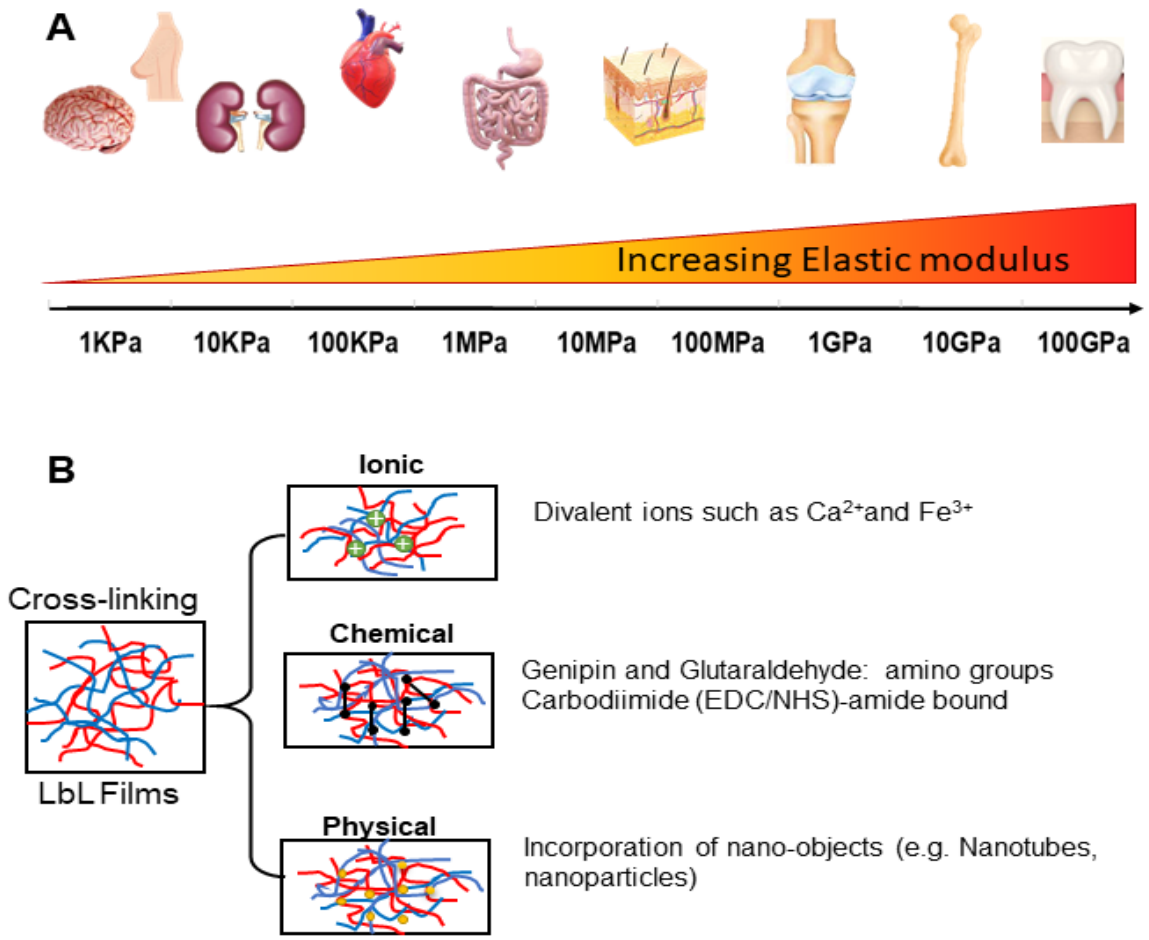

Figure 1.3: Mechanical properties of multilayered films (A) Mechanical properties that can be achieved to mimic the range of different elasticities. Soft tissue like the brain exhibited low stiffness, whereas tissue exposed to high mechanical such as bone, Adapted from [69].

1.5 Overview of polysaccharides as biomaterials and their metal ions complexation

Polysaccharides are long-chain molecules consisting of repeating units of monosaccharide bonded together by glycosidic linkages [134] [45]. They can extend in the structure from linear to branched-chain molecules. Polysaccharides can be obtained from various sources, such as microbes, plants, algae (e.g. alginate), and animals (e.g. chitosan and hyaluronic acid). Because of the biodegradability, biocompatibility, non-toxicity and natural abundance of polysaccharides in mammals, including humans, as a component of cell surfaces (e.g, syndecans) and extracellular matrix components (e.g, proteoglycans, HA), make them an attractive choice and interestingly in the development pharmaceutical and biomedical areas such as cell encapsulation, wound healing, drug delivery, tissue engineering, and protein binding [135-137]. Additionally, the polysaccharide holds other advantages, i.e. chemical

modification, controlled release and ease of availability [134]. In addition, many polysaccharides have different functional groups, such as hydroxyl or carboxylic and amine, which can be complexed with multivalent ions [138].

Review on Polysaccharides in this study

Chitosan (Chi)

Chitosan is derived from the deacetylation of chitin (50% of free amine form) from the natural crustacean exoskeleton or the cell wall of fungi [139]. Chitosan is a liner polysaccharide consisting of β- (1-4) linked 2-amino-2-deoxy-D-glucose (D-glucosamine) and N-acetamido-2-deoxy-D-glucose (N-acetyl-D-glucosamine) units [140]. Chitosan becomes soluble and dissolves in diluted acidic solutions due to its pKa value, which typically falls within the range of 6.46 to 7.32 [141]. It is insoluble at physiological pH value in water with pH above pKa value, as well as in alkaline solutions. This leads to the protonation of the amino group of glucosamine at a low pH value, and chitosan becomes a polycation with high charge density. Therefore, it can electrostatically interact with negatively charged (polyanions) to form stable polyelectrolyte complexes [142]. The chemical properties of chitosan are remarkable, including the high nitrogen content, hydrophilicity, and viscosity, crystallinity, insolubility in water and organic solvents. Chitosan is used as a chelating complexing agent with metal ions through interaction with –OH and $–NH_2$ groups (see **Figure 1.4**) [143]. Furthermore, Chi possesses numerous biological activities such as antioxidant, antimicrobial, anticoagulant and anti-inflammatory [144]. Chi exhibits anti-bacterial activity against various types of microorganisms, including fungi, viruses and bacteria due to its cationic nature, which contributes to its biocidal properties [145, 146]. It is considered a biodegradable, bioresorbable, biocompatible polysaccharide. These characteristics make Chi ideal candidates for tissue engineering, wound healing, drug/gene delivery and regenerative medicine applications [139].

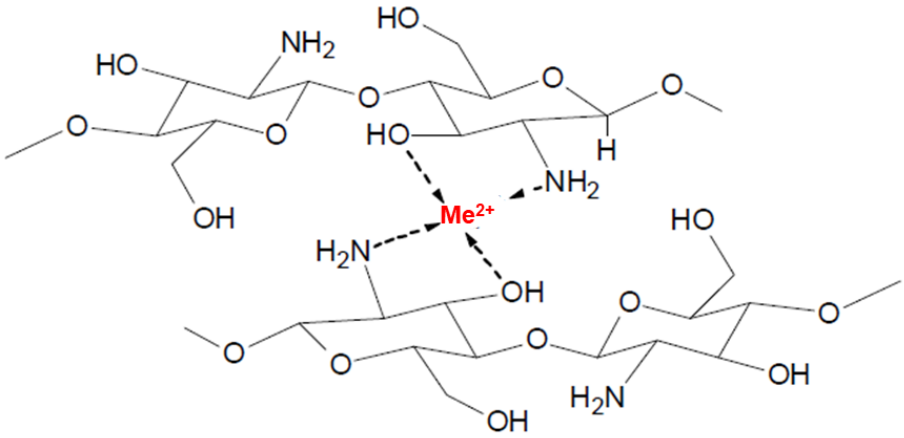

Figure 1.4: Suggested structure of metal complexes with chitosan. Copyright [143].

Alginate (Alg)

Alginate belongs to the family of linear polysaccharides obtained from brown seaweeds. It is a block copolymer consisting of two uronate sugars, β-D-mannuronic (M) acid and α-L-guluronic acid (G). The alginate chain can be divided into three blocks: the GG block containing L-guluronic acid unit only, the MM block containing D-mannuronic acid units only and the MG block with alternating units of both D-mannuronic acid and L-guluronic acid (**Figure 1.5 a**). These monosaccharides contain carboxylic acid functional groups, which are responsible for the polyanionic character of alginate [147]. The presence of di/trivalent metal ions (e.g. calcium, magnesium, barium and iron) results in strong interaction with the carboxylic groups of guluronic acid (G) of different chains, resulting in the formation of hydrophilic junctions known as “egg box” model [148] (**Figure 1.5 b**). Alginate is a polyanion that interacts with oppositely charged polyelectrolytes, such as chitosan, to form polyelectrolyte complexes [149, 150]. In the formation of alginate gels with transition metal (TM) cations, covalent bond formation takes precedence over electrostatic interactions in the polyelectrolyte solutions [96]. The abundant of $-COO^-$ groups on the backbone of alginate, make the electrostatic interaction between metal ions and polyanion stronger than that between starch based anion and metal ions [151]. Its biocompatibility, low toxicity [152], biodegradability, and cost-effectiveness [153], makes alginate highly attractive for various m applications. Alginate based wound dressings, not only serve as barrier but also maintain a moist environment, enhancing wound healing. Due to alginates exhibiting low protein adsorption and the lack of cell receptors, they serve as a specific model for cell culture and biomedical and tissue regeneration studies.

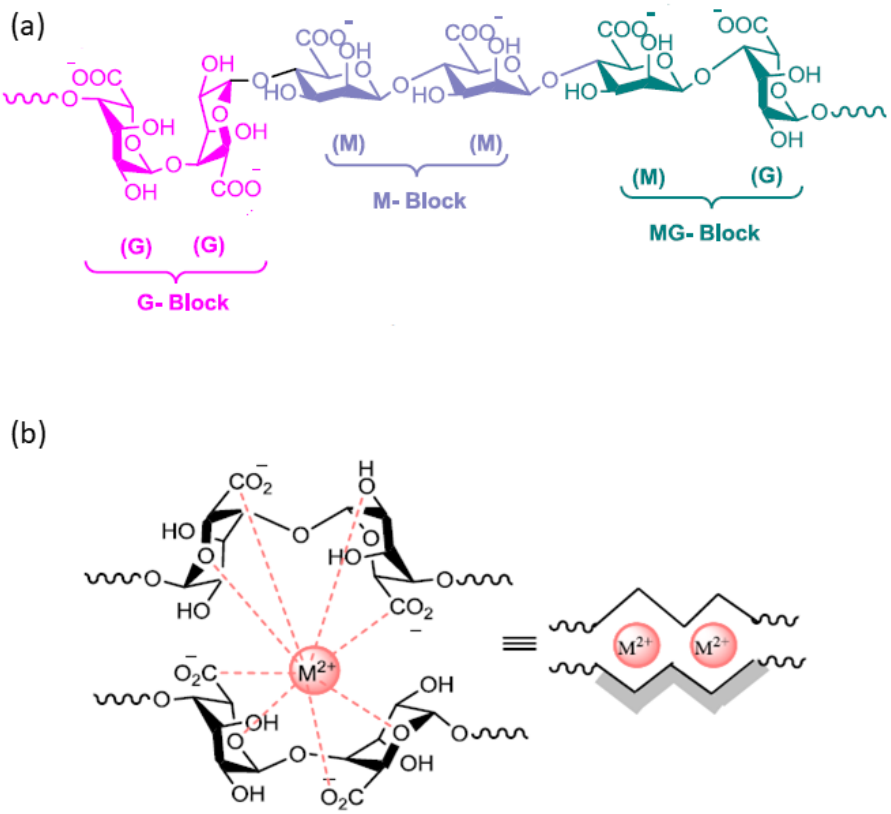

Figure 1.5: Structure of (a) alginate and (b) Egg-box" representation. (adapted from [148]).

Hyaluronic acid (HA)

Hyaluronic acid (HA) is a type of GAG, serving as another anionic polyelectrolyte that represents a critical constituent of many tissues' extracellular matrix. It is a high molecular weight GAG composed of repeating disaccharides of D-glucuronic acid (GlcA) and N-acetyl-D-glucosamine (GlcNAc) linked by a glucuronidic β bond. Each monosaccharide is connected through alternating beta-1,4 and beta-1,3 glycosidic bonds (**Figure 1.6**) [154, 155]. Owing to free carboxyl groups on GlcA units, HA has a polyanionic character that allows the formation of associates with polycations such as chitosan to obtain multilayer formation. Moreover, HA can act as a ligand, coordinating with metal ions through its carboxylate and hydroxyl groups. This interactions occurs via oxygen atoms particularly O-1 in the equatorial plane [156]. HA is the only non-sulfated GAG and does not bind to a protein core to form proteoglycans [17]. HA is an essential component of the ECM in cartilage due to its hydrogel-like elasticity and viscosity, high molecular weight, and moderate anionicity [17, 157]. The molecular weight of HA depends on the tissue and species. In humans, the highest concentrations of HA are found in umbilical cord, synovial fluid, skin, and eye with a molecular weight of around $2x10^6$ Da but this decreases with age progression [158]. High molecular weight HA exhibits anti-angiogenic,

immunosuppressive and anti-inflammatory properties, while low molecular weight HA is highly angiogenic, immunostimulatory and displays pro-inflammatory properties [159]. Due to viscoelastic properties, plays HA a crucial role in filling the intercellular spaces between various components such as collagen, the cellular environment, and blood lymph vessels. In the extracellular space HA is typically bound to matrix proteins (hyaladherins) [160]. HA also plays an important role in the immune response through interaction with specific cell-surface receptors, like CD44 and RHAMM (receptor for HA-mediated motility) [156, 161]. HA is a key regulator inflammation, where it is cross-linked by different hyaladherins such as CD44 and TSG-6 (tumor necrosis factor-stimulated gene-6), forming a pericellular coating around cells. This coating not only protects the cells from inflammatory mediators but also acts as an immunosuppressive by preventing ligand access and inhibiting phagocytosis by macrophages and monocytes [159, 162]. HA has many advantages including biocompatibility, biodegradability, and non-toxic, making it extensive use in various clinical applications include wound healing coatings and the creation of new scaffolds like microgels, hydrogels, its use in joint fluid for arthritis [157]. Moreover, HA's consistency, biocompatibility, and hydrophilicity make it an excellent ingredient in cosmetic creams, and it is utilized as a dermal filler and treatment of osteoarthritis [155, 163].

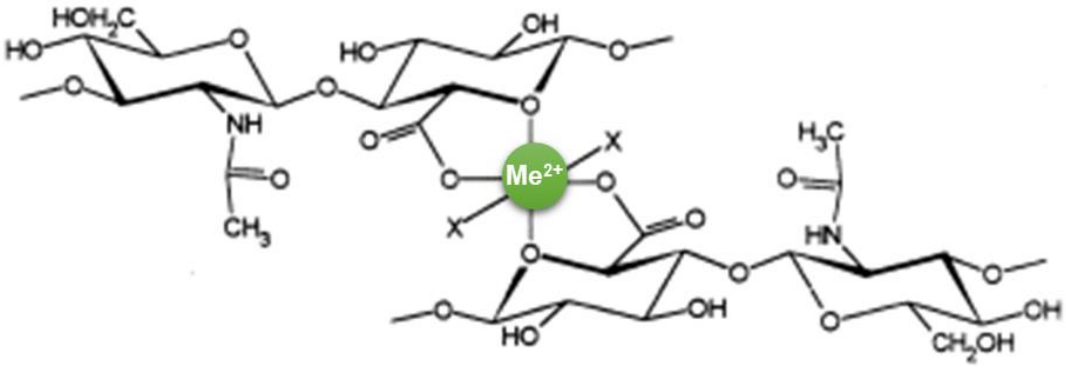

Figure 1 6: : proposed structure of metal ions (Cu^{2+}) with HA complex (adapted from [156]).

1.6 Biology of mesenchymal stem cells, including multipotent cell lines

Stem cells play an essential role in promising studies of tissue engineering due to their unique ability to differentiate into diverse connective tissue phenotypes, encompassing bone, cartilage, muscles, tendons, and ligaments [164]. Stem cells can differentiate into various types, including embryonic and extraembryonic such as totipotent, pluripotent, and multipotent stem cells. Totipotent stem cells from the inseminated oocyte, are characterized by their ability to generate an entire organism, including both embryonic and extraembryonic tissues such as placental tissue [165]. Pluripotent stem cells have capacity for self-renew and give rise to the

three primary germ cell layers during early embryonic development, ultimately contributing to the formation of the adult body. Multipotent stem cells have limited differentiation potential and can only differentiate into cells belonging to the same specific tissue lineage [165]. And allow the formation of all ectoderm, endoderm, and mesoderm cell layers [166]. In 1970 Friedenstein et al. discovered mesenchymal stem cells in bone marrow [167]. Over the last few years, MSCs have been isolated from various adult tissue sources. Human MSCs (hMSCs) are present in postnatal organs and tissues and can also be isolated from sources like dental pulp [168], marrow, adipose tissue [169], and several neonatal tissues [170], including the placenta [171]. Mesenchymal stem cells are multipotent and have ability to adhere and differentiate into several cell types, such as osteoblasts, chondrocytes and adipocytes (fat cells that give rise to marrow adipose tissue) [170, 172], further expressing surface molecules such as CD90 (thy-1), CD44 (hyaluronan receptor), CD105 (transforming growth factor-b receptor III), CD73 (ecto five nucleotidases) and not CD 34, CD 45, CD11b, CD19 and HLA-DR [173, 174].

Moreover, MSCs cells have two characteristics, i.e. ease of isolation and low immunogenicity stimulation. Owing to their characteristic capacity for both self-renewal and differentiation [175, 176], MSCs can be used to improve clinical treatment techniques in various skeletal tissues like (tendon, muscle and marrow stroma) [172], the bone [177], fat [178], and articular cartilage [178, 179] (**Figure 1.7).** In vivo, adhesion molecules such as cadherins play crucial roles in mediating the MSCs cell niche, including self-renewal, differentiation, cellular organization, and tissue integrity. They influence MSC behaviour by mediating cell-cell and cell-matrix interactions, which guide stem cell maintenance, migration, and response to signalling cues [180]. However, in vitro cultivation of MSCs can lead to reduced cell-cell interaction, prompting an increase in integrin-based focal adhesions. MSCs interact with ECM molecules, such as fibronectin, laminins, and collagen receptors, which play a critical role in adhesion, migration, and differentiation [180]. The physical characteristics of the niche have been observed to impact integrin binding and the formation of focal adhesions, both of which play a role in regulating the differentiation of MSCs [181]. The mechanical properties (stiffness, elasticity, etc.) and topography of the ECM have an impact on the cell interaction with their environment, cell spreading, orientation, and gene expression. This effect is mediated by mechanosensors and mechanotransducers, hence guiding cell differentiation [182]. For example, it has been shown that MSCs cultured on a softer surface guide the cells toward adipogenic and chondrogenic differentiation, whereas those grown on a stiffer substrata have a greater osteogenic [183].

Besides that, a microenvironment built of PEM made of extracellular matrix components of GAG can also provide MSCs with appropriate proliferation and differentiation [61]. For instance, in vitro culture of human adipose-derived stem cells (hADSCs) on PEM, treated with growth factor (e.g. bone morphogenetic proteins), promoted osteogenic differentiation [61].

Additionally, MSCs also have the capacity to produce chemokines, growth factors, and cytokines, which serve to stimulate and regulate a local response to regenerating microenvironments and repairing tissue. These molecules can exert their effects directly on the MSCs themselves (autocrine response) or on neighbouring cells (paracrine response) [184]. The paracrine activity of these factors can be employed to investigate the behaviour of the cells. The paracrine factors establish a complex network that contributes to the stability and amplification of the regenerative response [184]. Moreover, the MSCs can be guided to differentiate via induced culture media with specific chemical factors. For adipogenic differentiation; MSCs are typically cultured in medium supplemented with isobutylmethylxanthine (IBMX), dexamethasone (Dex), and insulin. IBMX directly induce C/EBPβ expression, while Dex activates C/EBPδ expression by binding to intracellular glucocorticoid receptor [185]. Insulin role is to promote glucose uptake for triglycerides synthesis, thus inducing of adipogenic differentiation. On the other hand, MSCs cultured in osteogenic medium, which includes (Dex), ascorbic acid phosphate and β-glycerophosphate are guided to differentiate into osteogenic cells. This promotes cell proliferation [186], resulting increase level of phosphate ions for mineral deposition of ECM [187]. Transcription factors that play a role in initiating and promoting the differentiation process are targets of various signaling pathways, either through direct or indirect interactions. In the osteogenic process, multiple signaling pathways, including transforming growth factor-ß (TGF-ß), bone morphogenic proteins (BMPs), Wnt/ß-Catenin and fibroblast growth factor (FGF), among others. These factors collaborate to the differentiation an osteoblast progenitor into a mature osteoblast [188]. The osteogenic process starts with signalling cascade by ligand binding to the heteromeric complex of types I and II serine/threonine kinase receptors on the cell surface [188]. BMPs increase the transcription of core-binding factor-1/Runt-related family 2 (Cbfa1/Runx2) that regulates osteogenic differentiation. The most important BMPs are BMP-2, -4, and -7 which are expressed in cartilage and bone [188, 189]. Furthermore, the combination of BMPs with collagen and hydroxyapatite induces bone formation [119]. However, the osteoinductive effect of the BMPs is affected by the concentration[188]. Many signalling pathways can induce conversion between osteogenesis and adipogenesis that are connected with two key transcription factors: PPARγ (peroxisome proliferator-activated receptor γ) direct differentiation to adipogenic, whereas Osterix and Runx2 (Runt related transcription factor 2) are master regulators of osteogenic of MSCs [189, 190]. During the differentiation, the Nel-like protein type I (NELL-1) promoting osteogenic differentiation and inhibiting adipose differentiation of MSCs [191]. Another signalling pathway involves a transcriptional co-activator with a PDZ-binding motif as known (TAZ), which is acts a transcriptional modulator of MSC. It enhances osteogenic differentiation while suppressing adipogenesis [192]. Several metabolic processes have been shown to affect stem cell fate

decisions, including mitochondrial metabolism [193], oxidative stress [194], and glucose uptake [195]. Increasing mitochondrial metabolism and generating reactive oxygen species (ROS) promoted adipogenic differentiation [196]. The induced hypoxic condition in human adipose tissue MSCs (hAT-MSCs) enhanced the ability to differentiate into adipocytes and osteocytes [197]. In recent years, mesenchymal stem cells (MSCs) have gained recognition for their remarkable therapeutic potential. They are now widely employed in the field of regenerative medicine, particularly in autologous tissue grafts, which are considered the leading approach for reconstructing damaged bone tissue. Additionally, MSCs can be used in biocompatible scaffolds for implants to heal many tissues, without causing adverse side effects or further tissue damage [164].

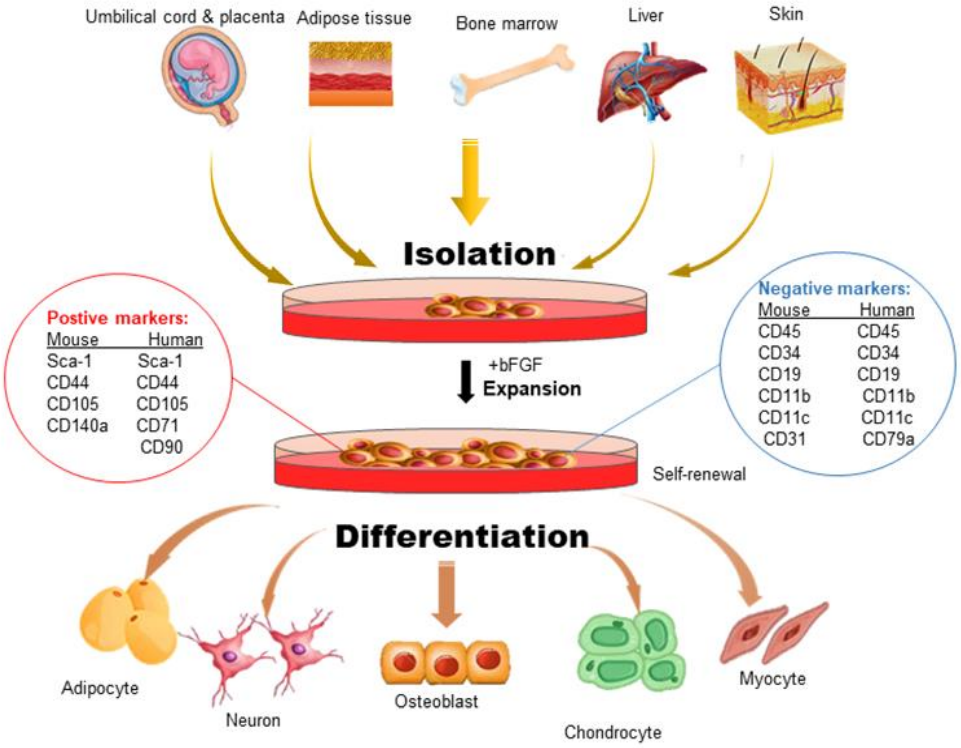

Figure 1.7: Isolation, expansion, and differentiation of MSCs. MSCs can be isolated from various tissues of either human or mouse. A combination of positive and negative markers is used to determine the purity of MSCs. In addition to self-renewal, these multipotent MSCs can also undergo differentiation in culture. The MSCs are their differentiation ability to cell lineages such as adipocytes and osteoblast- copyright from [198].

1.7 Effect of metal ions on cell metabolism and function (including cell differentiation)

Metal ions play essential functional roles in biological processes such as metabolism, catalysis, and cell signalling. Furthermore, metal ions often serve as cofactors for enzymes.

For instance, the alkali metal ions like sodium (Na+) and potassium (K+) present in our body fluids are responsible for maintaining fluid and electrolyte balance, regulating acid-base homeostasis, and sustaining cell membrane potential. This is crucial for generating action potentials, which are essential for processes like neurotransmission, muscle contraction, and heart function [199]. Essential metal ions such as copper (Cu^{2+}) and iron (Fe^{3+}) are crucial for maintaining cell membrane integrity, DNA stability, and participating in vital cellular processes like electron transfer and catalysis. However, an excess of these essential metals can prove lethal to cells [200]. In addition, metal ions opened up the prospect of widespread application in bone tissue engineering strategies [201, 202].

Here further focus is on metal ions that already used in this work.

Calcium (Ca^{2+}) is the most abundant metal in the body; approximately 99% of calcium is located in bones and teeth, while the remaining is distributed in other tissue. Calcium ions (Ca^{2+}) act as second messengers in many signalling pathways and play a critical role in regulating a wide range of physiological cell functions, including cell motility, muscle, heart contraction, the secretion of hormones like insulin (IGFs), nerve impulse transmission and cellular differentiation, proliferation [203, 204]. Calcium also promotes early stages of adipogenic differentiation by inducing cyclic adenosine monophosphate (cAMP) as a second messenger, This, in turn, triggers various physiological changes at cellular level such as proliferation, differentiation, migration and survival,. Furthermore, calcium-cAMP pathway regulates several gene expression involved in adipogenic differentiation through PPARγ (peroxisome proliferator-activated receptor gamma) [205, 206].

Calcium ions can activate intracellular signalling pathways, including the mitogen-activated protein kinase (MAPK) pathway, by activating protein kinases such as calcium/calmodulin-dependent protein kinase (CaMK). One of the critical steps in the MAPK pathway is the phosphorylation of extracellular signal-regulated protein kinases 1 and 2 (ERK1/2), which are activated by a dual-specificity kinase called mitogen-activated protein kinase kinase (MEK) [207]. Additional extracellular calcium activates an extracellular G-protein-coupled receptor called calcium sensor receptor (CaSR) [208]. Hence, activation of the CaSR and ERK1/2 signalling pathway has been shown to enhance cell proliferation, survival, and osteogenic differentiation of bone marrow-derived mesenchymal stromal cells (MSCs) [207, 209].

Cobalt (Co^{2+}) is an essential trace element for metabolism for all organisms. Further, it is a cofactor forming vitamin B12 and other cobalamin and a necessary coenzyme for cell mitosis. Moreover, cobalt is essential in synthesis of amino acids and some proteins, such as (methyl malonyl-CoA carboxyl transferase and aldehyde decarbonylase) [210]. The cobalt ions signal cells for low O_2 pressure by stabilizing HIF-1a, which induces the excretion of factors such as erythropoietin that support cell survival in a hypoxia environment and stimulate the production of red blood cells, as well as improve wound closure and avoid bacterial infection [211, 212].

Cobalt is a hypoxia agent, which can activate hypoxia-inducible factor-1 (HIF-1) in mesenchymal stem cells and then activates (HIF-1α) the production of vascular endothelial growth factor (VEGF) [213]. Hence cobalt enhances angiogenesis by activating hypoxia-inducible factor-1 (HIF-1) [214].

Moreover, cobalt enhances osteogenic differentiation via the production and expression of VEGF in endothelial cells [215]. Cobalt chloride has been shown to enhance the production of anti-inflammatory mediators such as prostaglandins (PGE_2) and inhibit the inflammatory cytokines such as tumour necrosis factor α (TNF-α) in human umbilical cord blood-derived MSC (hUCB-MSCs) under hypoxic conditions. The mechanism by which cobalt chloride exerts these effects is through the activation of the extracellular regulated kinases (ERK) signalling pathway in a hypoxia-inducible factor-1 alpha (HIF-1α)-MicroRNA-146a-mediated signalling pathway [216].

Copper (Cu^{2+}) plays a vital role in the human body's diverse physiological and metabolic processes through enzyme interaction [217, 218]. Copper is an essential nutrient, and it acts as a cofactor of redox enzymes, cytochrome oxidase (which produces Adenosine triphosphate ATP that is involved in the production of cellular energy) and Cu/ Zn superoxide dismutase [219]. Cellular copper homeostasis and utilization are regulated for several processes involving uptake, transportation to tissues, and export of excess copper to prevent harmful effects [218]. It has antibacterial properties and can stimulate angiogenesis and synthesis of the deposition of collagen fibres [220]. Moreover, it also stimulates the immune system to struggle and fight inflammation, repair injured tissues, and enhance healing [221]. These features give rise to catching attention for the use of copper in the field of tissue regeneration.

Iron (Fe^{3+}) is essential for energy metabolism and a variety of cellular processes [146-148], such as oxygen transport, ribonucleic acid (RNA), proteins, synthesis of deoxyribonucleic acid (DNA), and cell growth and differentiation related to iron [222]. Iron participates in a large number of metalloproteins such as heme protein (non-enzymatic) (e.g. haemoglobin and Myoglobin), and heme enzymes are involved in electron transfer (e.g. cytochromes, b, f oxidase) and with oxidase activity [203, 222]. Further, iron is loosely bound to low molecular weight compounds such as the procollagen proline hydroxylase and the procollagen lysine hydroxylase [223]. Both enzymes affect proline hydroxylation, and lysine remains in fibres of collagen. In contrast, a lack of iron gives rise to abnormal synthesis of maturation (physical and cognitive maturation) and collagen metabolism [224, 225]. Iron stimulates several signalling pathways in MSC, such as Wnt and ROS. Wnt signalling regulates MSC fate, bone remodelling and homoeostasis, as evidenced by its role in the osteogenic differentiation of BM-MSCs in adult marrow [226, 227]. ROS also affect MSC proliferation and differentiation, where regulated levels of ROS enhance the osteogenic differentiation of MSCs[194].

Motivation

In the field of tissue engineering and regenerative medicine, constant efforts have been made to design and develop functional nanostructured materials at the molecular level that possess specific bioactivity. One critical aspect of these materials is the bioactivity of metal ions, which play an essential role in various biological systems and cellular processes. This property makes metal ions highly relevant for applications in tissue engineering, where controlling cellular behaviour is paramount for successful tissue regeneration.

The primary goal of this study is to develop biomimetic surfaces that incorporate coordinated functional groups of polysaccharides with metal ions, thus allowing precise control over cell adhesion and growth. To achieve this, the layer-by-layer (LBL) assembly technique was employed to create multilayered films composed of two different polyanions. The first polyanion, hyaluronan, is known for its bioactive properties and its ability to interact with cells, making it a valuable component for promoting cellular adhesion. The second polyanion, alginate, does not inherently possess bioactivity or cell receptors but can still be used as a structural component in the multilayers. These polysaccharides were paired with the polycation chitosan, which is known for its biocompatibility and versatility in biomedical applications. Importantly, the multilayers of both systems [Chi/HA] and [Chi/Alg] were loaded with metal ions of different types and concentrations to explore their influence on the properties and bioactivity of the surface coatings. The study aims to investigate several key aspects of these multilayered systems. The first task of the study was to characterize the multilayers formation, effect of exposure PEM multilayers to metal ions on surface properties were studied in terms of wettability and surface charge. These properties are critical for influencing cellular interactions. Secondly, the biological response to multilayers of different metal ion concentrations was examined, with a focus on protein adsorption, cell adhesion, and proliferation. These are fundamental parameters for assessing the potential of the multilayers in tissue engineering applications. Finally, we studied the ability of these systems to induce adiopgenic and osteogenic differentiation of cell by gene expression analysis, immunofluorescence (IF) staining, and histochemical and fluorescence assays. Overall, the different approaches of biomaterial coatings showed promising outcomes for developing multifunctional surface coatings for implant surfaces and tissue engineering scaffolds. The results are reported herein.

Chapter 2: Materials and Methods

2.1. Materials

Table 1 shows the listing of reagents used in this work. Further, **Table 2** shows the list of antibodies and cell culture stains, while **Table 3** illustrates the prepared buffers and solution.

Table 1: Reagents used during the PhD work

Chemical reagents	Company	Lot-/Charge- No.	Specification
11-Mercaptoundecanoic acid (MUDA)	Sigma-Aldrich GmbH (Taufkirchen,Germany)	12103BE	95%
Antibiotic-antimycotic-solution (AAS)	Promocell, (Heidelberg, Germany Germany)	D09766P	
Acetic acid	Carl Roth GmbH + Co. KG (Karlsruhe, Germany)	15570541	
Ammonium hydroxide (NH4OH)	Carl Roth GmbH + Co.KG (Karlsruhe, Germany)	224214695	
β-Glycerophosphate	Alfa Aesar (Ward Hill, USA)	10170879	
Bovine serum albumin (BSA)	Carl Roth GmbH + Co.KG (Karlsruhe, Germany)	067254757	
Chitosan	Heppe Medical Chitosan GmbH (Halle, Germany)	212-270312-01	85/500
Calcium chloride dihydrate	Carl Roth GmbH + Co.KG (Karlsruhe, Germany)	01888370	≥99%
Cobalt chloride hexahydrate	Carl Roth GmbH + Co.KG (Karlsruhe, Germany)	245230236	≥99%
Copper (II) chloride dihydrate	Carl Roth GmbH + Co.KG (Karlsruhe, Germany)	375234053	≥99%
Dexamethasone	Sigma-Aldrich GmbH (Taufkirchen,Germany)	BCBCN3450V	
Dimethylsulfoxide (DMSO)	Sigma-Aldrich GmbH (Taufkirchen,Germany)	BCBK5723V	
Dulbecco's Modified Eagle's Medium (DMEM)	Sigma-Aldrich GmbH (Taufkirchen,Germany)	0000541112	1g/L glucose
Eagle's Basal Medium (EBM)	Sigma-Aldrich GmbH (Taufkirchen,Germany)	SLBL3380V	
Ethanol absolute	AppliChem Panreac ITW Companies (Darmstadt, Germany)	9N011428	≥99.8%
Fetal bovine serum (FBS)	Biochrom AG (Berlin, Germany)	0429B	
Hyaluronic acid sodium salt from Streptococcus equi	Sigma-Aldrich GmbH (Taufkirchen,Germany)	BCBR8383V	
Hydrogen peroxide (H_2O_2)	Carl Roth GmbH + Co.KG (Karlsruhe, Germany)	04524423	

Iron (III) chloride hexahydrate	Carl Roth GmbH + Co.KG (Karlsruhe, Germany)	206239044	≥99%
Isopropanol	Carl Roth GmbH + Co.KG (Karlsruhe, Germany)	242185327WW	
L-Ascorbic acid2*phosphate sesquimagnesium salt hydrate	Sigma-Aldrich GmbH (Taufkirchen,Germany)	SLBH6695V	
Mowiol 4-88	Calbiochem (Darmstadt, Germany)	475904/ B73224	
Oil Red	Sigma-Aldrich GmbH (Taufkirchen,Germany)	046K0666	
Paraformaldehyde	Sigma-Aldrich GmbH (Taufkirchen, Germany)	021305090	4%
Bicinchoninic acid assay (BCA)	Pierce, ThermoFisher Scientific, Germany	TF268879	
QBlue® viability test	BioChain (Newark,CA, USA).	B802107	
Sodium Alginic acid (low viscosity)	Alfa Aesar (ThermoFisher Kandel GmbH) (Kandel; Germany)	Z01B005 / W21E046	
Sodium chloride (NaCl)	Carl Roth GmbH + Co.KG (Karlsruhe, Germany)	339109045	≥99.5%
Triton X-100	Sigma-Aldrich GmbH (Taufkirchen,Germany)	084K0027	
Trypsin/EDTA	Biochrom AG (Berlin, Germany)	12143	0.25%/0.02%

Table 2: Antibodies and cell structures stains

Antibodies	Company	Lot-No.	Specification	Dilution
Primary antibodies				
monoclonal mouse anti-Vinculin IgG	Santacruz Biotechnology	047m4764V	hVIN-1 monoclonal mouse	1:50
CD44	Dianova, Hamburg, Germany		Mouse monoclonal	
Perilipin (G-2)	SC-Biotechnology, Germany	D2214	Rabbit monoclonal	1:100
Osteocalcin (F1-100)	SC-Biotechnology, Germany	E3013	Rabbit polyclonal	1:100
Col 1 A2 (H-9)	SC-Biotechnolog, Germany y	G0312	Mouse monoclonal	1:100
Glut4 (H-61)	SC-Biotechnology, Germany	A3114	Mouse polyclonal	1:100

osteocalcin	SC-Biotechnology, Germany		Rabbit polyclonal	1:100
Secondary antibodies				
Cy2-conjugated IgG	Jackson immune research,Germany	121076	Goat anti-mouse	1:100
Cy3-conjugated IgG	Jackson immune research, Germany	96173	Goat anti-rabbit	
BODIPY® 558⁄568 Phalloidin	Invitrogen, Germany	25710W		1:1000
TO-PRO®-3 Iodide (642⁄661)	Invitrogen, Germany	612354		1:500
All primary and secondary antibodies were diluted in 1% BSA to reduce unspecific binding and the background.				

Table 3: Buffers and media composition

Buffers and solutions	**Chemical composition**	
0.1% Triton X-100	0.1% (v/v) Triton X-100 dissolved in PBS	
1% BSA	1% (w/v) BSA dissolved in PBS	
Phosphate buffered saline (PBS)	2.7 mM KCl, 137 mM NaCl, 1.4 mM KH2PO4, 4.3 mM Na2HPO4, pH 7.4	
RCA clean	H_2O : NH_4OH : H_2O_2 = 5:1:1 (80°C)	
Dexamethasone 510 µM	Dexamethasone dissolved in ethanol and diluted in DMEM.	
L-Ascorbic acid-2-phosphate 50 mg/mL	L-Ascorbic acid dissolved in DMEM	
Mowiol	20 g Mowiol dissolved in 80 mL PBS and 40 mL glycerol	
β-Glycerophosphate 1 M	β -Glycerophosphate dissolved in PBS	
Eagle's Basal Medium (EBM)	without FBS	2 mM L-glutamine, 1.5 g/L sodium bicarbonate, Earle's salts
	With FBS	additionally, 10% of FBS
Dulbecco's modified Eagle's medium (DMEM)	without FCS	Low glucose concentration 1 g/L glucose, 1% AAS, without sodium pyruvate
	with FCS	additional, 10% of FCS

Table 4: List of equipments used.

Equipment	**Company**
Centrifuge (HERMLE Z 400 K)	Hermle Labortechnik GmbH (Wehingen)
CO2 Air-Jacketed Incubator	NUAIRE (Minnesota)
Confocal laser scanning microscopy, CLSM 710	Carl Zeiss Micro-Imaging GmbH, Jena, Germany
plate reader	FLUOstar, BMG LabTech, Germany
UV chamber	(Bio-Link BLX, LTF Labortechnik, Germany)

2.2. Methods

2.2.1 Surface cleaning

The substrates used for the experimental procedures were standard round glass coverslips Ø 12 mm for use in 24 multi-well plates, and (10*20) mm^2 for the flow chamber used in zeta potential measurements (Menzel GmbH, Bielefeld, Germany). 150 mm silicon wafers (Si-Mat, Kaufering, Germany) were cut to the desired size (10X10) mm^2 and (37X17) mm^2 for ellipsometry measurements. They were cleaned according to Radio Corporation of America (RCA-1) protocol to remove organic residues from the silicon wafers [228]. The procedure uses a solution of ammonia 25%, hydrogen peroxide 35%, and water (1:1:5, v/v/v). First, water and ammonia solution were mixed and heated to 75 - 80°C. Hydrogen peroxide was added to the solution while turning off the heater. All samples were immersed for 15 min in this solution, washed with ultrapure water six times for 5 min each, dried with a stream of nitrogen, and used immediately for further deposition of multilayers.

2.2.2 Polyelectrolyte multilayer (PEM) formation

The PEM was built up based on the alternating adsorption of chitosan (Chi) as polycation and alginate (Alg) or hyaluronic acid (HA) as polyanion, to achieve a total number of 10 layers with Alg or HA as a terminal layer $[Chi/Alg]_5$ and $[Chi/HA]_5$. Further PEMs formation was performed at pH 4 to allow ion pairing interaction between the positively charged amino group of Chi and the negatively charged carboxyl group of Alg or HA [126, 229].

All polyelectrolytes (PEL) were dissolved in 150 mM NaCl, and the pH was adjusted to pH 4.0 by addition of 0.1 M HCl. The cleaned samples were first coated with a Chi layer (1 mg/mL) at room temperature (RT) for 15 min while gently shaking, followed by three times rinsing with a solution of sodium chloride (150 mM, pH 4.0) for 5 min. After that, the samples were alternately incubated in Alg or HA solutions with 1 mg/mL for 15 min to achieve 10 layers. Excess PEL solution was removed by rinsing with NaCl solution (150 mM, pH 4.0) thrice for 5 min after each layer. Afterwards, the multilayers were placed in metal ion solutions (Ca^{2+}, Co^{2+}, Cu^{2+}, and Fe^{3+}) of different concentrations (5, 10, and 50 mM) for 15 min followed by three times rinsing with 150 mM NaCl for 5 min each. The resulting multilayers were then denominated as $[Chi/Alg]_5$ or [Chi/HA]5 -Me;C, where Me stands for the type of metal ion and the subscript C for its concentration.

2.2.3 Freestanding film formation

The freestanding multilayer films of $[Chi/Alg]_{100}$ and $[Chi/HA]_{100}$ were fabricated using the LbL method. Films containing 100 bilayers of (2 mg/ mL) chitosan and (5 mg/ mL) alginate (/

hyaluronic acid were fabricated using an automated dip coating device (DR01, Riegler & Kirstein, Berlin, Germany). The freestanding films Chi/HA were assembled on poly(propylene), (Thermhex Waben GmbH, Halle, Germany) to permit the fabrication and detachment of films. At the same time, glass slides (Thermo Scientific, Hungary) were used as substrates to fabricate the Chi/Alg. The coating duration for each polyelectrolyte was 5 min with a 2.5 min washing step between each coating. Dip coating was performed at room temperature with a dipping speed of 0.8 cm/s. After all the coating cycles, the films of $[Chi/Alg]_{100}$ and $[Chi/HA]_{100}$ were carefully detached from the substrates with the help of a spatula and forceps. Afterwards, the films were cut into circular disks of 12 mm diameter and placed inside 24-well plates. The films were incubated with metal ions solutions at the highest concentration (Cu^{2+}, Co^{2+}, Ca^{2+}, and Fe^{3+}). After 30 min incubation, the films were rinsed thrice with 0.15 M (NaCl) for 5 min each. (**Figure 2.1**).

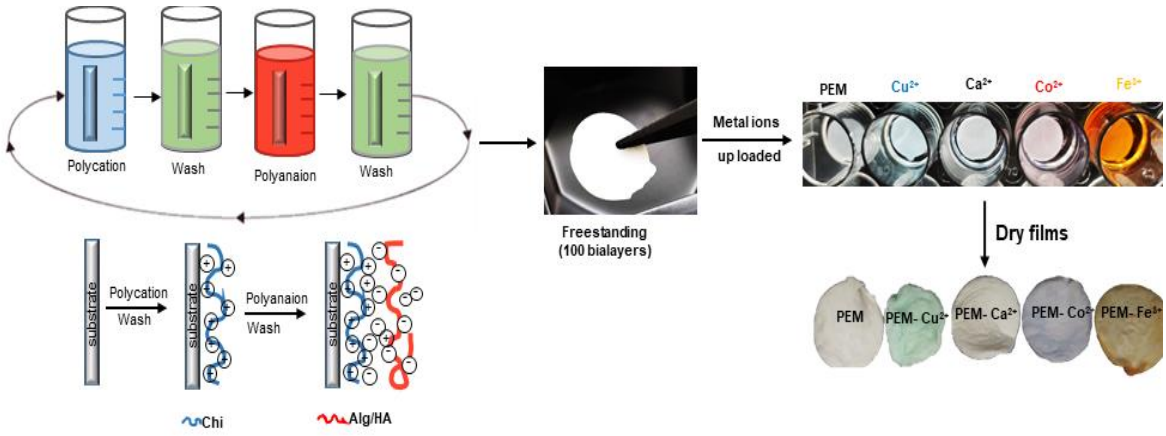

Figure 2.1*:* Illustration of freestanding multilayer film preparation, doping with a high concentration of 50mM of Ca^{2+}, Co^{2+}, Cu^{2+} and 10mM Fe^{3+}, and dry films appearing stained by metal ions

2.3 Characterization of physical properties of multilayers anduptake of metal ions

2.3.1 Surface plasmon resonance (SPR)

The layer growth and PEMs multilayer formation were investigated by IBIS-iSPR equipment (IBIS Technologies B.V., Enschede, Netherlands). Polarized light is reflected through a hemispheric prism with a refractive index of n = 1.518 onto a gold-coated sensor (IBIS Technologies B.V., Enschede, The Netherlands). A shift in the angle (m°) is observed upon the binding of molecules at the gold–liquid interface of the gold coating sensor due to the change of refractive index [230]. Before measurements, the gold sensor was coated with 11-mercaptoundecanoic acid (MUDA) and placed into the iSPR flow cell, which was equilibrated with 0.15M sodium chloride pH 4.0 to establish a stable baseline. The solutions were injected

at a flow rate of 3µL/s at 25 °C, then washed with NaCl three times for 5 min, followed by polycation (Chi) for 15 min, and polyanion (Alg or HA) was injected for 15 min. PEM formation was continued until ten single layers were formed. After each rinsing step, the average angle shift values (m°) were used to plot the graphs.

2.3.2 Ellipsometry

Ellipsometry is an optical technique widely used in biomaterials to measure the change in the film thickness and refractive index (RI) at the interface. This technique is susceptible to changes in the polarization state of an elliptically polarized light beam reflected by the interface [231]. This study determined the thickness of PEM formation with a J. A. Woollam Co, Lincoln, NE, USA device provided with WVase32 software. The film thickness and refractive index were measured under dry and wet conditions. For the measurement in dry states, the PEM were assembled on a silicon wafer (10x10mm²) in vitro and dried with a stream of nitrogen. Following that, the samples were placed in device and scanned with angles 65°, 70°, 80°, and 85° within the wavelength range of λ = 375-1000 nm. Data were obtained from five different spot points on each sample, using three separate samples. The refractive index (RI) of 1.4 was used in all samples because it is recommended for such native polysaccharides surface [232]. For the wet conditions, the formation of PEMs and the measurment of film thickness was performed in situ, where the silicon wafer (37X17 mm^2) was mounted to ellipsometer stage and fixed with 500µL liquid cells with a static scanning angle of 70°. Polyelectrolytes (Chi and Alg/HA) were injected into the sample and allowed to interact with the surface at RT for 15 min. The polyelectrolyte solution was removed and exchanged by washing with NaCl solution (150 mM, pH 4.0) thrice for 5 min after each layer. A single scan was achieved to obtain the final thickness. The thickness of the PEMs was obtained by fitting the experimental data to an additional Cauchy layer for the optical properties of the polymer film: $n(\lambda) = A_n + B_n/\lambda^2 + C_n/\lambda^4$. Here, negligible B_n and C_n were considered to be zero. Measurements were performed three times, and means, and standard deviation were calculated.

2.3.3 Inductively coupled plasma mass spectrometry (ICP-MS) analysis

ICP-MS analysis was used to measure the amount of metals in multilayers; the wafers/glasses coated with plain multilayer and doped with metal ions subsequently were immersed in concentrated 67% (w/v) nitric acid HNO3 (trace metal grade; Normatom/ ProLabo) at 70 °C for 2 h. The samples were diluted to a final concentration of 5–6% (w/v) in nitric acid. Indium and germanium were added as internal standards at a final concentration of 2/20 ppb and 5% isopropanol. Elemental analysis was performed via inductively-coupled plasma mass spectrometry (ICP-MS) using a Cetac ASX-560 (Teledyne, Cetac Technologies, Omaha

USA), a Micro Flow PFA-200 nebulizer and an iCAP-RQ ICP-MS instrument (Thermo Fisher Scientific, Bremen) operating with a collision/reaction cell and flow rates of 5 mL min^{-1} of He/H2 (93%/7% [13,3: 1]), with an Ar (4.8) carrier flow rate of 0.72 L min^{-1} and an Ar (4.8)-plasma makeup flow rate of 15 L min^{-1}. Data acquisition for each sample was made in triplicate using Qtegra Version 2.10.3324.83 software (Thermo Fisher Scientific). An external calibration curve was recorded with ICP-multielement standard solution XVI (Merck) or ICP-single-element standards (Merck/PerkinElmer) in 5% nitric acid. The sample was introduced via a peristaltic pump and analysed for calcium (Ca43), iron (Fe56), cobalt (Co59), copper (Cu63) and other element contaminations in triplicates for blank measurement and quality/quantity threshold calculations based on clean substances (glass) and plain multilayers were used. The results were transformed from ppb sample volume-dependent into ng metal per area (cm^2). The results are given in mass per area [ng /cm^2] and molarity [µM] are based on a surface area of 1.131 cm^2 by 12 mm diameter, volume of 2.26 x 10^{-9} L by 21 and 18 nm thickness of hydrated [Chi/Alg] and [Chi/HA] multilayers respectively, and the molecular mass of each element.

2.3.4 Fourier-transform infrared (FTIR) spectroscopy

The native polysaccharides and freestanding films contained 100 bilayers of [Chi/Alg], and [Chi/HA] doped with metal ions (at highest concentrations) were scanned by Fourier transform infrared (FTIR) spectroscopy (IFS 28, Bruker, Germany) after freeze-drying of the PEMs films. The scanned measurement of samples was 24 times and collected over the range of (4000–400 cm^{-1}) with a resolution of 4 cm^{-1}.

2.3.5 Water contact angle (WCA) measurements

The contact angle is a quantitative measure of the wetting of a solid by a liquid. It is the angle liquid forms at the three-phase boundary where a liquid, gas (usually air), and solid intersect. Here, the sessile drop method determines the static water contact angle (WCA) of the wettability of multilayer surfaces. Decrease of wettability, resulting in a higher WCA and, thus, higher interfacial energy, which is related to a lower surface free energy and vice versa [233]. The static water contact angle was measured with the OCA15+ system (Dataphysics, Filderstadt, Germany). The experiments were conducted by placing five water droplets on each sample. The device dispensed 5 µL of fresh ultrapure water with a flow rate of 0.5 µL /s. The software of the OCA15+ device recorded at least 10 independent measurements for each droplet. The data were used to calculate the means and standard deviations.

2.3.6 Zeta potential measurements

Zeta (ζ) potential measurements are widely used to study materials' colloidal stability and surface charge by recording the electrokinetic potential, such as electrophoresis and streaming potential [234]. This study measured the zeta potential with a SurPASS Electrokinetic Analyzer (Anton Paar, Graz, Austria). Specially manufactured glass coverslips with a size of 10X20 mm^2 were modified with multilayer formation done by dip-coating before the zeta potential studies, according to the protocol described in **Section 2.2.2**. The modified coverslip was mounted on the gap flow cell with double-sided tape. The gap was adjusted manually to achieve a flow rate of 100–150 $mL \cdot min^{-1}$ at a maximum overpressure of 300 mbar. 1mM KC solution was used as model electrolyte. The pH titration solution from 2.5 to 10.0 (acid-based pH) was adjusted using 1 M sodium hydroxide (NaOH). Then the measurement was carried out by an automated titration program using titration steps of 0.25µL from pH 10.0 to 2.5 pH. The ζ - the potential was determined using the streaming current and calculated.

2.3.7 Atomic force microscopy and nanoindentation

AFM is a scanning probe microscopy with a high resolution, which can be applied to analyze in situ dry or hydrated samples. The surface morphology of PEMs was investigated with atomic force microscopy (AFM), where the program Nanowizards IV (JPK/Bruker, Berlin, Germany) was used to determine topography in ambient air using fast nanoindentation (Quantitative Imagingt- Mode), and mechanical properties in intermittent contact mode in a standard liquid cell (JPK/Bruker) with 150 mM NaCl (pH 4). Force-constant calibration was carried out by the thermal noise method [235]. Here the force map of an area of 2.5 X 2.5 μm^2 was recorded for each sample with a resolution of 512 X 512 $pixel^2$ to represent the morphological nature of the layers as well as the elastic modulus. The AFM probe tip was verified twice using scanning electron microscopy to measure the radius of the indenter and prove the tip geometry consistency after completing all measurements. After the processing procedure, Young's moduli were calculated from the indentation curves using the advanced Hertzian model [236]. JPK Data of Processing V5.0.85 and Gwyddion V2.49 software were utilized for data post-processing and elastic modulus analysis.

2.4 Biological studies

2.4.1 Serum protein adsorption measurements

The capability of the PEMs to bind serum proteins was quantified using a bicinchoninic acid assay (BCA). The PEMs were fabricated in 96-well plates (Greiner Bio-One), as described in **Section 2.2.2.** After that, 250 mL of Eagle's Basal Medium (EBM) supplemented with 10% fetal bovine serum was added to the PEM, which were then incubated at 37°C for 4 h. After

incubation, the medium was aspirated, and the wells were washed twice with (PBS) phosphate buffered saline pH 7.4. Subsequently, 250 mL of working reagent of the BCA protein assay was added to each well and allowed to react at 37 °C for 30 min. Then 225µl supernatant of each well was collected and transferred into a new 96-well plate (Greiner). The absorbance was measured at 562 nm with a plate reader (FLUOstar, BMG LabTech, Ortenberg, Germany). Bovine serum albumin (BSA) was employed to create a calibration curve for calculating the amount of adsorbed serum protein.

2.4.2 Cell culture conditions

C3H10T1/2 embryonic mouse fibroblasts (clone 8) cells with multipotent properties were used in this study to investigate the effect of plain and metal ion doped PEMs multilayers on cellular processes such as adhesion, proliferation and differentiation. The cells were cultured in Eagle's Basal medium (EBM) supplemented with 2 mM L-glutamine, 1.5 g L^{-1} sodium bicarbonate, Earle's salts, 10% fetal bovine serum (FBS) and 1% penicillin/streptomycin (pen/strep, Promocell, Germany) at 37°C in a humidified 5% CO2/95% air atmosphere using a NUAIRE® DH Autoflow incubator (NuAire Corp., Plymouth, USA). Cells at 80% confluent cultures were washed with phosphate buffer (PBS) at 7.4 pH. Subsequently, the cells were incubated with 0.25% trypsin/ 0.02% ethylenediaminetetraacetic acid (EDTA) at 37°C for 5 min. Detached cells were observed with a bright field microscope, and trypsinization was stopped by adding EBM containing 10% FBS. The cell suspension was collected and centrifuged at 250xg for 5 min. After removing the supernatant, the cell pellet was resuspended in fresh culture medium and then seeded on PEM at different concentrations, depending on the assay.

The adhesion of cells was investigated on glass slides coated with plain [Chi/Alg] and [Chi/HA] multilayers or those doped with Ca^{2+}, Co^{2+}, Cu^{2+} and Fe^{3+} solutions of different concentrations (5, 10, 50 mM). The C3H10T1/2 cells cultured in the presence of 10% FBS in EBM were placed into 24 well plates at a density of $5x10^4$ cells.mL^{-1} at 37 °C in a humidified 5% CO2/95% air atmosphere for 4h. Then adherent cells were carefully rinsed once with pre-warmed PBS pH 7.4 to remove non–adherent cells. Subsequently, the remaining cells were fixed using 4% paraformaldehyde solution pH 7.4 at room temperature for 15 min and washed with PBS three times. After fixation, cells were permeabilized with 0.1% (v/v) triton X-100 for 10 min, and again the samples were rinsed twice with PBS. Nonspecific binding sites were blocked by incubation with 1% bovine serum albumin (BSA) solution in PBS at RT for 1 h. The focal adhesion complex was visualized with a primary mouse antibody raised against vinculin (1:50, v/v). In chapter 4, CD44, the surface receptor of HA was stained by incubation with a mouse monoclonal antibody raised against CD44 (Dianova, Hamburg, Germany). Specific monoclonal antibody binding was detected by incubation with a goat Cy2-conjugated anti-

mouse secondary antibody (1: 100). Actin cytoskeleton was visualized by incubating the samples with BODIPY® phalloidin (1:1000, v/v). Cell nuclei were visualized with TO-PRO®3 staining (1:500, v/v). Cells were incubated with each dye and antibody at room temperature for 30 min, followed by extensive washing with PBS three times and with ultrapure water after the last washing to avoid salt crystal formation. Finally, all samples were mounted on glass object holders using Mowiol 4-88. Samples were stored at +4°C and later examined with a confocal laser scanning microscope (CLSM 710, Carl Zeiss Micro-Imaging GmbH, Jena, Germany) equipped with 10X, 20X, and oil immersion 63X objective lenses. At least five images per sample with low magnification objectives (10X) were used to determine cell count and higher magnification objectives (20x, 63x oil immersion) for cell area measurements and focal adhesion visualisation, actin and nuclei. The images were processed with ZEN2012 software (Carl Zeiss). Image analysis by use of software ImageJ (version 1.46r) was applied to obtain cell count and area.

2.4.3 Cell proliferation studies

The cell growth was measured using a non-toxic QBlue® assay that estimates the metabolic activity of cells. The PEMs were fabricated in 96-well tissue culture. The samples were sterilized in an ultraviolet light (UV) chamber (Bio-Link BLX, LTF Labortechnik, Germany) at 254 nm (50 J cm^{-1}) for 30 min. Cells were seeded at a density 50.000 cells.mL^{-1} in EBS with10% FBS and incubated at 37°C / 5% CO_2 for 24 and 72h. The EBM medium was carefully removed and the samples were washed with sterile PBS once. Then 200µL of pre-warmed EBM containing the QBlue® reagent (ratio 1:10) was added, and the cells were incubated at 37°C for 3 h. The QBlue cell viability assay is based on reducing a non-fluorescent reagent (resazurin) into a highly fluorescent product (resorufin) by metabolically active cells. Therefore, only living cells can readily reduce this non-toxic reagent's increasing fluorescent intensity. The fluorescence intensity represents viable cells only and can be determined by a plate reader. Thus, 100 µL was collected from each sample and transferred to a black 96-well plate (Greiner Bio-one, Germany). The fluorescence intensity of viable cells was measured using a plate reader at an excitation wavelength of 544 nm and an emission wavelength of 590 nm (FLUOstar, OPTIMA, BMG LabTech, Offenburg, Germany). The EBM/QBlue solution without cell contact was used as a blank. The cell morphology and proliferation were visualized using phase contrast microscopy and an Axiovert 100 equipped with a CCD camera (AVT HORN) from Carl Zeiss Meditec GmbH (Oberkochen, Germany).

2.4.4 Cell differentiation studies

C3H10T1/2 cells were obtained from American Type culture Collection (ATCC; LGC Promochem, Molsheim, France) seeded on plain polyelectrolyte multilayers (PEMs) and

doped with a high concentrations of metal ions on the differentiation and cultured in Dulbecco's Modified Eagle's Medium (DMEM low-glucose concentration) supplemented with 10% FBS and 1% pen/strep at a density of 50.000 cells.mL^{-1} for 48 h to obtain a certain degree of confluence. After that, the samples and negative control was incubated with DMEM medium supplemented with 10% FBS and 1% pen/strep (***basal medium)***. In contrast, the cells were cultured in the presence of adipogenic or osteogenic medium as a positive control. The media composition is shown in **Table.5**. Cells were incubated at 37°C in a humidified 5% CO2/ 95% air atmosphere for three weeks, while the medium was changed twice weekly.

Table 5: Composition of different induction media used in differentiation study

	DMEM medium (Basal medium)	**Adipogenic medium**	**Osteogenic medium**
Pen/Strep	1%	-	-
FBS	10%	10%	10%
Dexamethasone	-	1µM	10nM
Ascorbic acid	-	-	0.2mM
β-glycerol phosphate	-	-	7mM
All components were dissolved in DMEM medium.			

2.4.4.1 Adipogenic differentiation

The adipogenic investigation of C3H10T1/2 cells was determined by histochemical staining of cells with oil red to evaluate the formation of fats vacuoles in the cytoplasm. Oil red stock solution was prepared by dissolving oil red powder in isopropanol to achieve a concentration of 0.5% (w/v) by heating. Subsequently, the solution was filtered with filter paper and stored at RT overnight. Then, the solution was filtered again with filter paper. Oil red working solution was prepared by diluting the stock solution with PBS pH 7.4 at a ratio of 3:2. A final filtration step with a 0.2 µm syringe filter is necessary before use to remove any particulate matter that may interfere with the staining process or cause artifacts in the analysis. Cells were rinsed and fixed as described earlier in the thesis (refer to paragraph 2.4.2). After fixation, cells were incubated in the dark with the oil-red working solution for 30 min. Thereafter, the cells were rinsed with ultrapure water three times and dried in the air before imaging. The cells were analyzed using the Axiovert 100 microscope (Car Zeiss, Oberkochen, Germany) equipped with a CCD camera.

Additionally, glucose transporter 4 (GLUT4) and perilipin as specific adipogenic differentiation markers were immunohistochemically stained using specific antibodies. GLUT4 is a sugar transporter protein abundant in adipocytes [237]. Perilipin is a protein crucial in modulating

adipocyte lipid metabolism. It is present many on the surface of lipid vacuoles, where is responsible for lipid storage [238]. The primary monoclonal antibodies were detected using fluorescently labelled secondary antibodies (CY2 for perilipin and CY3 for GLUT4, respectively). The actin cytoskeleton was visualized by incubating with BODIPY® -phalloidin. After a single wash once with ultrapure water, the samples were mounted onto object holders using Mowiol 4-88 mounting media.The cells were later examined with confocal laser scanning microscopy (CLSM) using a 40x oil immersion objective.

2.4.4.2 Osteogenic differentiation

The osteogenic investigation of the C3H10T1/2 on plain PEMs and metal ions doped PEMs with both basal, osteogenic medium was determined histochemical, and immunocytochemically stained for specific osteogenic markers. The deposition of calcium phosphate as an indicator of osteogenic differentiation of C3H10T1/2 cells was studied. The cells were stained with alizarin red-S solution to investigate the emergence of a mineralized matrix. Alizarin red (20 mg mL^{-1}) was prepared by dissolving alizarin red in distilled water and adjusting pH to 4.1–4.3 with 0.5% ammonia. The solution was filtered to discard any precipitations. Subsequently, the cells were washed once with PBS pH 7.4 and then fixed with 4% paraformaldehyde solution for 15min. After fixation, the cells were washed twice with distilled water, and then the cells were stained with Alizarin red S and incubated at RT in the dark for 45 min. Unspecific binding was excluded by washing cells with distilled water. The image cells were taken in transmission mode Axiovert 100 microscope equipped with a CCD camera. The osteogenic differentiation was further determined by immunohistochemically staining for specific markers of osteogenesis (collagen I and osteocalcin). The cells were rinsed with PBS and fixed as described in (section 2.4.2). For visualization of osteogenic markers, the cells were incubated with primary monoclonal antibodies raised against collagen I (mouse) and osteocalcin (rabbit) (1: 100) and conjugated secondary anti-mouse (CY2) and anti-rabbit (CY3) antibodies. The samples were studied and photographed with confocal laser scanning microscopy (CLSM 710) using a 40x oil immersion objective.

2.4.4.3 RNA extraction and Real-Time PT-PCR

C3H10T1/2 cells were seeded on plain [Chi/Alg], [Chi/HA] and doped metal ions PEMs and cultured in Dulbecco's Modified Eagle's Medium (DMEM; low-glucose concentration) (Sigma-Aldrich, Germany) supplemented with 10% FCS and 1% pen/strep at a density of $1x10^5$ cells mL^{-1} for 48 h. The composition of the media was the same as described above in **Table.6**. The cells estimate the osteogenic differentiation through culture for 14 days. During the

incubation time, the medium was changed twice per week. The RNA was extracted from samples using the Aurum Total RNA Mini Kit spin columns from BioRad (Hercules, CA, USA) according to the manufacturer's recommended procedure. First-strand cDNA was synthesized using an iScript Advanced cDNA Synthesis Kit for RT-qPCR (Biorad, Hercules, CA, USA) in 20 µL reactions, according to the manufacturer's instructions. RT-qPCR was carried out under standard enzyme and cycling conditions on a CFX Connect Real-Time PCR Detection System (Biorad, Hercules, CA, USA). Primer sets were pre-validated by Prime PCR Probe Assays from Biorad (Hercules, CA, USA) for osteogenic genes (ALP, RUNX2, Noggin, and Osterix). In addition, the housekeeping gene RPLP0 was used (see **Table.6**). Data were analysed using the BioRad CFX Manager Software 3.0 (Hercules, CA, USA). The conditions of real-time PCR were as follows: 95°C for 30 s followed by 39 cycles at 95°C for 15 s and 60°C for 30 s. The relative expression levels for each gene were calculated and normalized to the housekeeping gene RPLP0 by the DDCt method ($2^{-\Delta\Delta C_t}$).

Table 6: Primers of target and housekeeping genes for qRT-PCR

Symbol	Name	Assay ID
Osteoblast		
ALP	Alkaline phosphatase	qMmuCEP0027961
RUNX2	Runt-related transcription Factor-2	qMmuCEP0057696
NOG	Noggin	qMmuCEP0058332
SP7	Osterix	qMmuCEP0042201
Housekeeping gene RPLP0	60S acidic ribosomal protein P0	qMmuCEP0042968

Statistics

All statistical analysis was performed using Origin 8 software as means values and standard deviations (SD). A one-way ANOVA followed by a post-Tukey's test was carried out to evaluate the statistical significance of results for $p \leq 0.05$, which is labelled by an asterisk in the respective figures. Furthermore, the box whisker diagrams are shown where appropriate. The box indicates the 25th and 75th percentiles, the median (dash) and means values (black square), respectively, whereas the 95-5% confidence interval is represented by the whiskers.

3. Chapter 3: Results '' Effect of metal ions on physical properties of multilayers formation composed of alginate (Alg) and chitosan (Chi), and cell behaviour''

3.1. Characterization of multilayers formation and metal ions uptake

The physical characterization and surface properties of [Chi/Alg] multilayers were investigated by various methods. Moreover, the effect of doping [Chi/Alg] multilayers to metal ions on their physicochemical properties was studied to understand their influence on the behaviour of cells. The surface plasmon resonance (SPR) was used to investigate the multilayer growth of [Chi/Alg] (**Figure 3.1**). The deposition of the layers shows the exponential growth behaviour of the PEM system. The increase in the angle shift (m°) with the addition of each layer of polyelectrolytes is related to the increase in layer thickness. Ellipsometry was used to study the thickness of PEM (**Figure 3.1 b**), both in dry and hydrated states. The results of the ellipsometry measurements indicate that the adsorption equilibrium is reached rather quickly and suggests the exponential growth of layers, where the curve of layers growth were fitted as exponential and noted r square is 0.999. The multilayer thickness in the wet state is higher compared to the dry state is approximately 21 nm and 10 nm, respectively (see **Figure A.1a**). The observed increases in angle shifts are attributed to the increased layer thickness, exhibiting exponential growth corresponding to results from other studies [239].

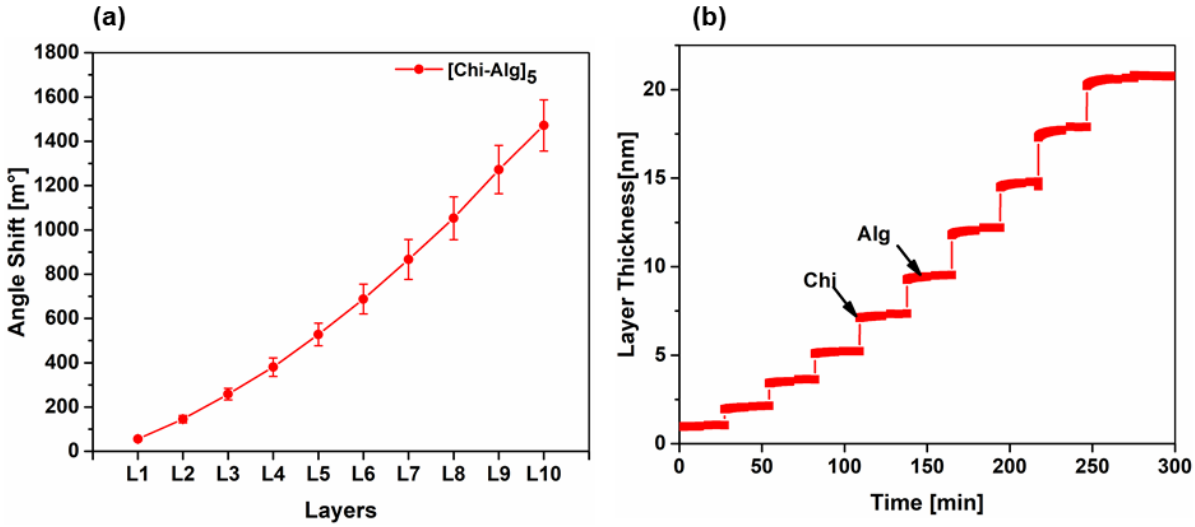

Figure 3. 1: (A) Multilayer growth of [Chi/Alg] measured by surface plasmon resonance angle shifts from the 1st to 10th layer. Odd layers: chitosan; even layers: alginate. **(B)** The wet thickness of the PEM system was measured by ellipsometry under dynamic conditions in a flow chamber. Results are given as means ± SD (n=3).

The quantity of metal ions incorporated into multilayers was determined using the ICP-MS technique's elemental analysis. For this purpose, the 5-bilayers Chi/Alg were used for loading 50 mM of Ca^{2+}, Co^{2+}, Cu^{2+} and 10 mM of Fe^{3+}, respectively. At the same time, the amount of metal ions was normalized to a plain multilayer. **Table 7** shows high concentrations of Fe^{3+} and Ca^{2+}, followed by lower concentrations of Cu^{2+} and Co^{2+}.

Table 7: Amounts of metal ions in $[Chi/Alg]_5$ multilayers prepared on glass. Results represent means ± deviation, n = 4.

Quantity of metal ions in multilayers	**$[Chi/Alg]_5 Ca^{2+}$**	**$[Chi/Alg]_5 Co^{2+}$**	**$[Chi/Alg]_5 Cu^{2+}$**	**$[Chi/Alg]_5 Fe^{3+}$**
[µM]	6.96 ± 0.47	0.041 ± 0.003	0.245 ± 0.040	8.71 ± 1.17
[ng / cm^2]	558.25 ± 37.70	4.89 ± 0.32	31.16 ± 5.08	972.36 ± 130.38

FTIR spectroscopy was used to investigate which the functional groups such as hydroxyl, carboxylic, amino groups of chitosan and alginate create ionic or coordinative bonds with the metal ions. The spectra of pure chitosan (Chi), alginate (Alg) and $[Chi/Alg]_{100,}$ prepared as freestanding films, were analyzed using FTIR spectroscopy. Moreover $[Chi/Alg]_{100}$ multilayers doped to the high concentration of metal ions were investigated.

The characteristic peaks of pure chitosan can be seen in **Figure 3.2 a.** The intense band was 3275 $cm^{-1,}$ and two weak bands appeared at 2881 and 2980 cm^{-1}. Then the absorption band of the amide I stretched at 1651 cm^{-1} as N–H deformations of a primary amine exhibited strong bands in the range of 1638-1575 cm^{-1}. Peaks at 1377 cm^{-1} and 1419 are associated with the stretching of C-N and deformation of C-H, respectively [97, 240]. The absorption bands at 1150 cm^{-1} of anti-symmetric stretching of the C-O-C bridge and C-N stretch and 1075 cm^{-1}, 1050 cm^{-1}, and 1030 cm^{-1} of skeletal vibrations involving the C-O stretching. **Figure 3.2 a** shows the spectrum of pure alginate (Alg) and the absorption bands related to hydroxyl or carboxylic groups at 3328 and 2980 cm^{-1}, respectively. The carboxylic (COOH) carbonyl group presented a strong, sharp band at 1592 cm^{-1} and a medium-sharp at 1404 cm^{-1}. Further, a small shoulder peak at 1722 cm^{-1}. The bands below 1320 cm^{-1} are attributed to the saccharide structure.

The spectra of $[Chi/Alg]_{100}$ multilayers films **Figure 3.2 b** presented the broadening of O-H and N-H stretching bonds at 3335 cm^{-1}The absorption band at 1600 cm^{-1} resulted from the overlap of -NH bending vibration of chitosan and carboxyl group asymmetric stretching vibration of alginate. The weak and moderate bands at 1600 and 1408 cm^{-1} can be related to the stretching

of COO- of the asymmetric and symmetric stretching of Alg molecules, respectively. The band at 1300 cm^{-1} is the skeletal vibration of alginate. In contrast, the bands at (950 and 1150 cm^{-1}) present sharp peaks of Chi and Alg saccharide rings, including symmetrical C-O-C stretching at 1078 cm^{-1} and skeletal vibration of C-O stretching at 1030 cm^{-1} [241].

Figure 3.2 b shows FTIR spectra of metal ions containing multilayers comparison to plain $[Chi/Alg]_{100}$,. It can be observed that there are only small differences., including a slight decrease in the intensity and the broad band at 3335 cm^{-1} (O–H and N–H stretching) in multilayers $[Chi/Alg]_{100}$ after doping to metal ions , as compared to plain $[Chi/Alg]_{100}$, while PEMs doping with Fe^{3+} led to increasing intensity broader peak than the plain Chi/Alg multilayers, could be related to residual water after drying of free-standing films. **Figure 3.2 c** shows an area of interest between 1200 and 1700 cm^{-1}. A slight shift of the bands to higher wavelengths is also observed in [Chi/Alg] multilayers containing the Ca^{2+} ions from the peaks 1408 cm^{-1} up to 1410 cm^{-1}. The band at 1600 cm^{-1} appears similar to the case of $[Chi/Alg]_{100}$ (**Figure 3.2 c**). However, a slight shift to a higher wavenumber is observed in the case of Cu^{2+} to 1606 cm^{-1}, indicating a redshift towards a longer wavelength. Conversely, the peak shows a slightly movement to lower wavenumber, specifically 1597cm^{-1} for Ca^{2+}, Co^{2+} and Fe^{3+} , suggesting a blue shift towards a shorter wavelength. The small peak at 1538 cm^{-1} became slightly wide with the addition of metal ions. A weaker intensity and slight movement to a higher/lower wavenumber in the range 1100 cm^{-1} and 1030 cm^{-1} peaks (C-O glycosidic bond) were observed for the Ca^{2+}, Co^{2+} and Cu^{2+} containing samples (**Figure3.2d**).

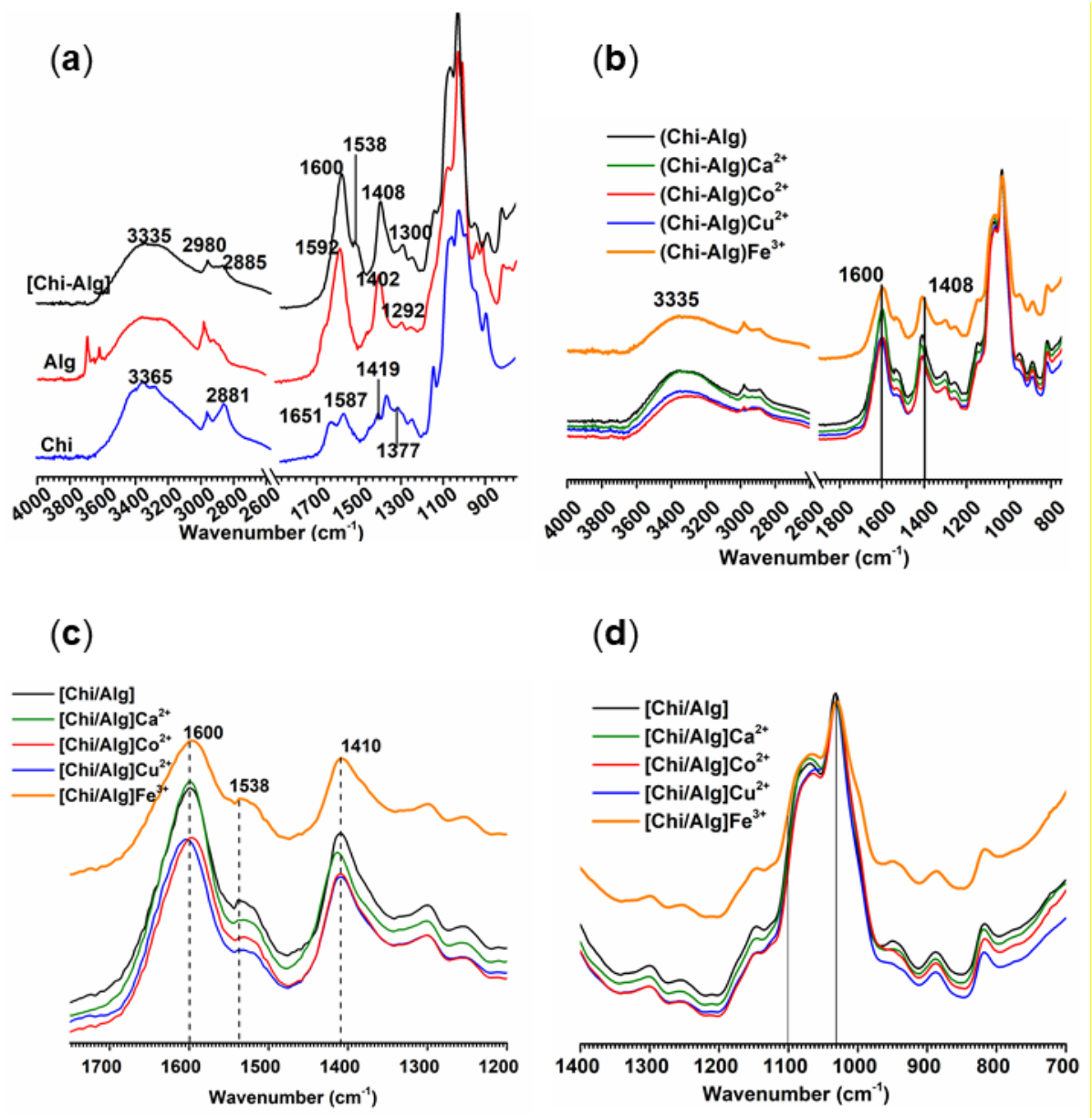

Figure 3. 2: (a) FTIR spectra of pure chitosan (Chi) and Alginic acid (Alg) as well plain multilayers $[Chi/Alg]_{100}$. **(b)** the spectra of multilayers doped with metal ions adding 50mM for Ca^{2+}, Co^{2+}, Cu^{2+} and 10Mm of Fe^{3+}. **(c)** FTIR spectra of the $[Chi/Alg]_{100}$-metal ions doped in the region of 1600–1400 cm^{-1}. **(d).** FTIR spectra $[Chi/Alg]_{100}$ doped with metal ions in the range of 1100-1030 cm^{-1}.

3.2 Physical properties of multilayers

3.2.1 Surface wettability

Figure 3.3 represents the determination of surface wettability of plain [Chi/Alg] and doped to metal ions. The plain PEM possesses a WCA of around 33°. A slight increase in WCA was seen after Ca^{2+}, Co^{2+}, and Cu^{2+} were added to [Chi/Alg] PEM. The WCA ranged between 33° to 42°. No difference in wettability was observed concerning the type and concentration of metal ions. The wettability of PEM treatment with 5 and 10 mM Co^{2+} and Cu^{2+} did not increase compared to the plain layer [Chi/Alg]. In contrast, the WCA significantly increased to around 82° in the multilayers containing a high concentration Fe^{3+}.

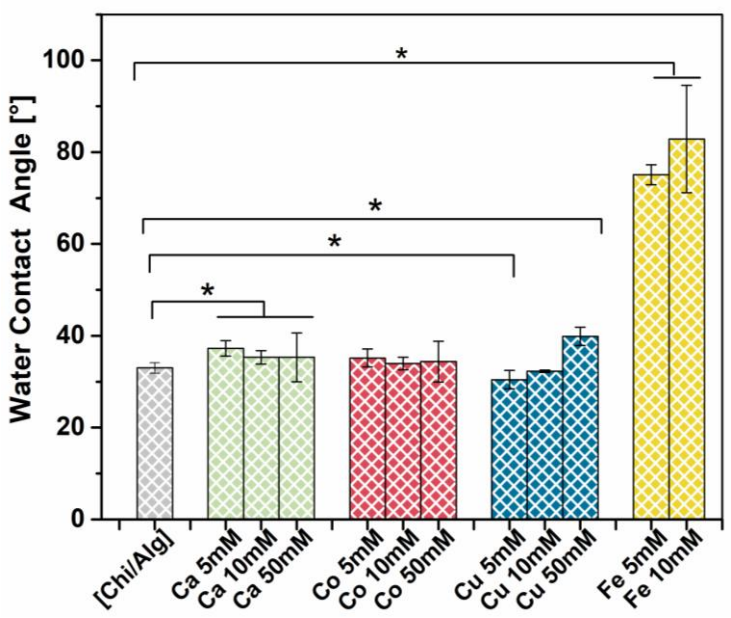

Figure 3.3: Static water contact angles (WCAs) of the plain $[Chi/Alg]_5$ and metal ion-doped PEM. [Metal ions used for doping PEM: **green** Ca^{2+}, **red** Co^{2+}, **blue** Cu^{2+}, and **yellow** Fe^{3+}. The results represent means ± SD (n = 12, *p < 0.05).

3.2.1 Zeta potential (ζ-potential)

The zeta potential measurements of plain PEM films and after exposure of [Chi/Alg] multilayers to metal ions high concentration (50mM of Ca^{2+}, Co^{2+}, Cu^{2+}, and 10mM of Fe^{3+}) are shown in **Figure 3.4.** The graph displays that the PEM with and without metal ions had positive potentials at highly acidic pH values, which all resulted in the sigmoidal progression of the zeta potential. The zeta potential did not significantly differ from plain [Chi/Alg] and multilayers exposed to Co^{2+} and Cu^{2+} ions. However, the Cu^{2+}, Ca^{2+} and Fe^{3+} incorporated into [Chi/Alg] multilayers introduces additional positive charges, especially at acidic values. The point of zero charges (PZC) is also shifted to a higher pH value of multilayers doped with Ca^{2+}

and Fe^{3+}. Despite the lower amount of Ca^{2+} comparison with Fe^{3+}, but show higher PZC. At physiological pH (7.4), there are no significant differences in negative surface charge between plain [Chi/Alg] and metal ion-doped PEM.

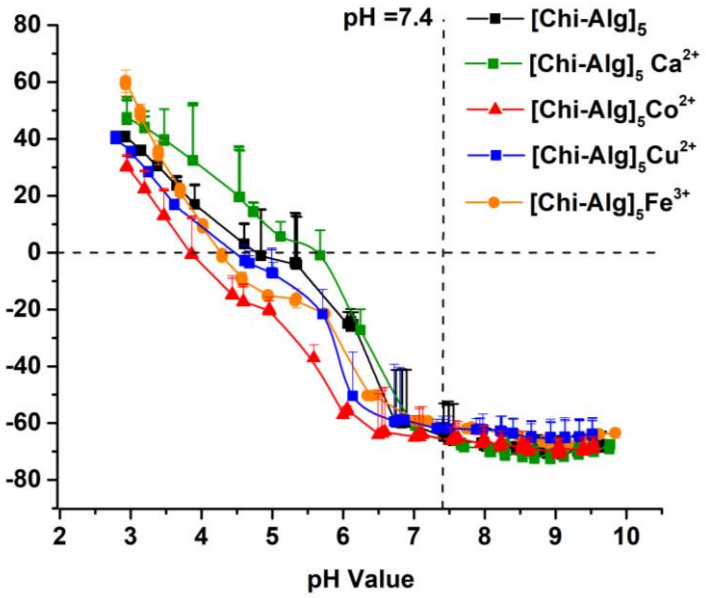

Figure 3.4: Zeta potential of plain PEM films (black) and metal ions- doped with high concentrations 50mM (**green** Ca^{2+}, **red** Co^{2+}, **blue** Cu^{2+}), and 10Mm **yellow** Fe^{3+}. All samples were measured twice (n = 2).

3.2.3 Atomic force microscopy (AFM) investigation

The PEMs were investigated with AFM to determine the surface topography. The measurements were performed in a hydrated state. **Figure 3.5a** displays plain [Chi/Alg] topography images and metal ions-doped PEMs. The plain multilayer was comparable to all different types of metal ions, excluding utilising the Fe^{3+}. Most sample surfaces exhibited granular surface morphologies. The plain [Chi/Alg] showed a small granular structure with (Sq = 3.4nm). In contrast, the roughness decreased when the [Chi/Alg] was doped with Ca^{2+} and Co^{2+}. However, Cu^{2+} presented less granular topography and increased roughness than plain [Chi/Alg] multilayers **(see Table 8)**. The multilayer containing Fe^{3+} shows more homogeneous surface topography and significantly increased surface roughness. The surface roughness of the [Chi/Alg] doped with Fe^{3+} was slightly higher than that of other metal ions. The mechanical properties of plain and metal ions containing [Chi/Alg] PEMs were investigated using nanoindentation to determine the different surfaces' elastic modulus, shown in **Figure 3.5b**, with the means values presented in **Table 8.** The plain [Chi/Alg] PEM possessed the highest modulus while adding metal ions to the [Chi/Alg] PEMs decreased E modulus. The multilayers containing Cu^{2+} resulted in the lowest E modulus with the narrowest peak, even though the

amount of incorporated ions was lower than the Ca^{2+} and $Fe^{3+,}$ and Ca^{2+} doped [Chi/Alg] existent at considerably higher concentrations.

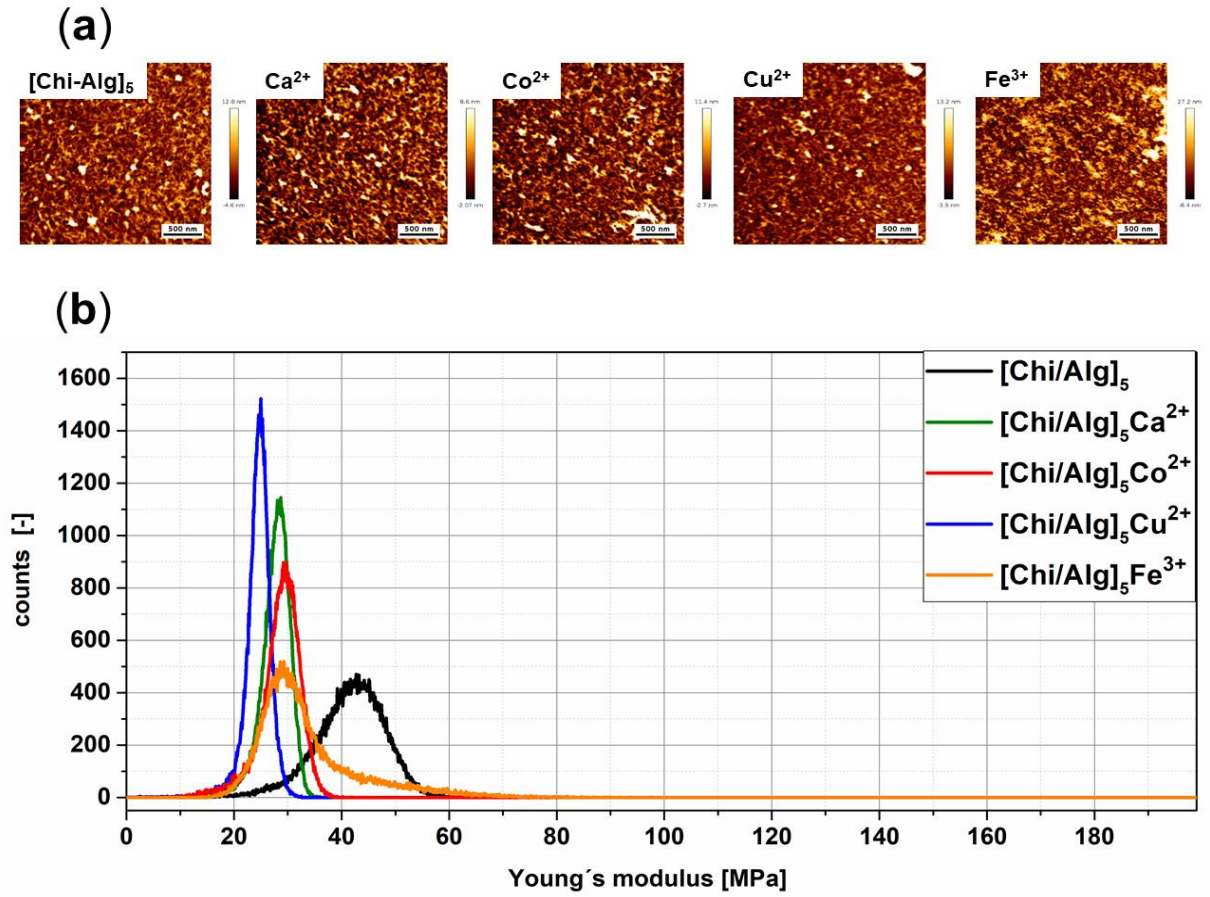

Figure 3. 5: (a) Surface topography of PEM doped with metal ions at concentrations of 50 mM for Ca^{2+}, Co^{2+} and Cu^{2+} and 10 mM for Fe^{3+}, respectively, measured by atomic force microscopy (AFM), (Scale bar = 500 nm). **(b)** Distribution curves of E modulus calculated from AFM force scan maps with a sum of 65536 single force curves per sample.

Table 8: Area Mean Roughness (**Sa**), Area Root-Mean-Squared Roughness (**Sq**), and Elastic Modulus (**E**) of plain and metal ion-doped [Chi/Alg] PEMs Measured with Atomic Force Microscopy (AFM).

	[Chi/Alg]	**Ca^{2+}**	**Co^{2+}**	**Cu^{2+}**	**Fe^{3+}**
Sq[a] [nm]	3.4	2.4	3.2	3.9	6.6
Sa[b] [nm]	2.1	1.6	2.2	1.9	5.2
E modulus (MPa)	42.4 ± 0.02	28.2 ± 0.01	29.3 ± 0.01	24.8 ± 0.004	29.7 ± 0.03

3.3 Biological studies

3.3.1 Protein adsorption

Serum protein adsorption is a sign of the ability to support cell attachment and growth because adhesive proteins promote cell attachment and proliferation on PEM [242]. Here the capability of [Chi/Alg] multilayers to bind proteins was evaluated using a standard BCA assay. Fetal Bovine Serum (FBS) 10% was used as the model protein mixture. **Figure 3.6** shows that a significantly higher amount of proteins was absorbed on [Chi/Alg] doped with metal ions compared to plain [Chi/Alg]. The quantity and type of metal ions do not appear to influence protein adsorption. Despite the concentration of Fe^{3+} ions in the PEM is much higher compared to other metal ions, as determined by ICP-MS studies, the amounts of adsorbed proteins did not exhibit a significant differences in all metal ion-doped [Chi/Alg] PEM.

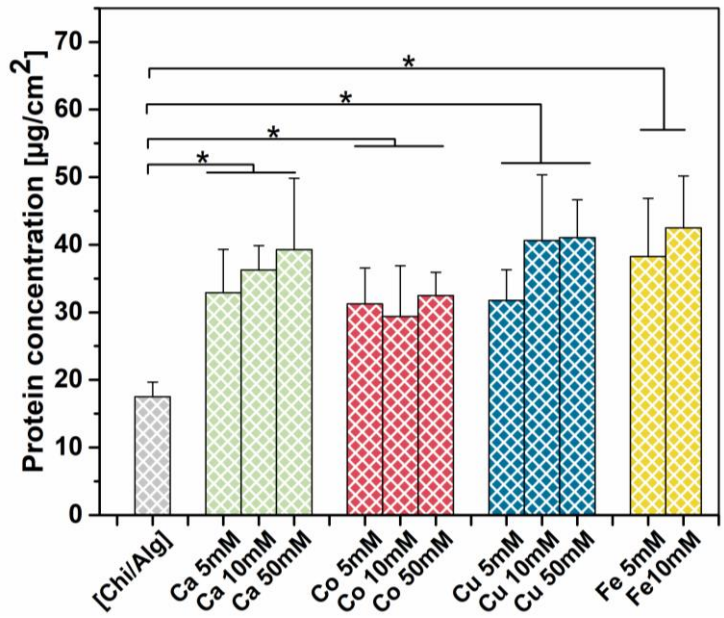

Figure 3.6: The measurement of serum proteins adsorbed on plain[Chi/Alg] (black) and metal ion-doped [Chi/Alg] PEMs using BCA assay [metal ions used for doping PEM: green Ca^{2+}, red Co^{2+}, blue Cu^{2+}, and yellow Fe^{3+}]. The means values ± SD (n = 6, *p < 0.05).

3.3.2 Cell adhesion

The adhesion of C3H10T1/2 grown on multilayers was investigated after 4h (**Figure 3.7**). The cell adhesion studies were performed by the quantification of cell number and cell area. These investigations are important to understand how surface properties of PEMs affect cell adhesion and subsequent cell differentiation [243]. **Figure 3.7**a shows that the multilayers containing Fe^{3+} had a higher number of cells regardless of the concentration. Furthermore, the low concentrations of Cu^{2+} doped [Chi/Alg] led to a significant increase in cell count, but

this effect decreased with higher concentrations. However, it appears that Ca^{2+} and Co^{2+} doped [Chi/Alg] did not affect the cell count regardless of their concentration. The Cu^{2+} and Fe^{3+} [Chi/Alg] stimulate cell spreading, which results in significantly increased cell area **Figure 3.7b**. Furthermore, the cell area significantly increased at higher concentrations (50Mm) of Ca^{2+}, Co^{2+} and Cu^{2+} compared to plain [Chi/Alg] multilayers. In contrast, there were no different effects on cell shapes and areas between plain [Chi/Alg] and Ca^{2+} and Cu^{2+} doped [Chi/Alg] at lower concentrations (5, 10 mM), as seen in CLSM images (**Figure 3.8**).

C3H10T1/2 cell adhesion was also studied by visualizing vinculin-positive focal adhesion (green staining), actin filament (red staining) and nuclei (blue staining) using CLSM after 4 h incubation. As shown in **Figure 3.8**, cells cultured on plain [Chi/Alg] and Ca^{2+} and Co^{2+} doped [Chi/Alg] at lower concentrations (5 and 10mM) had taken a round shape with the absence of fibrillar organization of actin and focal adhesion (FA) plaque formation. There, vinculin in focal adhesion was weakly expressed and primarily found in the perinuclear region, where actin fibres were organized only predominantly circumferentially. On the other hand, the Ca^{2+} and Co^{2+} doped [Chi/Alg] at higher concentration (50mM) slightly enhanced cell spreading, with the weak expression of FA, which displayed clearly at the periphery and to a lesser extent in the central region. Interestingly, the multilayers containing Fe^{3+} at low concentrations exhibited the highest cell spreading and longitudinal distribution of the actin filaments with well-expression of vinculin-positive focal adhesions at the end of the actin filaments in central regions in comparison to other metal ions-doped [Chi/Alg] at a similar concentration. Whereas the Cu^{2+} at lower and higher concentrations show more extensive cell morphology with the presence of organized longitudinal actin fibres, as well as distribution of the vinculin, indicating the presence of focal adhesions **Figure 3.8**.

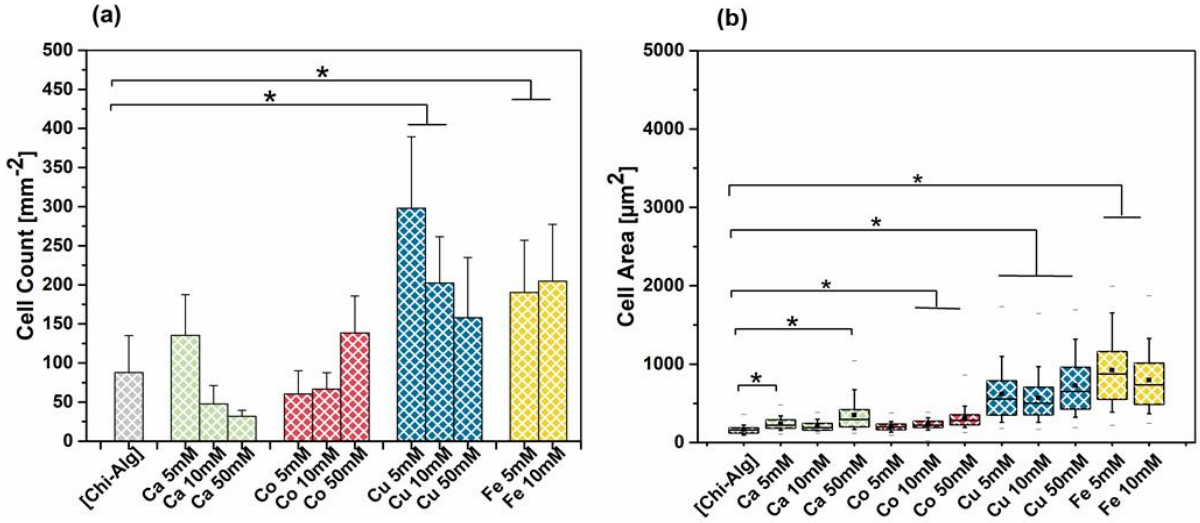

Figure 3.7: (a) Quantification of cell count per square; (means± SD) (b) and cell spreading area(µm^2) of C3H10T1/2 embryonic fibroblasts grown on plain and metal ion-doped [Chi/Alg] PEMs in EBM with 10% FBS for 4 h. The box plots with whiskers represent the first and third

quartiles, the median (dash) and means values (Black Square). Asterisks show statistical significance at $p \leq 0.05$.

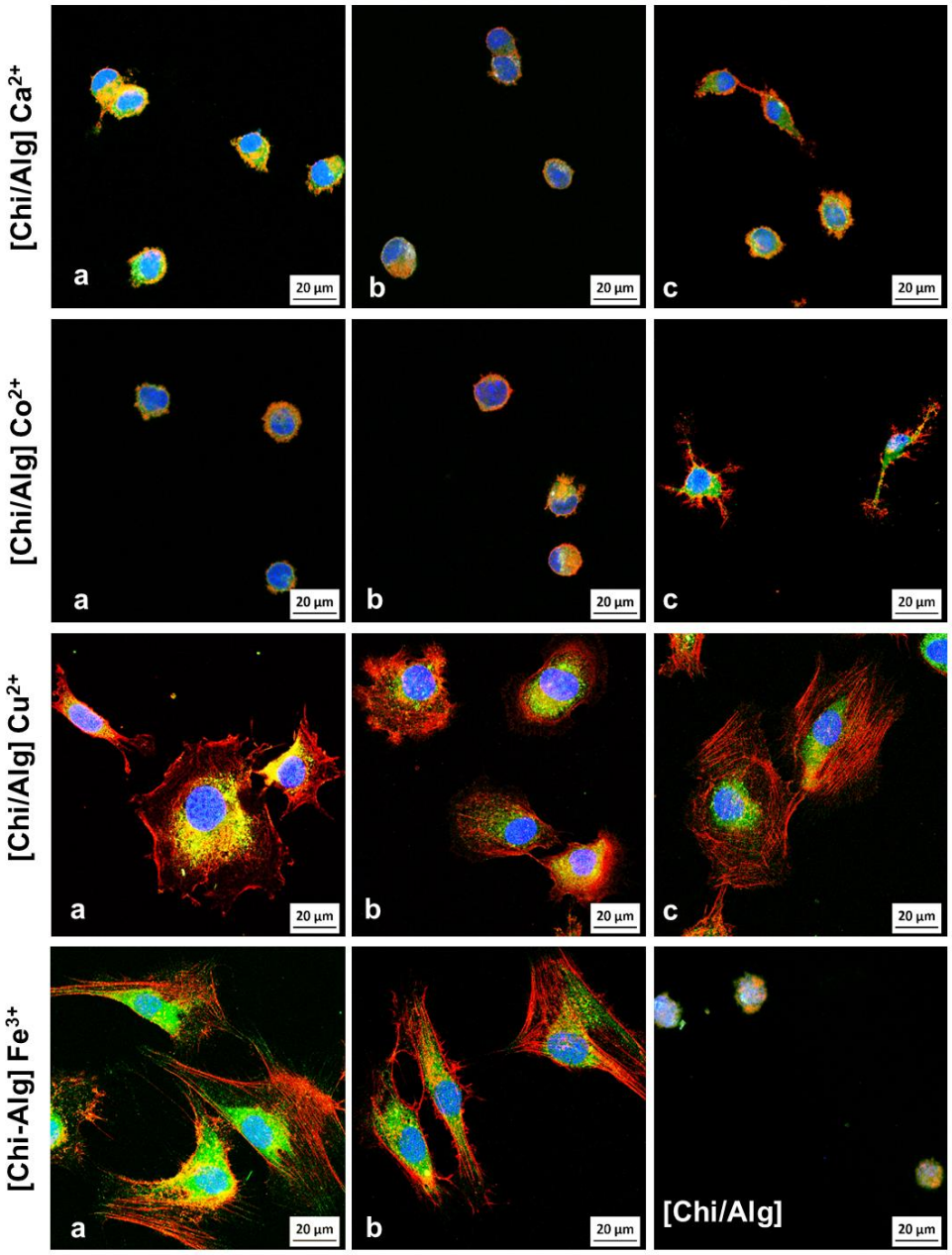

Figure 3. 8: Merged CLSM image of adherent C3H10T1/2 cultured on plain and metal ion-doped [Chi/Alg] after 4h of incubation. The cells are stained for filamentous actin (**red**), vinculin (**green**) and nucleus (**blue**). The concentration of Ca^{2+}, Co^{2+}, and Cu^{2+} was 5 (a), 10 (b), and 50 mM (c), respectively, while the Fe^{3+} was 5 (a) and 10 mM (b) used for doping multilayers [scale bar: 20 µm].

3.3.3 Cell proliferation

The growth of C3H10T1/2 was investigated on the plain [Chi/HA], and metal ions doped PEMs after 24 and 72h using Qblue® assay by measuring the fluorescence induced by metabolically active cells. The results are shown in Figures (3.9a and b), while the corresponding phase contrast images of the cells are shown in Figure 3.10. The quantitative measurement results of cell growth show that the multilayers containing Ca^{2+} significantly suppressed the number of cells found after 24 and 72 h of culture. The morphology of cells shown in the micrographs taken after 24 and 72 h (Figure 3.10) display that the cells culture on Ca^{2+} doped $[Chi/Alg]_5$ take a round morphology and shape aggregates similar to plain $[Chi/Alg]_5$ but with a lower density. Moreover, the Co^{2+}doped $[Chi/Alg]_5$ with low concentrations cause suppressed cell growth.

On the other hand, the high concentration of Co^{2+} doped [Chi/Alg] led to cell aggregation and a low number of adhered cells after 24 h, but after 72h, the cells' active number was increased and enhanced spreading was observed. These results are correlated to the microscope image in (**Figure 3.10**). The multilayers containing the Cu^{2+} independent of the concentration of Cu^{2+} showed no significant difference in the cells number than plain [Chi/Alg] after 24h. After 72h, the higher Cu^{2+} concentration (50 Mm) considerably enhanced the number of cells compared to plain [Chi/Alg]. Micrographs show that a higher concentration of 50 mM Cu^{2+} cells had a spread phenotype at 24h, and evident that cell spreading improved after 72h (see **Figure 3.10** lower panel). Interestingly, Fe^{3+} doped [Chi/Alg] with 5 and 10 mM visibly promoted cell growth and spreading. Cell quantity measured with Q Blue assays also revealed a significantly higher number of cells than on the plain [Chi/Alg] after 24 and 72 h (**Figure 3.9a, b**). The C3H10T1/2 cells grew fast enough to cover the surface after 24 h. The cells attained confluence after 72 h of culturing when 10mM Fe^{3+} was used, as seen in micrographs (**Figure 3.10** lower panel).

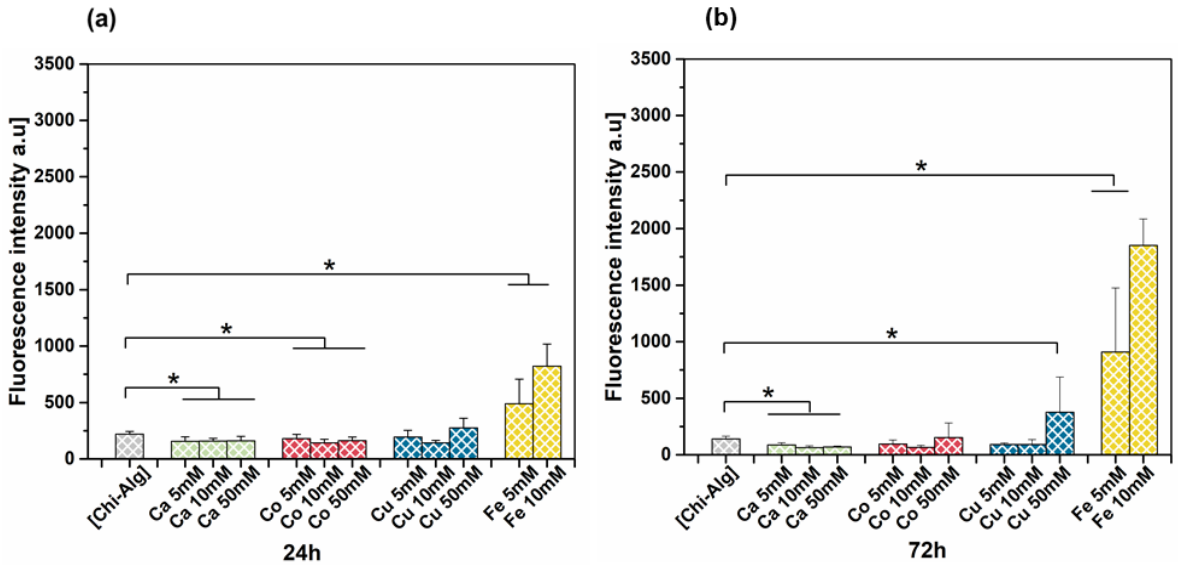

Figure 3. 9: Growth of C3H10T1/2 seeded on plain and metal ion-doped [Chi/Alg] in EMB with 10% FBS measured by the QBlue assay after 24 h (a) and 72 h (b) of culture. Results represent means ± SD, n=3.

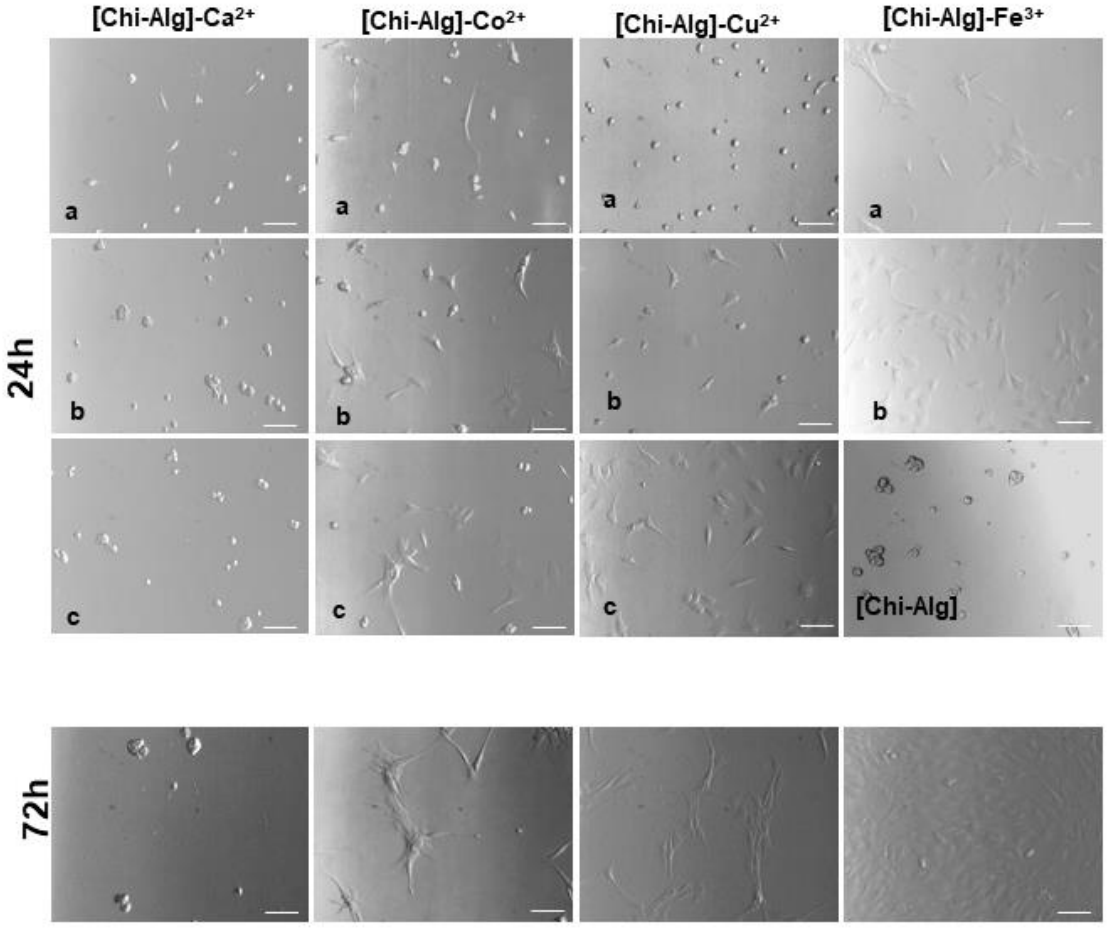

Figure 3. 10: Phase contrast images of cells cultured on plain [Chi/Alg] and metal ion-doped PEMs concentration 5(a), 10(b) and 50 mM(c), respectively, after 24 (upper panel). The (highest concentrations of metal ions) after 72 h (lower panel). [Scale bar: 100 mm].

3.4 Differentiation of C3H10T1/2 cells

C3H10T1/2 cells differentiation plated on plain [Chi/Alg] and metal ions-doped [Chi-/lg] PEMs. After cells reached almost confluence, differentiation was induced with basal medium (BM) or with adipogenic medium (AM)/osteogenic media (OM), as shown in **Table 5.**

3.4.1 Adipogenic differentiation

In adipogenic differentiation, the formation of lipid vacuoles was examined with Oil Red (**Figure 3.11a**). Positively stained lipid vacuoles were observed on cells plated in the presence of the adipogenic medium, further when cells cultured in the basal medium of [Chi/Alg] doped

with Fe^{3+} and Cu^{2+}. By contrast, the cells seeded on plain multilayers and Co^{2+} doped [Chi/Alg] observed no staining, while Ca^{2+} resulted in very small and faintly stained lipid vacuoles. Furthermore, adipogenic differentiation was evaluated by visualization of perilipin (green) and Glut4 (red) after cultivation in differentiation and control medium for three weeks (**Figure 3.11**). Plain and Co^{2+} doped [Chi/Alg] PEMs exhibit very little or no staining. There is either no or minimal staining of plain, and Co^{2+} doped [Chi/Alg] PEMs, which further establishes the lack of adipogenesis. **Figure 3.11** showed that Cu^{2+} and Fe^{3+} doped [Chi/Alg] enhanced the expression of both markers and stronger expression of perilipin and GLUT4 was found in C3H10T1/2 fibroblasts on Fe^{3+} doped [Chi/Alg]. On the other hand, the faintly positive staining of GLUT4 and perilipin in C3H10T1/2 cells was discovered when cultivated on [Chi/Alg] doped with Ca^{2+}.

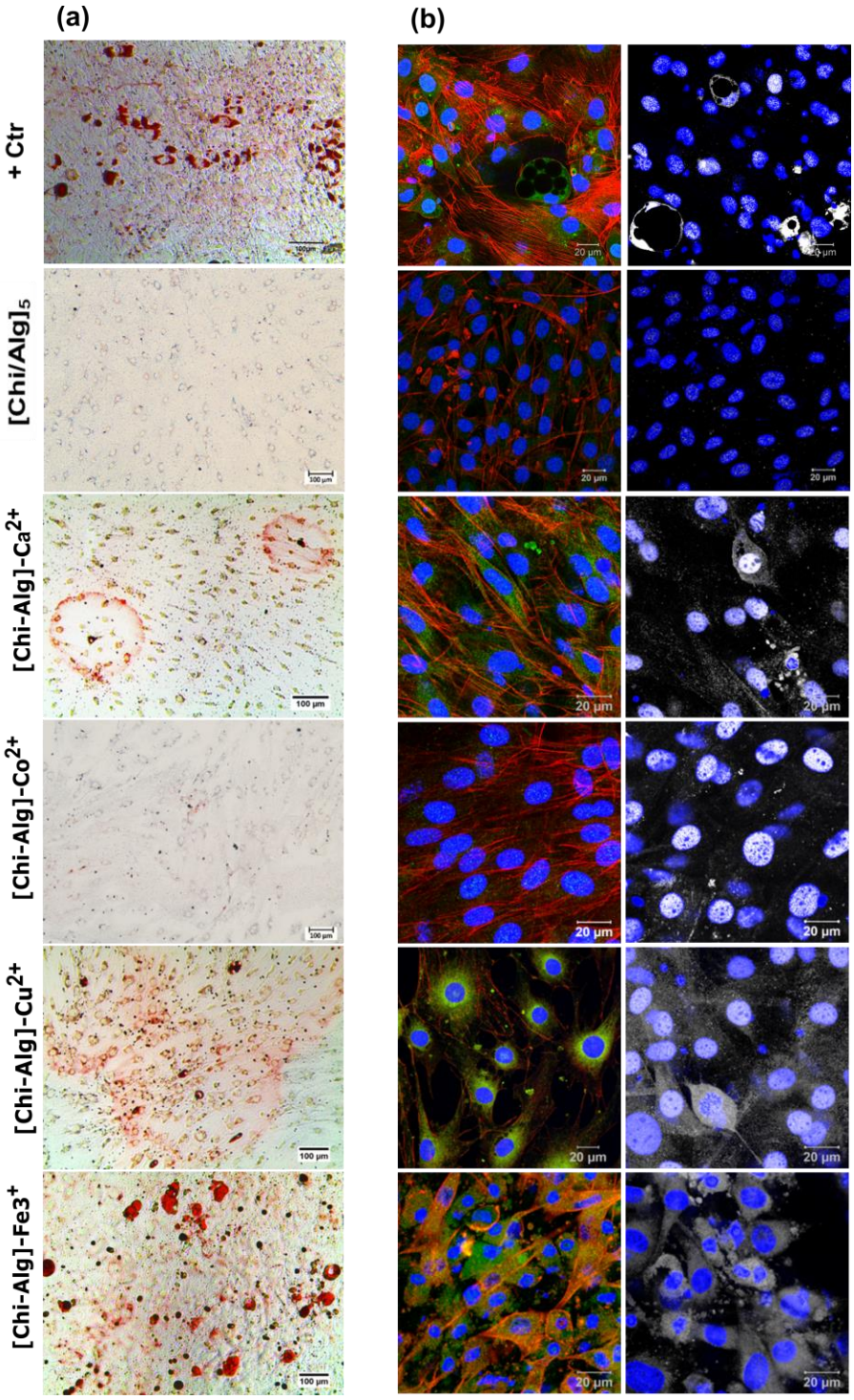

Figure 3. 11: Visualization of adipogenic differentiation of C3H10T1/2 fibroblasts cultured on the glass as Positive control, plain and metal ion-doped [Chi/Alg] PEMs (concentration of metal ions: 50 mM for Ca^{2+}, Co^{2+}, and Cu^{2+}, 10 mM for Fe^{3+}). (a) phase-contrast images of cells stained with oil red solution to investigate the formation of neutral lipid droplets in the cytoplasm (scale: 100 µm). (b) CLSM images of immunofluorescence staining for specific adipogenic markers. Left panel: perilipin (**green**), actin (**red**) and nuclei (**blue**). Left panel:

glucose transporter 4 (GLUT4, white) and nuclei (blue). The image was taken with CLSM 40x oil immersion objective [Scale: 20 µm].

3.4.2 Osteogenic differentiation

To evaluate the osteogenic differentiation of C3H10T1/2 cells on the plain [Chi/Alg] and metal ions-doped PEMs, the expression of osteogenic markers ALP, noggin, osterix and Runx2 was assessed using qRT-PCR at day 14 post-differentiation. As shown in (**Figure 3.12**), the cells treated with osteogenic media (OM) supplemented with dexamethasone, ascorbic acid and ß-glycerophosphate (positive control) exhibited an upregulation of osteogenic markers expression (ALP, Runx2, osterix, and noggin) compared to the negative control, which was treated with basal medium (BM). The expression levels in C3H10T1/2 cells cultured in BM were lower in the negative control than in the multilayer doped with metal ions. **Figure 3.12d** illustrates that osteogenic markers such as ALP and noggin showed increased expression upon metal ions exposure to multilayers when cells were cultured in BM, compared to plain PEMs multilayers. Specifically, Fe3+ doped [Chi/Alg] multilayers exhibited higher expression of ALP and noggin compared to plain [Chi/Alg]. Additionally, osterix expression on [Chi/Alg]-Fe^{3+} was significantly higher than in the positive control, while Runx2 expression of Fe^{3+} doped [Chi/Alg] was comparable to that of the positive control. Furthermore, [Chi/Alg]-Cu^{2+} multilayers demonstrated significantly higher ALP, noggin and osterix expression compared to negative control. Notably, when Co^{2+} was used for doping [Chi/Alg], there was an increase in RUNX2 expression compared to plain multilayers and the negative control.

Furthermore, calcium phosphate deposition at 24 days was assessed using Alizarin red staining (**Figure 3.13a**). The dye interacts with hydroxyapatite, producing a red stain highlight mineralized nodules, indicating an ECM rich in calcium phosphates. These nodules were observed in cells cultured on [Chi/Alg] doped with Cu^{2+} and Fe^{3+} even without of an inducing medium. Interestingly, staining was also observed in cells grown on [Chi/Alg]- Co^{2+} suggesting enhanced osteogenic differentiation and mineralization matrix formation. In contrast, plain [Chi/Alg] exhibited only faint staining. Another approach to evaluate the osteogenic differentiation was immunofluorescence staining of collagen I (Col, green) and osteocalcin (OCN, red) after three weeks' incubation in OM and BM media. As shown in **Figure 3.13b** positive staining confirmed the presence of Col and OCN. The expression of these markers was evident in positive control cells cultured in OM, whereas minimal staining of Col I and OCN was observed in the negative control, where C3H10T1/2 cells were maintained in basal medium. In contrast, C3H10T1/2 cells plated on plain [Chi/Alg] exhibited a weak Col and OCN expression. Notably, the expression of collagen osteocalcin appeared stronger in cells plated on [Chi/Alg]-Co^{2+}, particularly Cu^{2+} doped [Chi/Alg]. Interestingly, Fe^{3+} doping resulted in more

intense staining, further enhancing the formation of Col I fibrillary structure. Moreover, [Chi/Alg]-Fe^{3+} exhibited intense spot of Col I, OCN, along with increase cells spreading, indicating enhanced osteogenic differentiation.

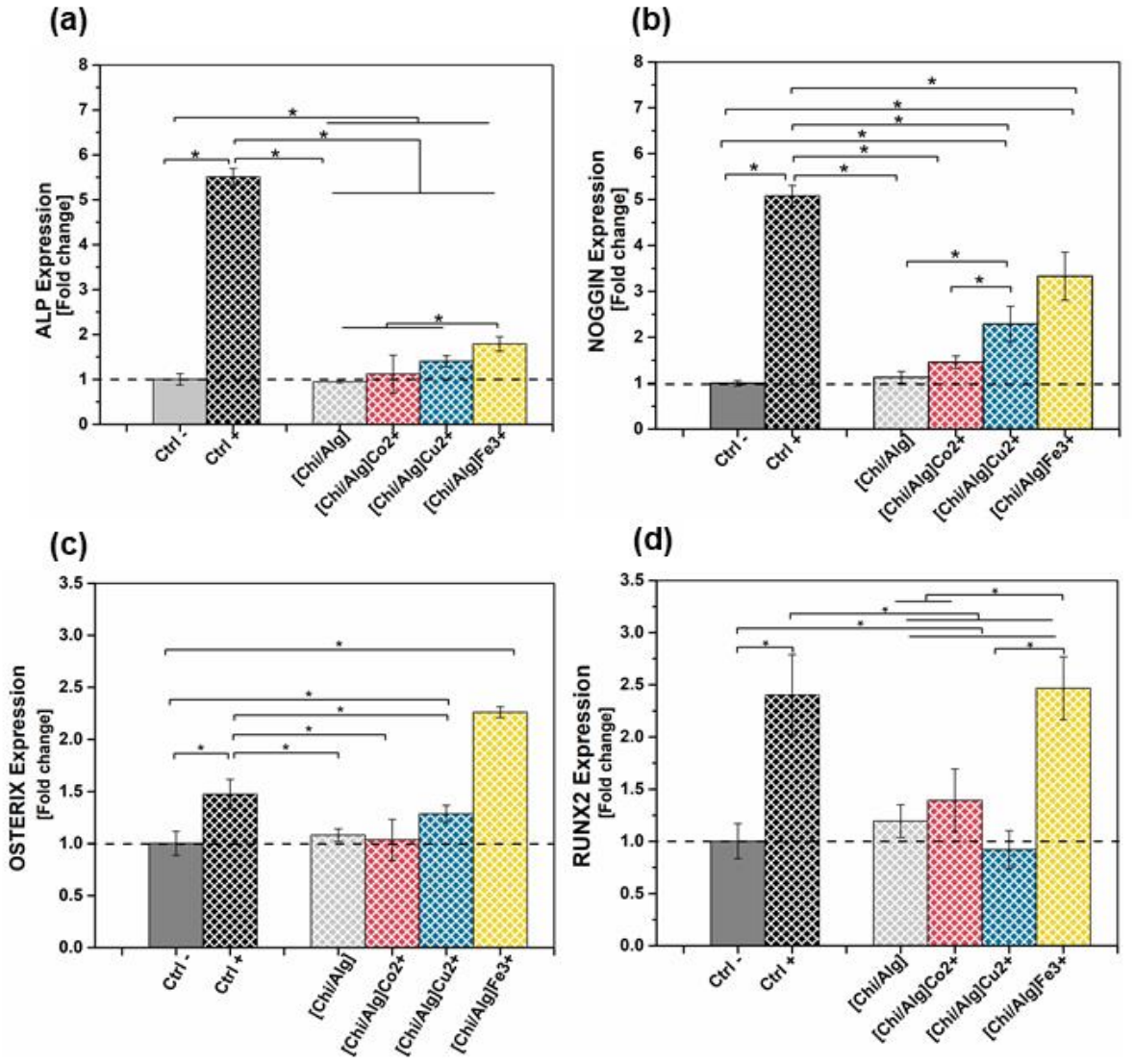

Figure 3. 12: Relative expression of ALP (a), Noggin (b), Osterix (c) and Runx 2 (d) of C3H10T1/2 cultured in basal medium (BM) on the plain [Chi/Alg] multilayers and doped with metal ions (Co^{2+}, Cu^{2+} and Fe^{3+}). RT-PCR determined the expression of cells at day 14 post-osteogenic differentiation. Relative gene expression presented as normalized to gene expression by C3H10T1/2 cultured on plain glass (negative and positive control).

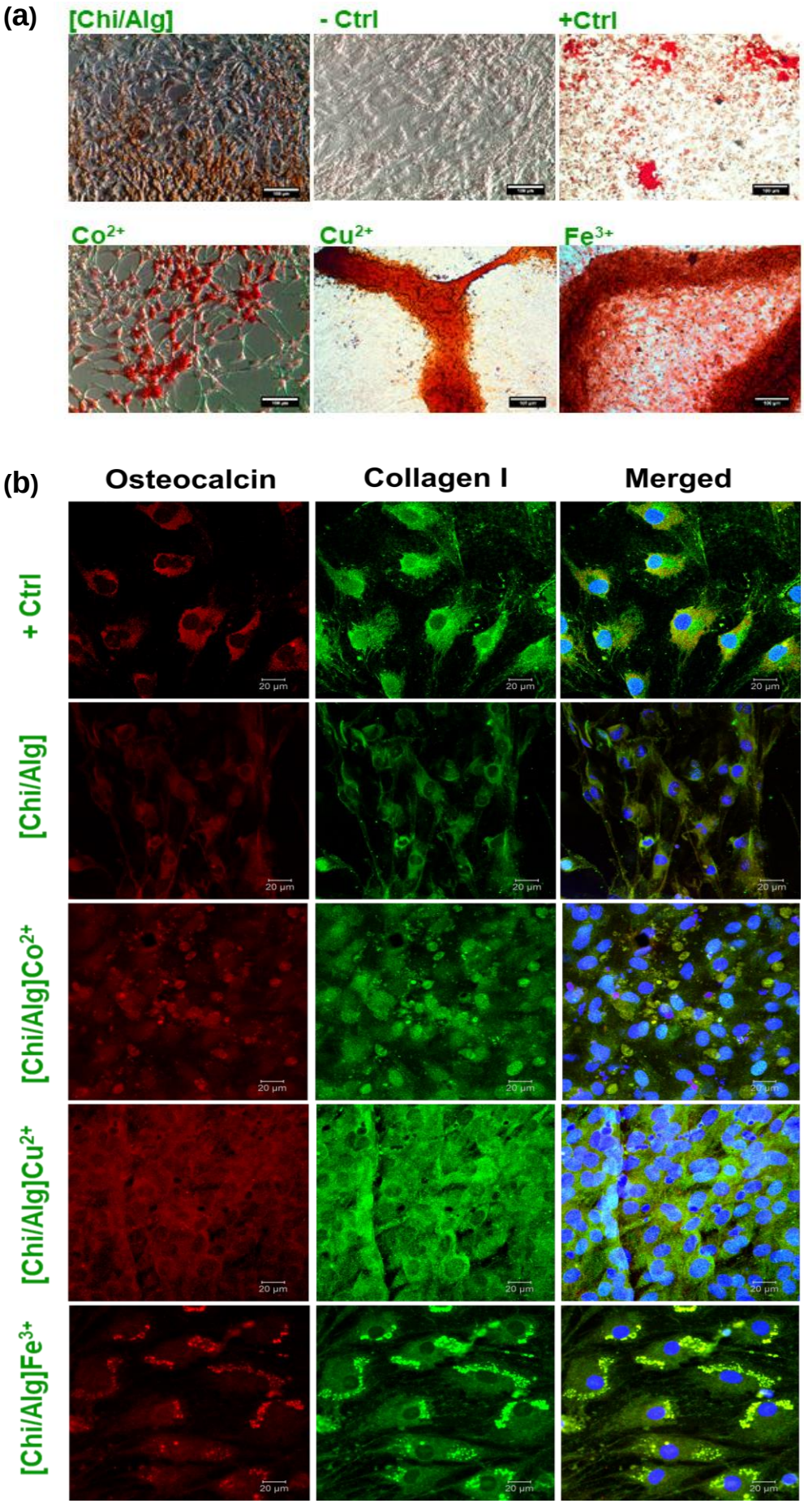
(a)
[Chi/Alg]
- Ctrl
+Ctrl
Co2+
Cu2+
Fe3+
(b)
Osteocalcin
Collagen I
Merged
+ Ctrl
[Chi/Alg]
[Chi/Alg]Co2+
[Chi/Alg]Cu2+
[Chi/Alg]Fe3+
20 µm

Figure 3. 13: (a) Visualization of osteogenic differentiation of C3H10T1/2 cells cultured on plain [Chi/ Alg] and exposed to metal ion (Co^{2+}, Cu^{2+} and Fe^{3+}) with basal medium (BM) and positive control cultured in osteogenic medium (OM). The calcium phosphate was detected at 24 days post-differentiation using histochemical staining with Alizarin Red S (scale: 100 mm). **(b)** Expression of osteogenic markers in C3H10T1/2 cultured on the plain [Chi/Alg] multilayers and doped with metal ions (Co^{2+}, Cu^{2+} and Fe^{3+}) in BM. Immunofluorescence staining of collagen I (Col I, green), nuclei (blue) and osteocalcin (red) in C3H10T1/2 at day 24 post-osteogenic differentiation in the presence of BM. [Scale bar 20 µm].

Chapter 4: Results ''Effect of metal ions on polyelectrolyte multilayers made of hyaluronic acid (HA) and chitosan (Chi), surface properties and cell response''

4.1 Studies on multilayer formation, thickness and complexation of metal ions

Multilayer growth and thickness of [Chi/HA] was studied by using analytical techniques surface plasmon resonance (SPR) and ellipsometry, respectively. **Figure 4.1a** shows that an increase in SPR angle shift (m°) for each successive layer of polyelectrolyte was similar to that of the preceding layer, leading to the PEM system growing nearly linear and increasing in their thickness. The PEM build-up process was monitored by measuring the increase in film thickness after PEM assembly using ellipsometry. **Figure 4.1b** shows that the equilibrium adsorption states of the polyelectrolytes were reached relatively quickly. The overall thickness of the multilayers in the dry conditions was ~8.9 nm (**Figure. A.1b**). in comparison, their thickness in wet conditions was ~18 nm (**see Figure. 4.1b**). The growth of the [Chi/HA] multilayer studied by SPR and ellipsometry demonstrated a similar growth behaviour and thickness as observed in previous studies conducted under comparable conditions [244, 245].

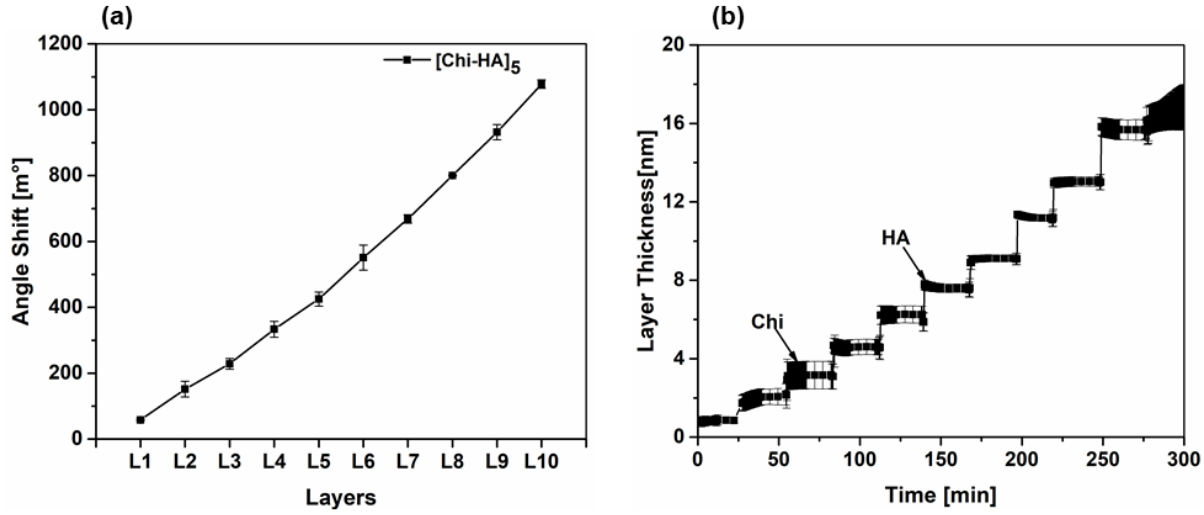

Figure 4.1:(A) layer growth of PEM system of [Chi/HA] measured with surface plasmon resonance (SPR). Odd layers numbers correspond to polycation (Chi), and even layers numbers correspond to polyanion (HA). **(B)** Thickness of [Chi/HA] multilayers measured by ellipsometry in situ (wet conditions). Results represent (means ±SD of three independent experiments*).*

The quantity of metal ions taken up by the multilayer [Chi/HA] was measured by ICP-MS using the highest concentration of metal ions for uploading, such as 50 mM for Ca^{2+}, Co^{2+}, Cu^{2+} and

10 mM for Fe^{3+}, respectively. **Table 9** displays the quantity of metal ions in multilayers with the highest concentration for Fe^{3+} and Ca^{2+}, followed by a much lower concentration of Co^{2+} and Cu^{2+}.

Table 9: Quantities of metal ions on [Chi/HA] multilayers determined by ICP-MS

Amount of metal ions within multilayers	**$[Chi/HA]_5Ca^{2+}$**	**$[Chi/HA]_5Co^{2+}$**	**$[Chi/HA]_5Cu^{2+}$**	**$[Chi/HA]_5Fe^{3+}$**
[µM]	0.166 ± 0.09	0.006 ± 0.00	0.018 ± 0.00	19 ± 0.24
[ng/cm²]	13.31 ± 7.19	0.69 ± 0.06	2.34 ± 0.02	926 ± 26.24

"The doping concentration of 50 mM (Ca^{2+}, Co^{2+}, Cu^{2+}) and 10 mM (Fe^{3+}). Results represent means ± S.D., n = 3.

The spectra of pure chitosan (Chi), hyaluronic acid (HA) and multilayers $[Chi/Alg]_{100}$ prepared as freestanding films were examined by FTIR spectroscopy (**Figure 4.2**). After that, the PEM multilayers were doped with a high concentration of metal ions, where the functional groups of both (Chi) and (HA) that were involved in complex formation with metal ions were investigated by FTIR spectra. For the description of the spectra of pure chitoasn, (see **Chapter 3, section 3.1**). The spectra of HA **shown in Figure 4.2a** present a broad absorbance band at 3275 cm^{-1}. The band at 2900 cm^{-1} is attributed to the stretching vibration of the C-H bonds. Furthermore, the protonated carboxylate group causes the two-carbonyl bands at 1608 and 1730 cm-1. The peak at 1555 cm^{-1} is associated with the amide II vibration [246]. Hyaluronic acid also exhibits bands at 1400 cm^{-1}. The strong bands represented between 1200 and 900 cm^{-1}. **Figure 4.2a** shows the $[Chi/HA]_{100}$ multilayers presented a relatively strong band at 3275$cm^{-1;}$ the stretching bonds of O–H and N–H shifted to 3300cm^{-1}, discovering a new small band at 1317cm^{-1}. The multilayers [Chi/HA]100 displayed new stretches (C–O and C–N amide II) bands at 1317cm^{-1}, and further stretch of the carboxylic group of HA was observed weak and moderate at 1602 and 1404 $cm^{-1,}$ respectively. The stretching region of saccharide units is between 1200 and 900 cm^{-1}. There was no significant change between the spectra multilayers $[Chi/HA]_{100}$ after adding metal ions and [Chi/HA]. The moderate band at 1602 cm^{-1} observed slight movement to a higher wave number (redshift) to 1605 cm^{-1} when Co^{2+} or Ca^{2+} were used. Further, multilayers containing Fe^{3+} and Cu^{2+} present up to 1608 cm^{-1}. In metal ion-containing [Chi/HA] multilayers, the peaks at 1404 cm^{-1} slightly shift toward longer wavelengths at 1406 cm1 for Co^{2+} and Cu^{2+} and 1410 cm1 for Ca^{2+} and Fe^{3+} (**Figure 4.2b**). The cobalt and iron doped to multilayers exhibit a lower intensity and slight movement to the higher wavenumber at 1070 cm^{-1} (**Figure 4.2d)**.

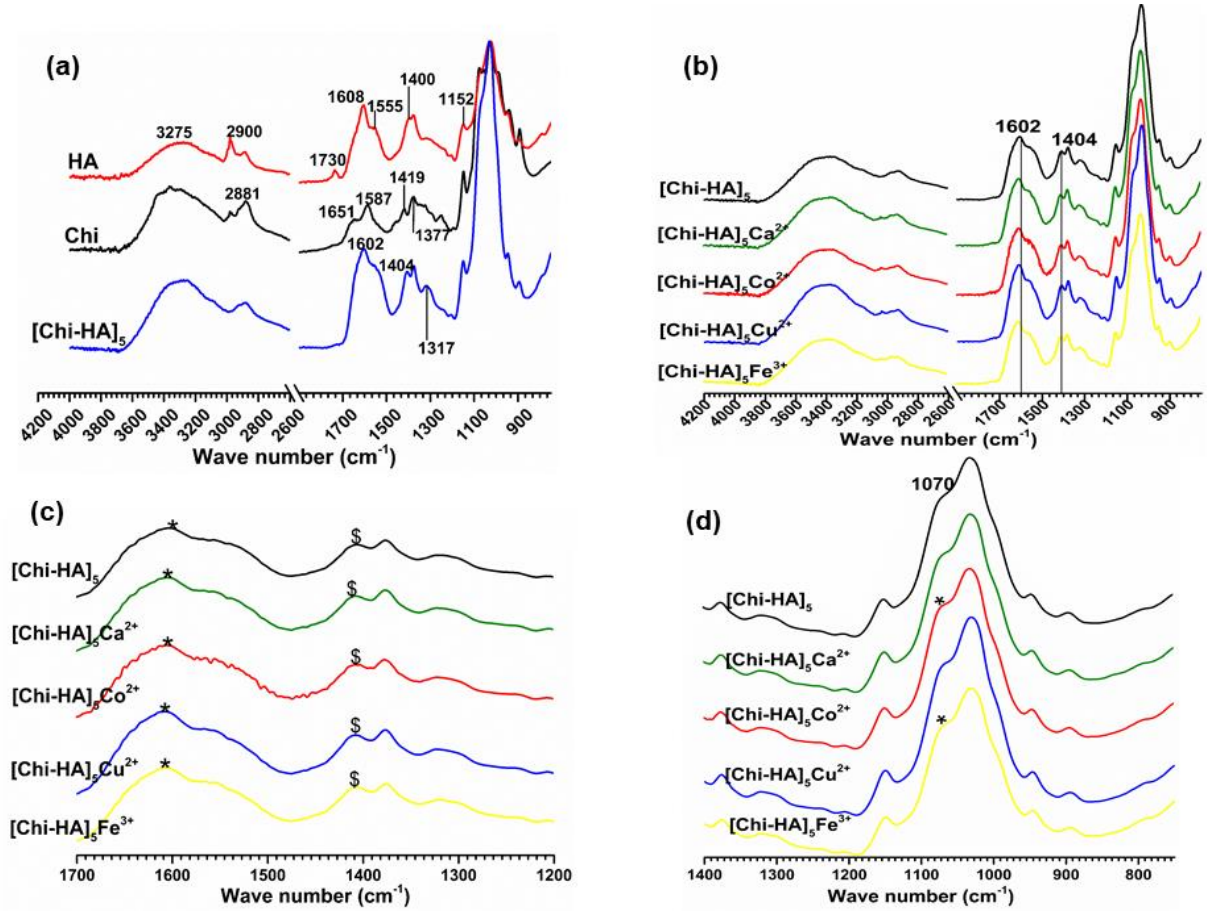

Figure 4.2: **(a)** FTIR spectra of pure chitosan (Chi), hyaluronic acid (HA) and dry $[Chi/HA]_{100}$ multilayer films. **(b)** after exposure of [Chi/HA]100 multilayers to metal ions using concentrations of 50 mM for Ca^{2+}, Co^{2+}, and Cu^{2+} and 10 mM for Fe^{3+}. **(c)** FTR spectra after exposure of $[Chi/HA]_{100}$ to metal ions in the range of 1600–1400 cm^{-1}, (*, $) indicate small changes in the spectra. **(d)** FTIR spectra after exposure of $[Chi/HA]_{100}$ to metal ions in the range of 1100–1030 cm^{-1}.

4.2 Characterization of surface properties

4.2.1 Static water contact angle (WCA)

Static water contact angle (WCA) measurements were applied to investigate the wettability properties of the terminal layer of plain [Chi/HA] multilayers and after doped with different metal ions and their concentration. **Figure 4.3** shows that all samples were hydrophilic with slight differences in the range of 35° ± 5°, depending on the type and concentration of metal ions. For instance, treating [Chi/HA] multilayers with Ca^{2+}, Co^{2+} and Cu^{2+}, resulted in a slight decrease in WCA, but the change was not significantly. In contrast, treatment multilayers [Chi/HA] with Fe^{3+} ions led to a significant increase in WCA, reaching up to 73° compared to plain [Chi/HA].

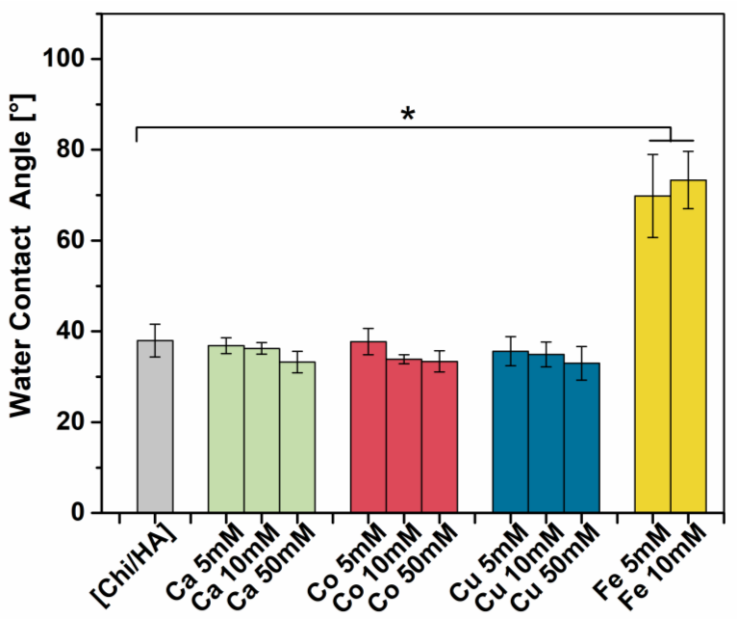

Figure 4.3: Static water contact angle measurements using the sessile drop method to characterize surface wettability of plain (HA) and [Chi/HA] doped with a metal ion. (Ca^{2+} **green,** Co^{2+} **red**, Cu^{2+} **blue**, and Fe^{3+} **yellow**). The results represent mean ± SD (n = 15, *p < 0.05).

4.2.2 Zeta potential (ζ-potential)

The zeta potential measurements were performed on plain [Chi/HA] multilayers with HA as the outermost layer and after exposure of the [Chi/HA] to metal ions. **Figure 4.4** shows that the multilayers did not significantly differ from plain [Chi/HA] and those exposed to Co^{2+} and Cu^{2+} ions, which is consistent with the low metal ions concentrations detected in ICP-MS studies. In contrast, the multilayers doped with Ca^{2+} and Fe^{3+} exhibited a more positive potential at a high acidic value than the plain [Chi/HA] multilayer. The point of zero charges (PZC) for the Co^{2+} and Cu^{2+} doped PEMs was found at pH 4.2, similar to PZC of the plain multilayers. However, the PZC slight shifted to higher pH values of 4.6 and 5.8 of Fe^{3+} and Ca^{2+} doped PEMs, respectively, indicating a more positive potential. All PEMs displayed similar negative zeta potentials at physiological pH 7.4.

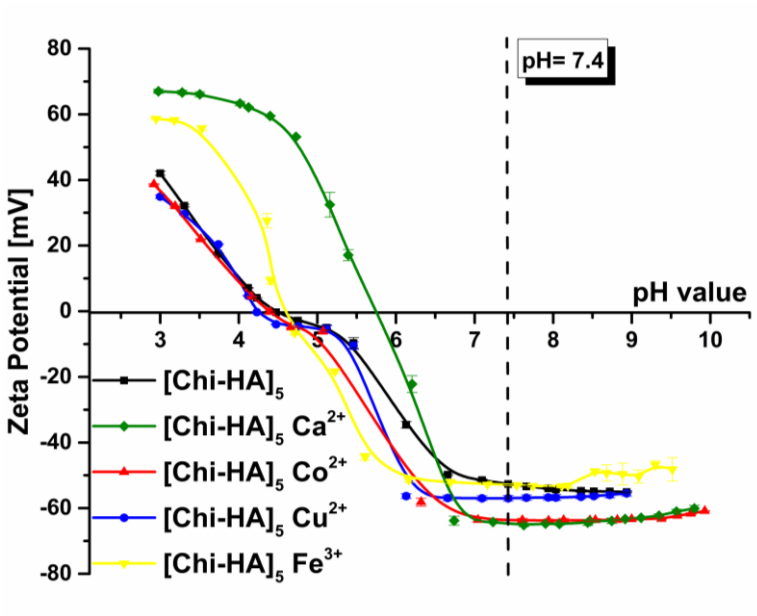

Figure 4.4: Zeta potential measurements of the plain (black) and $[Chi/HA]_5$ multilayers exposed to metal ions at the highest concentrations 50 mM (Ca^{2+} **green**, Co^{2+} **red**, Cu^{2+} **blue** and 10 mM Fe^{3+} **yellow**). Results are means ± SD of two independent experiments.

4.2.3 Atomic force microscopy (AFM)

Figure 4.5 presents the results of AFM studies, providing insights into the topography of plain PEM compared to metal ions-doped [Chi/HA] PEM. The topography of plain PEMs and metal ions-doped were similar, with no significant difference among the types of metal ions, except for multilayer containing Fe^{3+}. The surface morphology of all samples appeared granular, with minor variations in roughness depending on the kind of metal ion (see **Table 10**). The granular structure of the PEMs was associated with increased surface roughness after [Chi/HA] PEMs were treated with Cu^{2+} and Co^{2+}. In contrast, [Chi/HA] multilayers exhibited a smoother surface (sq = 4.4 nm). Previous studies report that the granular structure [Chi/HA] multilayers are linked to the film formation process [247]. Despite Fe^{3+} doped [Chi/HA] displaying a less granular and more homogeneous surface, it exhibited the highest roughness (sq = 11.7 nm). The mechanical properties of PEM were studied in a liquid environment by nanoindentation, as shown in **Figure 4.5a.** The elastic modulus distribution graphs indicate that plain [Chi/HA] PEM had the highest modulus, whereas metal ions-doped [Chi/HA] exhibited a lower E modulus. Among them, Co^{2+} doped [Chi/HA] had the lowest elastic modulus and the narrowest peak were in, while other metal ions resulted in a wider distribution of the elastic modulus with a similar effect.

Table 10: Area roughness parameters (area mean roughness (**Sa**) and area root mean squared roughness (**Sq**), and the elastic modulus (**E**) distribution of the plain [Chi/HA] and with high concentrations of metal ions were measured by AFM..

	$[Chi/HA]_5$	**Ca^{2+}**	**Co^{2+}**	**Cu^{2+}**	**Fe^{2+}**
Sq[a] [nm]	4.4	4.9	6.5	5.3	11.7
Sa[b] [nm]	2.8	2.7	4.2	3.4	7.9
E modulus (MPa)	71.3 ± 0.06	61.6 ± 0.05	45 ± 0.03	49.9 ± 0.03	62 ± 0.08

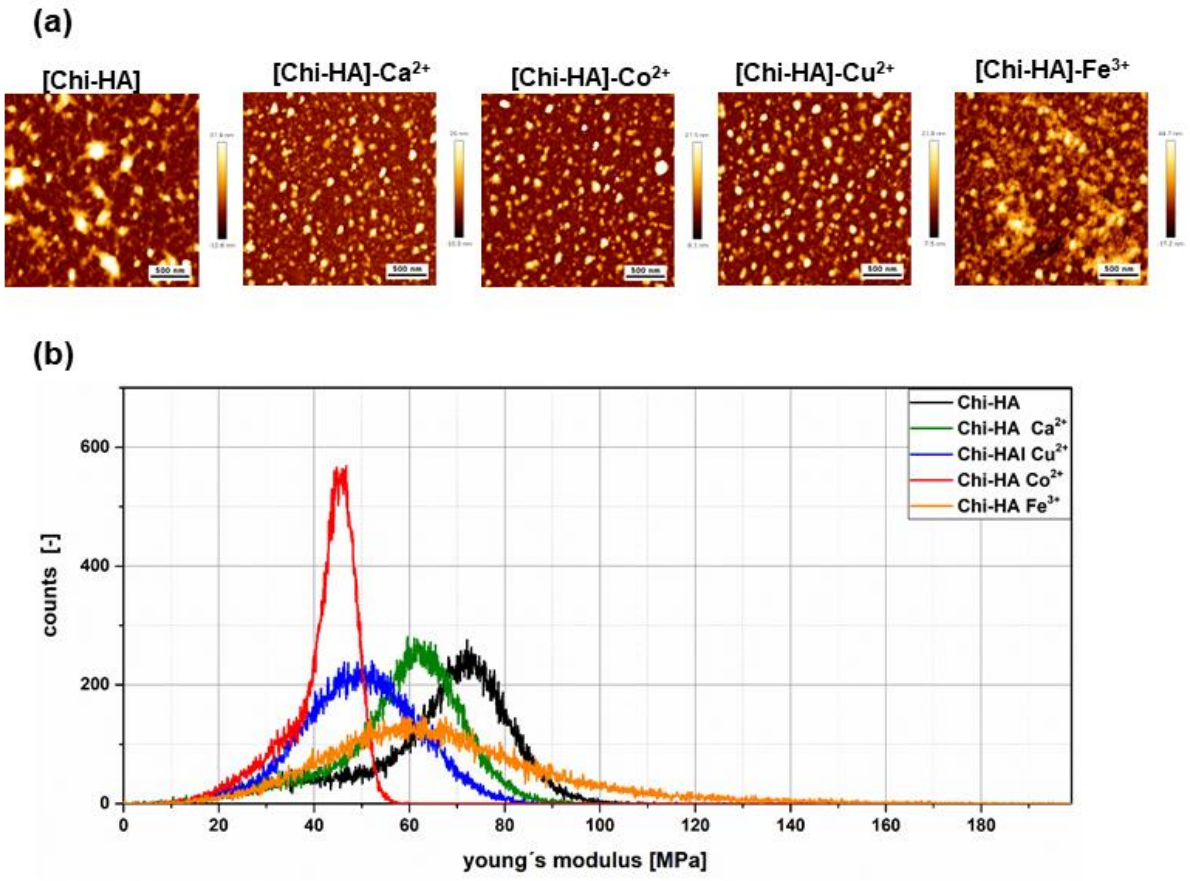

Figure 4.5: **(a)** Surface topography of [Chi/HA]5 multilayers doped with the highest concentrations of 50 mM of Ca^{2+}, Co^{2+}, and Cu^{2+} and 10 mM of Fe^{3+} measured by AFM (scale bar = 500nm). **(b)** Distribution curves of Young's modulus performed at the intermittent contact mode of AFM in 150 mM NaCl solution with a force map of an area of 2.5 X2.5 mm^2 (scale bar = 500 nm).

4.3 Biological studies

4.3.1 Protein adsorption

The ability of proteins to bind to [Chi/HA] multilayers was assessed by using a BCA assay. A 10% FBS solution was used as a model to evaluated the propensity of protein adsorption on plain [Chi/HA] and metal ions-doped PEMs. The adsorption of serum proteins might be used to detect the presence of vitronectin and other adhesive proteins, which can promote the adherence of the cells to multilayers [31]. The capability of the PEMs to bind serum proteins is shown in Figure 6, [Chi/HA] doped with Cu2+ and Fe3+ at high concentrations (50 and 10mM, respectively) exhibited significantly more protein adsorption relative to plain [Chi/HA]. On the other hand, the Ca^{2+} and Co^{2+} doped [Chi/HA] PEMs had no significant effects on protein adsorption compared to plain [Chi/HA].

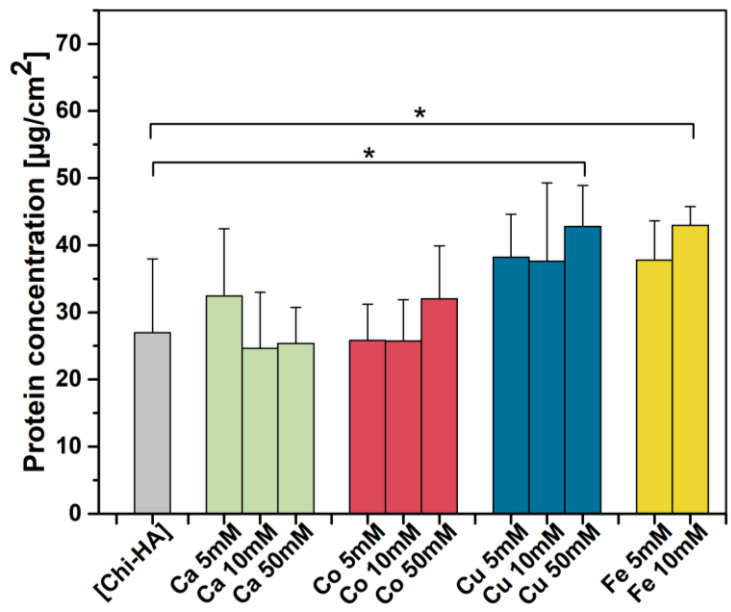

Figure 4.6: Quantity of serum protein adsorption on [Chi/HA] multilayers (**black**) and metal ions-doped PEMs determined by BCA assay, dependent on the concentration of metal ions (Ca^{2+} **green**, Co^{2+} **red**, Cu^{2+} **blue**, and Fe^{3+} **yellow**). Results represent means ± SD (n = 6, *p < 0.05).

4.3.2 Cell adhesion

Adhesion and spreading of embryonic fibroblasts (C3H10T1/2) on plain and metal ion-doped [Chi/HA] multilayers was investigated after 4 h. Cells were stained for a cellular structure including the nucleus, actin cytoskeleton and vinculin in focal adhesions. Immunohistochemical staining and image analysis was performed to determine cells count**.** **Figure 4.7** shows the significant decrease in cell count within the increase in the metal ions

concentration of Co^{2+} and Cu^{2+}. However, the quantification of the cell count did not reveal significant differences independent of the concentration of $Ca^{2+,}$ and Fe^{3+} doped [Chi/HA] compared to plain [Chi/HA]. In addition, the cell area was more extensive for PEM doped with Fe^{3+} observed at low concentrations of 5mM (**Figure. 4.7b**). By contrast, the cell area of [Chi/Alg]5 doped with Ca^{2+} and Co^{2+}, and Cu^{2+} at lower concentrations was significantly different compared to plain [Chi/HA].

On the other hand, the concentration (10 and 50 mM) effect of doped metal ions on cell spreading was exhibited, significantly larger than those on the plain [Chi/HA] multilayers. Furthermore, the cell adhesion studies were carried out by staining the actin cytoskeleton (red) expression and organization of vinculin (green) to detect focal adhesion (FA) formation and cell nuclei (blue) using CLSM (**Figure. 4.8**). The cells seeded on plain [Chi/HA] showed poor vinculin expression. In contrast, cells seeded on [Chi/HA] doped with Ca^{2+} and Co^{2+} showed more vital vinculin expression but no observed organisation development in focal adhesion plaques at 5mM concentration. By contrast, cells seeded on Fe^{3+} doped [Chi/HA] at lower concentrations (5mM) showed a longitudinal distribution of the actin filaments and enhanced vinculin expression in focal adhesion at the end the actin filaments but also in central regions. On the other hand, all metal ions- doped [Chi/HA] at 10 mM concentrations showed enhanced vinculin expression in focal adhesion and vinculin molecules were located at the periphery and in central regions accompanied by the growth of actin stress fibres.

Nevertheless, additionally, when Ca^{2+} and Co^{2+} with higher concentrations (50mM) were utilized resulted in a reduction in cell size and less expressed vinculin with the disappearance of focal adhesions. In addition, this study examined whether receptors recognizing HA, such as CD44, are involved in the adhesion process. C3H10T1/2 cells were seeded on plain [Chi/HA] and metal ions-doped PEMs at high concentrations. Cell morphology was analysed by immunofluorescence microscopy staining CD44 (green), actin polymerization (red) and cell nuclei (blue) labelling. **Figure 4.9** shows that positive staining of CD44 in peripheral regions of cells cultured on [Chi/HA] doped metal ions, as well discovered as clusters in the periphery but was not present in cells on the plain PEM.

Moreover, the clustered appearance of CD44 was found in both Co^{2+} and Cu^{2+} doped [Chi/HA], with both showing significant CD44-positive staining in the nuclei of permeabilized cells. In contrast, cell-seeded on plain [Chi/HA] exhibited weaker CD44 staining in the nucleus. Visual observations were supported by quantitative analysis of these findings, which showed that both copper and cobalt ions induced more intense nuclear staining of CD44 as measured by the intensity ratio of CD44 nuclei to cytoplasm using Image J. (**Figure. 4.9b**).

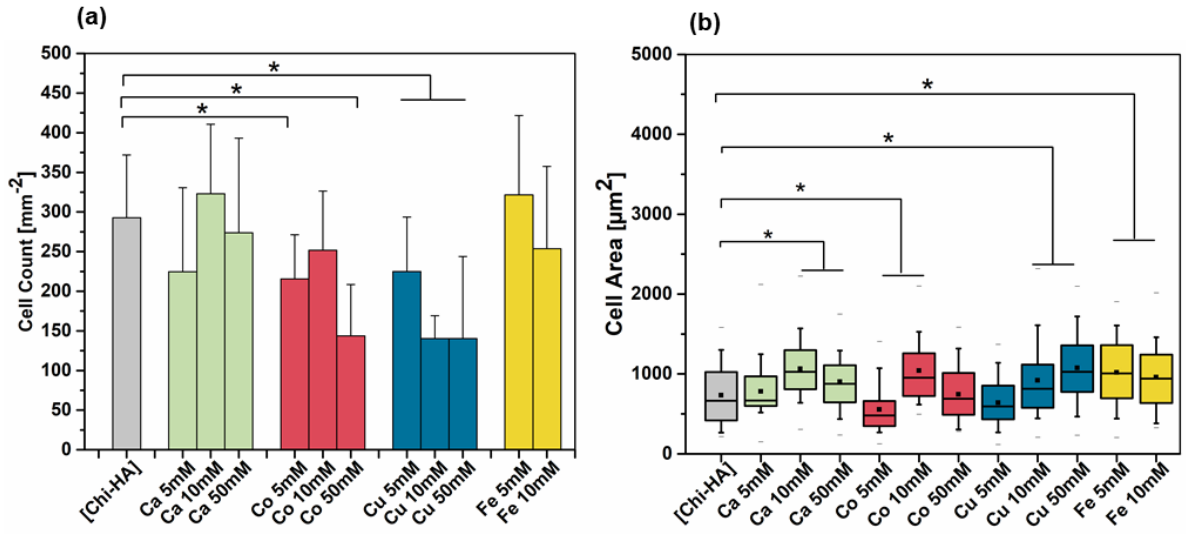

Figure 4.7: Cell count (a) and area (b) of cells seeded on plain and metal ions-doped [Chi/HA] with different concentrations in EBM with 10% FBS for 4h. The box-whisker plots in panels (b) and (c) indicate the 25th and 75th percentile, and the median and means values (black square), respectively (means ± SD).

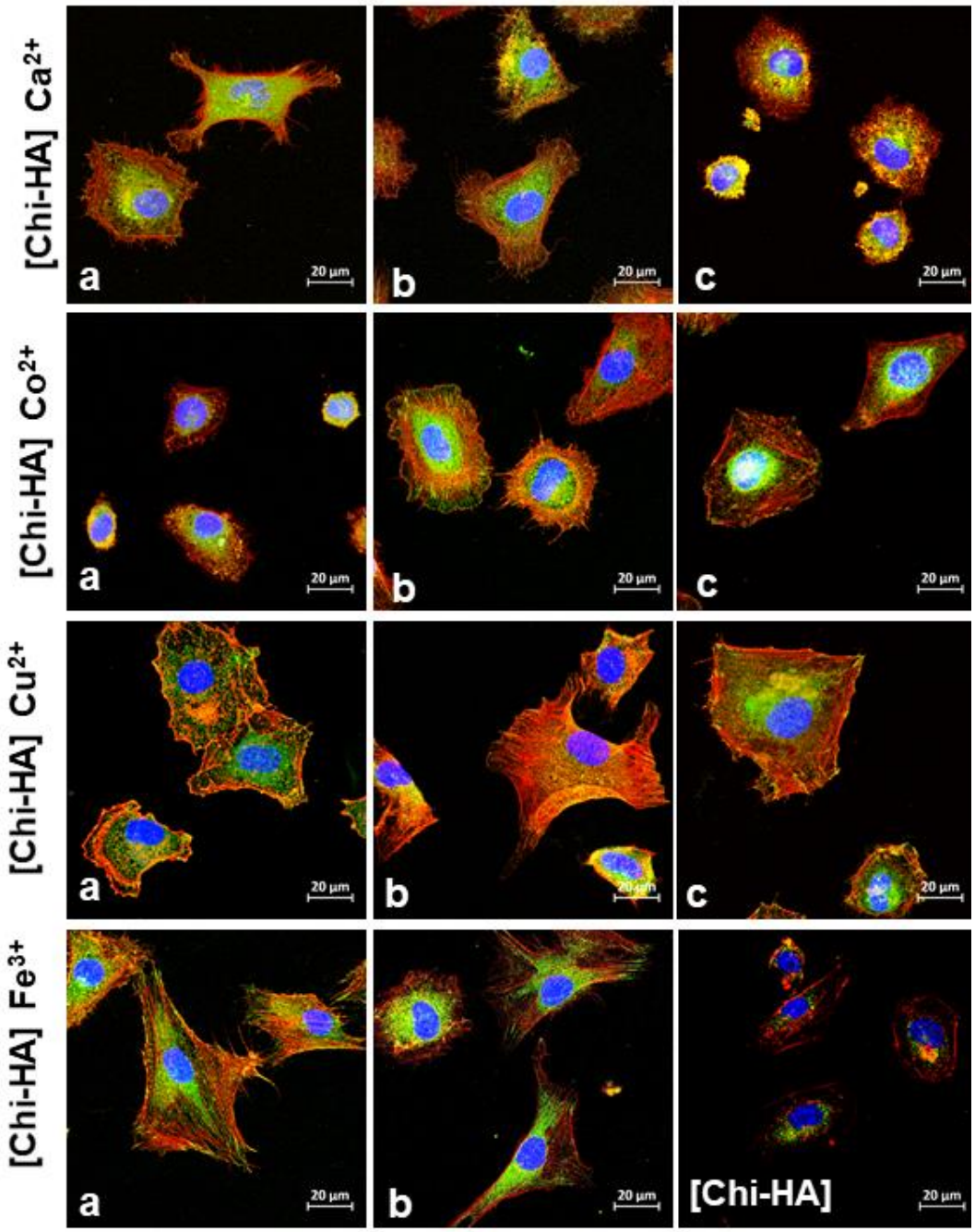

Figure 4.8*:* Cell morphology of C3H10T1/2 embryonic fibroblasts after 4 h incubation on plain and metal ions -doped [Chi/HA]. Concentrations of Ca^{2+}, Co^{2+}, and Cu^{2+} was 5 (a), 10 (b) and 50 mM (c), while the Fe^{3+} was 5 (a) and 10 mM (b) respectively. Cells were stained for actin filaments (**red**), vinculin (**green**) and nuclei (**blue**) [scale bar: 20 mm].

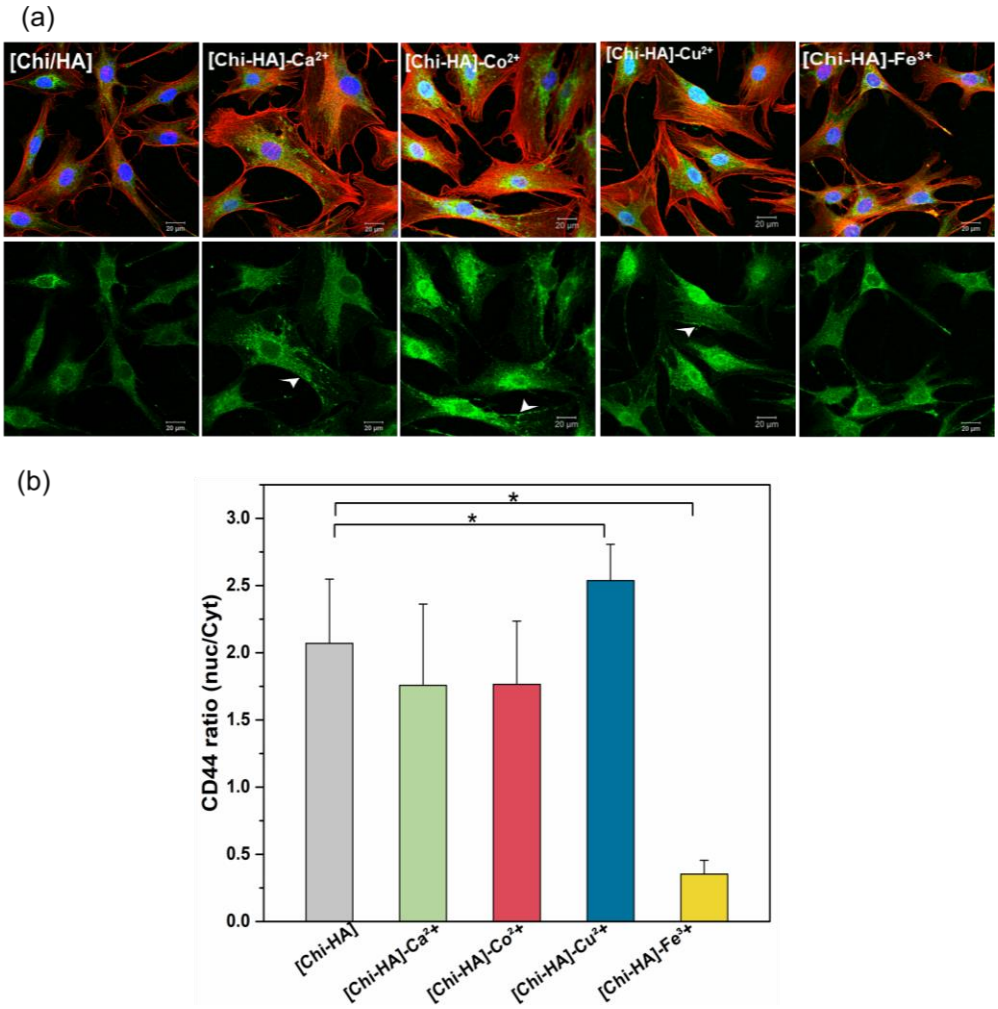

Figure 4.9: (a) Merged CLSM image of adherent C3H10T1/2 cells stained for actin filaments (**red**), CD44 (**green**) and nuclei (**blue**) in the upper lane and for CD44 only lower lane. (b) The intensity ratio of nuclei to cytoplasmic staining of CD44 in C3H10T1/2 embryonic fibroblasts after 24 h incubation on plain and [Chi/HA] multilayers doped with 50 mM Ca^{2+}, Co^{2+}, and Cu^{2+} or 10 mM Fe^{3+}. White arrows in the micrographs indicate peripheral cell areas of increased CD44 expression. For quantification of the intensity ratio, Fiji ImageJ was used.

4.3.3 Cell growth

The proliferation of C3H10T1/2 cells on the plain [Chi/Alg] and metal ions doped PEMs was studied after 24 and 72 h by QBlue assay quantifying viable cells, as shown in **Figure 4.10 a & b**. In contrast, the corresponding phase contrast images of the cells are shown in **Figure 4.11**. The cells seeded on plain [Chi/HA] showed increased metabolic activity during incubation. Additionally, the micrographs in **Figure. 4.11** show that the C3H10T1/2 formed almost confluent layers on [Chi/HA] after 24 h. The plain multilayers showed that cells almost confluent layer after 4h. According to the results from the QBlue assay, the use of Ca^{2+} had an inhibitory and concentration-dependent effect on the number of cells after 24 of culture. It

also revealed a significantly reduced number of cells after 72 h compared to plain [Chi/HA] multilayers. **Figure 4.11** shows that after 24h, the cells cultivated on [Chi/HA] doped with Ca^{2+} relatively round morphology and formed aggregates compared to the flat spread of cells on plain [Chi/HA] multilayers. Here, the impact of Ca^{2+} concentration was not observable. The [Chi/HA] doped with Co^{2+} inhibited the cells' quantity after 4h if compared to plain [Chi/HA]. However, a higher concentration of Co^{2+} (50 mM) doped [Chi/HA] exhibited a higher cell number and promoted cell spreading was found after 72h (see **Figure 4.10b**). These findings correspond to the microscopy image shown in **Figure 4.11**. In contrast, low concentrations of cobalt 5 and 10mM displayed cells aggregate and a low number of spread cells. The Cu^{2+} doped [Chi/HA] multilayers had a similar number of cells compared to plain [Chi/HA] after 4h. The number of cells decreased after 72h than on plain multilayers; however, it slightly reduced as the Cu^{2+} concentration increased from 5 to 50 mM. The micrographs demonstrate that the cells already exhibited a spread phenotype at a low concentration of 5 mM Cu^{2+} and that this phenotype did not alter when the concentration was raised. The [Chi/HA] doped with $Fe^{3+,}$ even at a low concentration of 5 mM, stimulated cell growth and spreading. Moreover, the Q blue assay detected that increase in the number of cells to the plain [Chi/HA] after 24h and a comparable number after 72h (Figure4.10a and b). Additionally, micrographs in **Figure 4.11** show that the cells growing and reached confluence after 24 h when Fe^{3+} at 10mM concentration was utilized.

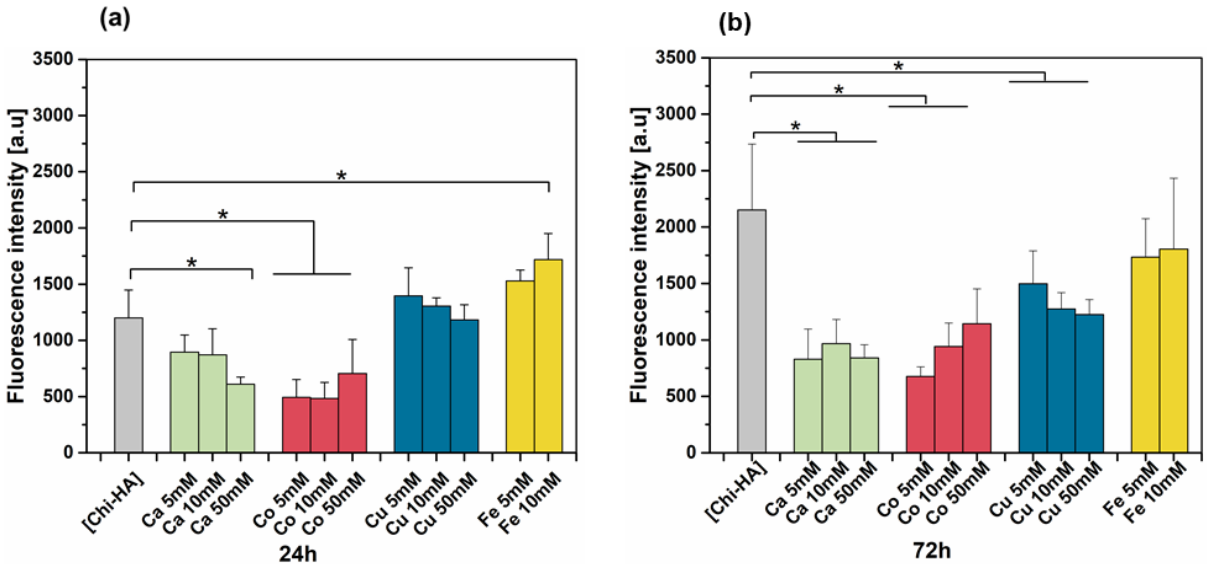

Figure 4.10: The proliferation of C3H10T1/2 cells cultured on plain and metal ion-doped [Chi/HA] multilayers. The Q Blue viability assay evaluated the metabolic activity after 24 h (a) and 72 h (b) of culture. The results represent the means ± SD of three independent experiments.

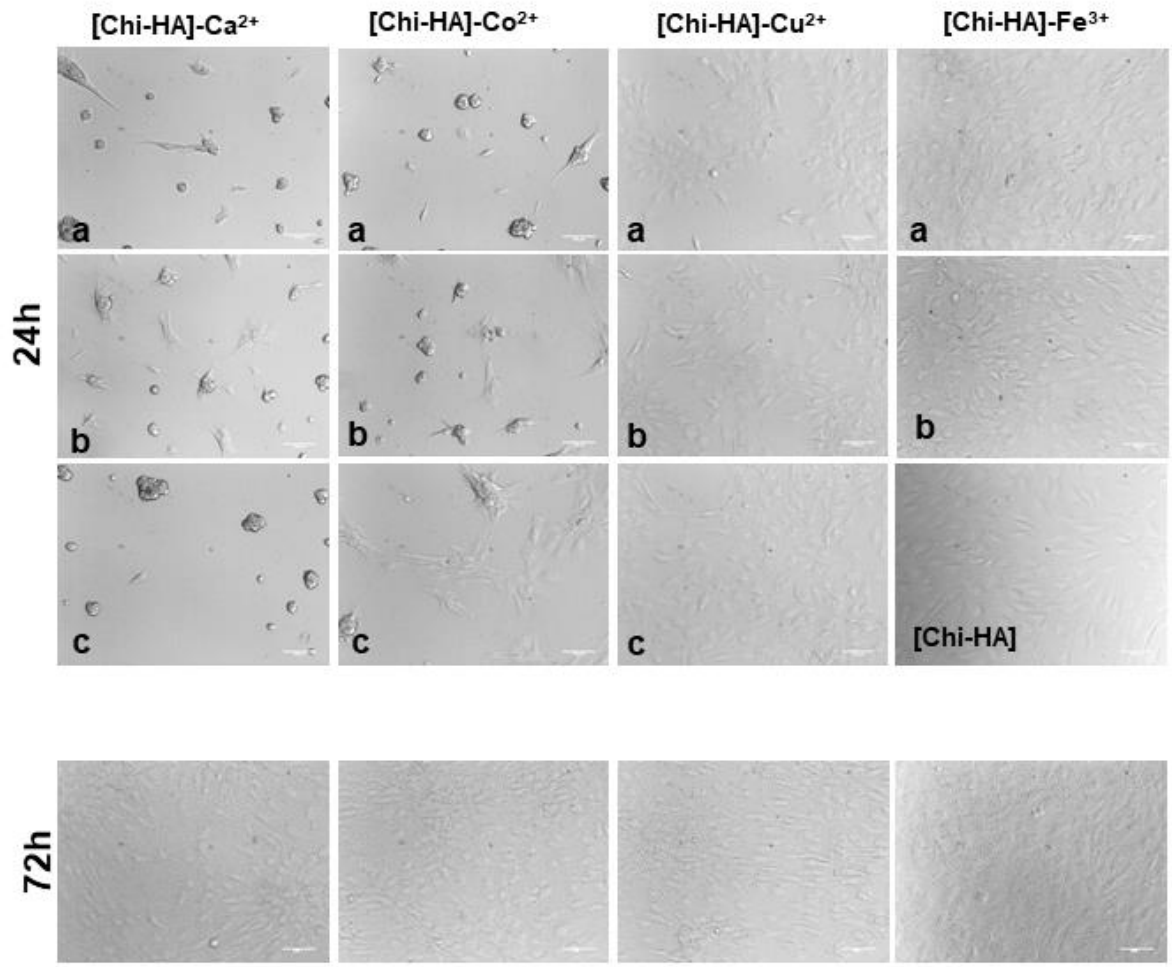

Figure 4.11: Phase contrast images of C3H10T1/2 cells cultured in 10% FBS for 24 h on the plain [Chi/HA] and metal ions-doped PEMs. Metal ion concentrations of 5 (a), 10 (b) and 50 Mm(c) were used after 24h (upper panel). High concentrations represent in the lower panel.

4.4 Differentiation of C3H10T1/2 cells

4.4.1 Adipogenic differentiation

The influence of (Ca^{2+}, Co^{2+}, Cu^{2+}, Fe^{3+}) ions loaded on PEM composed of hyaluronan and chitosan was studied on adipogenic differentiation of multipotent embryonic mouse fibroblasts C3H10T1/2 cell line. The lipid vacuoles were stained with histochemistry oil red (**Figure 4.12a**). Lipid vacuoles were absent in the cells cultured on plain [Chi/HA] and Co^{2+} doped PEMs. Contrarily, intense positive staining of vacuoles was observed when cells were grown in the presence of the adipogenic medium, and on the [Chi/HA] doped with Ca^{2+}, Cu^{2+} and Fe^{3+}. Immunohistochemically staining for perilipin and GLUT4 were performed to assess adipogenic differentiation after 21 days cultivating. **Figure 4.12b** shows the loss or weak staining of both markers in cells seeded on Co^{2+} doped multilayers, indicating the absence of

adipogenesis. In contrast, plain [Chi/HA] exhibited some perilipin expression. However, the remarkable finding was that cells seeded on the [Chi/HA] doped with Ca^{2+} to formed aggregates cells, with positive staining of lipid vacuoles, as well as the expression of GLUT4 and perilipin. Most interestingly, it was observed that Ca^{2+} and particularly Cu^{2+} and Fe^{3+} metal ions significantly promote perilipin and GLUT4 expression. Further, perilipin, forming lipid droplet, was predominantly localized on the cell surface and throughout the cytoplasm. In addition, it appeared in a few puncta as a ring on the lipid droplet. Additionally, adipogenic markers were strongly expressed in cells seeded in a basal medium on multilayer treatment with Cu^{2+} and Fe^{3+}, similar to the specific differentiation medium (**Table 5**).

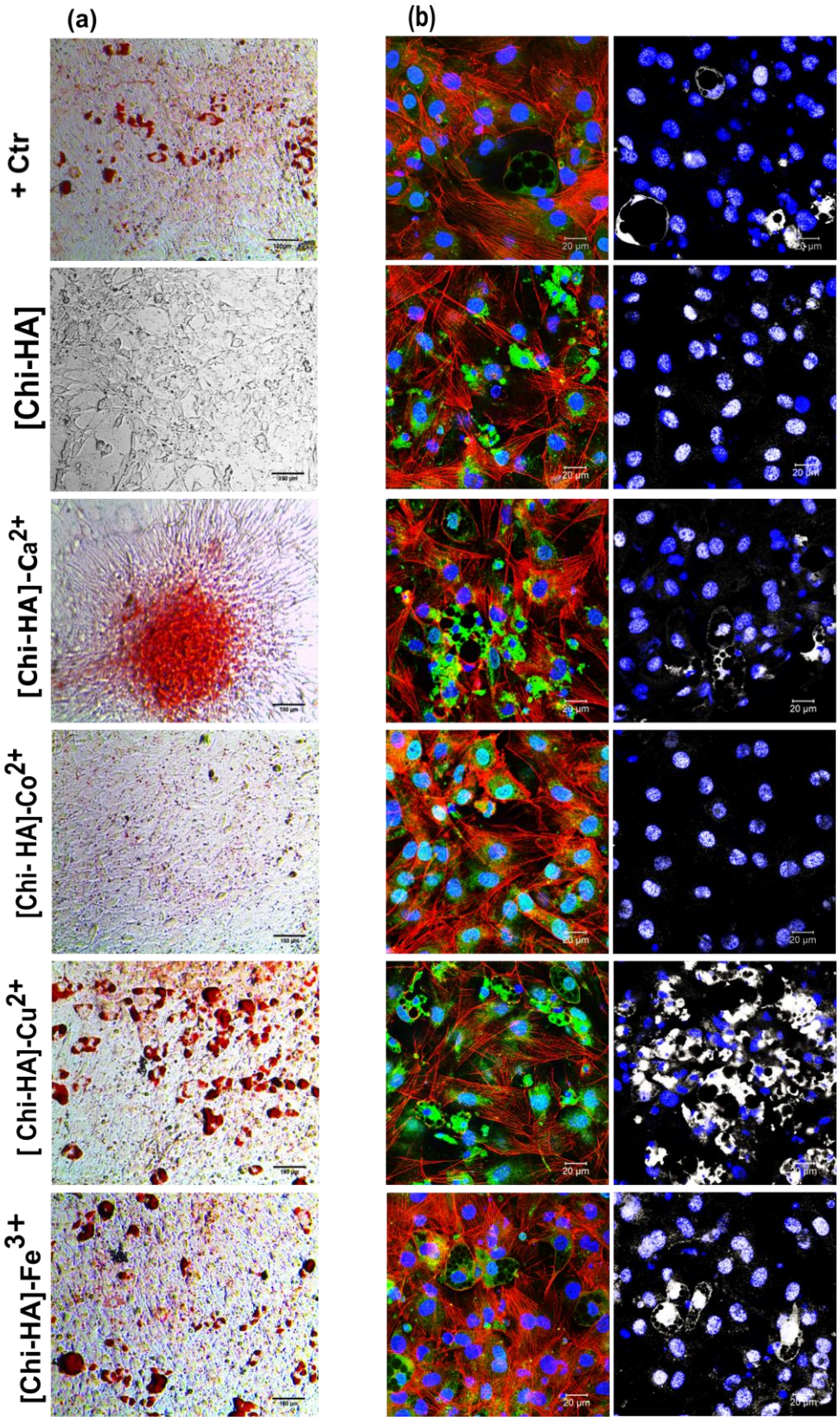

Figure 4.12: Representation of adipogenic differentiation of C3H10T1/2 cells grown for 21 days on plain and metal ion (highest concentration) doped [Chi/HA]. (a) Histochemical staining oil red to detection of lipid vacuoles (scale: 100 mm). (b) CLSM micrographs of cells immunofluorescence staining for specific adipogenic differentiation markers. (b) Cells were

stained for perilipin (**green**) and actin (**red**) and the nuclei (blue) (left lane) and glucose transporter 4 (GLUT4, white) and the nuclei (**blue**) (right lane) [scale: 20 mm].

4.4.2 Osteogenic differentiation

To determine the effect of the molecular composition of [Chi/HA] and metal ion-doped PEMs on osteogenic differentiation of C3H10T1/2, we examined the expression of osteogenic specific genes such as ALP, noggin, osterix, and Runx2 by qRT-PCR at day 14 after differentiation. The results presented in Figure.4.13 indicate that cells cultured in osteogenic media (OM) media containing dexamethasone, ascorbic acid, and ß-glycerophosphate (positive control) showed a significant upregulation of osteogenic gene expression compared to the negative control, where cells were treated with basal media (BM). Interestingly, even in the cells cultured in basal medium, metal ion-doped [Chi/HA] promoted upregulation of osteogenesis related genes. Some of these changes were statistically significant, surpassing the expression levels seen in positive control. Notably, the highest levels of ALP and noggin expression were observed in cells cultured on the Fe^{3+} doped [Chi/HA], regardless of whether the cells were cultured in plain [Chi/HA] or OM medium.

In contrast, no significant difference in the expression of Runx 2 was detected among the different metal ion-doped PEM. However, the expression of Osterix varied significantly between the across the metal ion-doped PEM, particular when the cells cultured on Fe^{3+} and Co^{2+} PEMs showing higher osterix expression of than the positive control. It is also notably that the expression of these genes was generally higher in the metal ion-doped [Chi/HA] compared to plain [Chi/HA] multilayers and the negative control. To further confirm the formation of the osteogenic matrix of C3H10T1/2 on the plain [Chi/HA] and metal ion-doped PEM, Alizarin Red S was performed after three weeks to visualize the deposition of calcium phosphate (see **Figure 4.14**). As expected based PCR results, no positive staining was obsorved in cells treated with BM on plain [Chi/HA] and negative control. In contrast, mineralized nodules staining was evident when Co^{2+} especially Cu^{2+}, were used for doping [Chi/HA].

In contrast, more pronounced positive staining for mineralised matrix formation was obsorved on Fe^{3+} doped [Chi/HA] (**Figure 4.14**). The immunofluorescence staining shown in **Figure 4.14 b**, was used to detect the expression of the bone-specific ECM protein collagen I (Col I, green staining), osteocalcin (OCN, red staining) and blue nuclear staining, in C3H10T1/2 cells and cultured in either BM or OM after three weeks days of induction. As seen in Figure 4.14 b**,** positive staining of Col and OCN was observed in positive control when the cells were cultured in OM. Additionally, metal ions-doped [Chi/HA] multilayers promoted intense staining of the fibrillar structure of newly synthesized Col I and osteocalcin, particularly when cells were

cultured on Fe^{3+} and Cu^{2+} doped [Chi/HA] in BM. Interestingly, Co^{2+} doped [Chi/HA] exhibted increased spreading and some Col I staining. In contrast, no visible staining of Col I and osteocalcin was observed on plain multilayers.

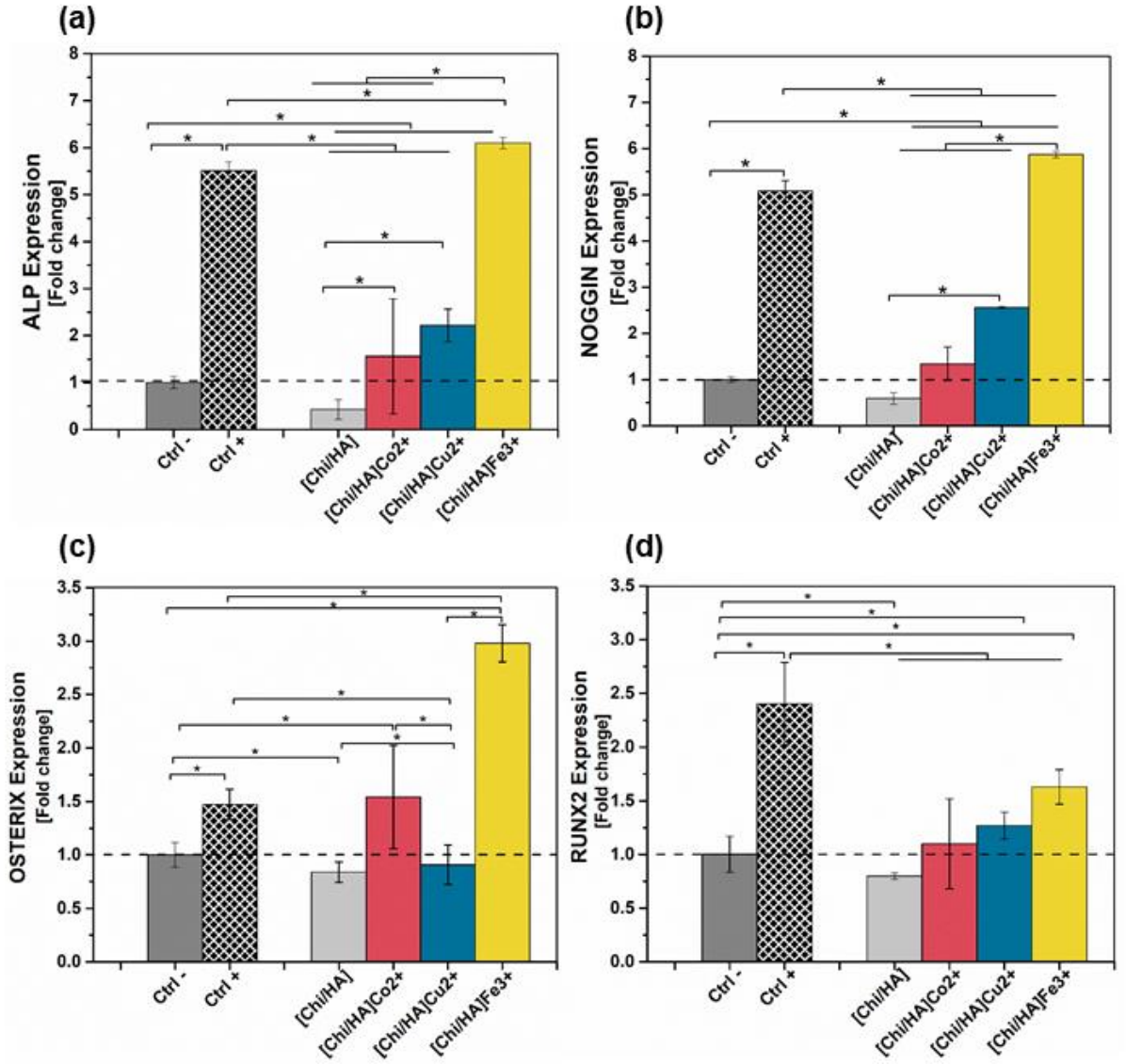

Figure 4.13: Relative expression level of osteogenic-associated genes in C3H10T1/2 cultured in basal medium (BM) grown on the plain [Chi/HA] multilayers and doped with metal ions (Co^{2+}, Cu^{2+} and Fe^{3+}). ALP (a), Noggin (b), Osterix (c) and Runx 2 (d) of expression of cells at day 14 post-osteogenic differentiation was determined by RT-PCR.

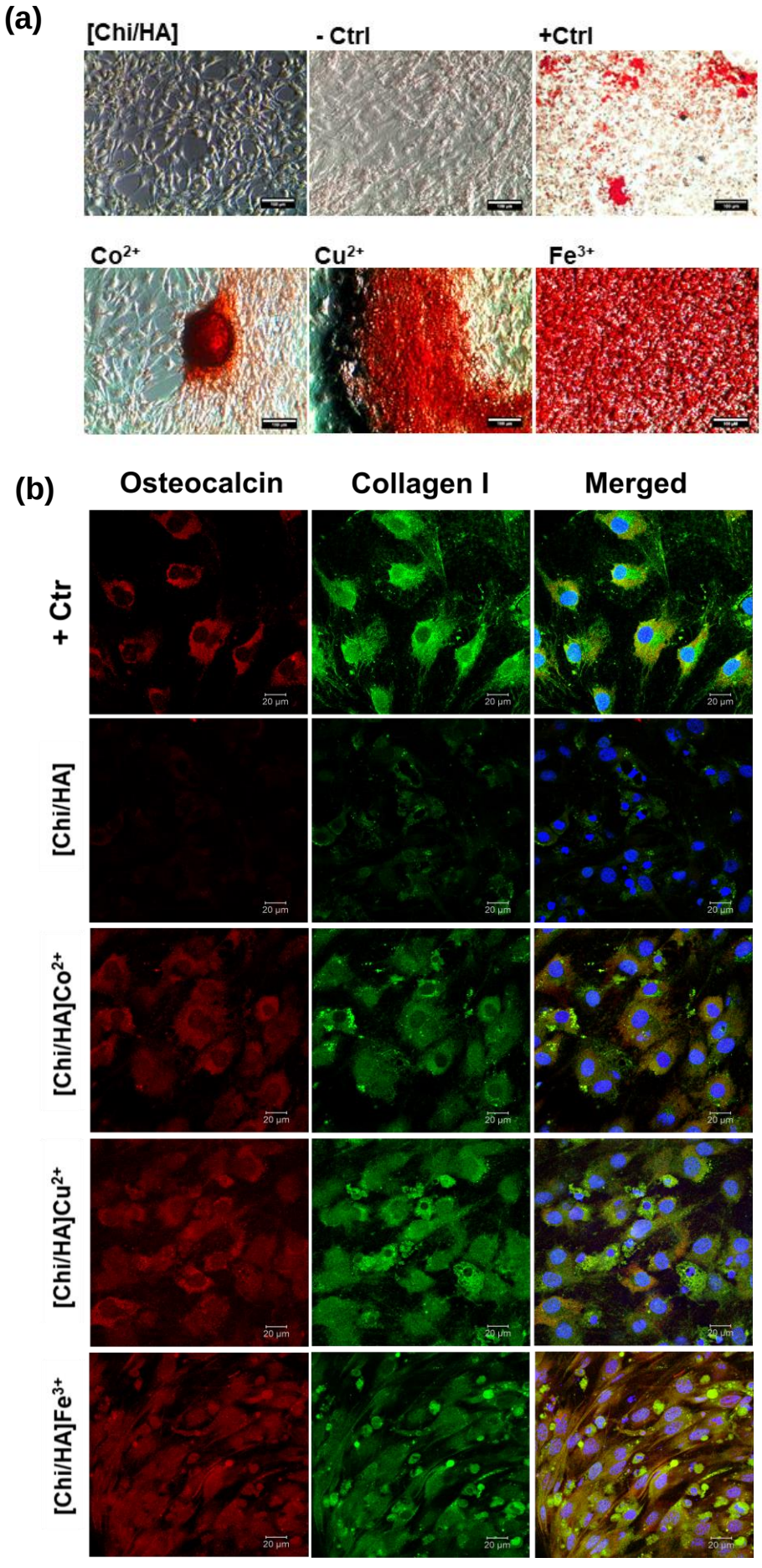
(a)
[Chi/HA]
- Ctrl
+Ctrl
Co2+
Cu2+
Fe3+
(b)
Osteocalcin
Collagen I
Merged
+ Ctr
[Chi/HA]
[Chi/HA]Co2+
[Chi/HA]Cu2+
[Chi/HA]Fe3+
20 µm

Figure 4.14: Determining osteogenic differentiation of C3H10T1/2 placed on the plain [Chi/HA] multilayers and doped with (Co^{2+}, Cu^{2+} and Fe^{3+}). **(a)** Alizarin red S solution to investigate the formation of the mineralized matrix (scale bar: 100 µm). **(b)** Immunofluorescence staining of collagen I (Col I, **green**), nuclei (**blue**) and osteocalcin (**red**) in C3H10T1/2 at day 24 post-osteogenic differentiation in the presence of BM. [Scale bar 20 µm].

Chapter 5: Discussion

This thesis focuses on studying the effects of metal ions (Ca^{2+}, Co^{2+}, Cu^{2+}, and Fe^{3+}) doped into polysaccharide-based PEMs. Chitosan serves as the polycation, and either alginate or hyaluronan serves as the polyanion, loaded with metal ions. The study aims to quantify the amount of ions taken up, identify the functional groups to which they are bound, and analyze their effects on the surface and intrinsic properties of multilayers, which subsequently influence on cell interactions. The particular focus of this work lies in exploring and comparing the effects of different types of metal ions on adipogenic and osteogenic differentiation of stem cells. The first part of the discussion centers on the characterization of multilayer formation and metal ion uptake. Subsequently, we examine the impact of exposing PEMs to metal ions on the physical properties of multilayers and the biological response of multipotent embryonic mouse fibroblasts (C3H10T1/2), including cell adhesion, growth, and differentiation. This is discussed in the following section. Finally, conclusions and suggestions for future investigations are drawn.

5.1 The physical characterization of polysaccharide-based PEM

The growth of [Chi/Alg] and [Chi/HA] multilayers formation was successfully tracked using surface plasmon resonance (SPR) and ellipsometry. The growth of the PEMs was investigated SPR through angle shift (m°) measurements, which revealed an increase in the adsorbed mass for both systems. [Chi/HA] showed a nearly linear growth pattern, whereas the angle shift for [Chi/Alg] was higher, indicating more exponential growth. This behavior is characteristic of PEMs based on polysaccharides, which is related to the in-and-out diffusion of one of the polyelectrolyte layers (PEL). Ellipsometry confirmed that both [Chi/Alg] and [Chi/HA] reached adsorption equilibrium quickly, with dry film thicknesses of 10 nm and 8.9 nm, respectively, and hydrated thicknesses of 21 nm and 18 nm. The observed difference in growth are attributed to the varying charge densities and pKa values of Alg and HA. Alginate with a higher charge density due to four carboxylic groups per dimeric, formed thicker films and exhibiting exponentially growing layers. Additionally, at pH 4, chitosan is protonated and interacts with the negatively charged polyanions, forming stable polyelectrolyte complexes [142]. NaCl at 150 mM was used to reduce electrostatic attractions, leading to bulkier multilayer structures [248]. The stronger interactions between Chi and Alg resulted in more compact films despite Alg having a lower molecular weight, wheras the lower charge density of HA allowed for a more relaxed conformation. Metal ions play a critical role in modulating protein activity and cellular functions. In this study, polyelectrolyte multilayers (PEMs) composed of chitosan (Chi) and alginate (Alg), hyaluronic acid (HA) were doped with various metal ions, including calcium (Ca^{2+}), cobalt (Co^{2+}), copper (Cu^{2+}), and iron (Fe^{3+}), which

interact with their functional groups. Ca^{2+} and Fe^{3+} ions, in particular, can be deposited in greater amounts within the PEMs, leading to increased positive ζ potentials and, in the case of Fe^{3+}, higher water contact angles, these changes may be related to the character of Ca^{2+} and Fe^{3+} ions as hard Lewis acids while Co^{2+} and Cu^{2+}, ions as Lewis acids of intermediate strength had no significant effects in this regard [249, 250]. An intriguing discovery was that the introduction of metal ions reduced the elastic modulus of the PEMs, making them less rigid than plain PEMs. Fourier transform infrared (FTIR) spectroscopy revealed that metal ions primarily interacted with the carboxylic groups of alginate and hyaluronic acid, while the hydroxyl and amino groups remained unaffected. Changes in wetting properties and surface potential were linked to improved adhesion and proliferation of multipotent C3H10T1/2 fibroblasts, compared to the non-adhesive properties of plain [Chi/Alg] multilayers. Specifically, PEMs doped with Cu^{2+} and Fe^{3+} significantly enhanced cell attachment and promoted cells differentiation, suggesting that metal ions not only alter surface characteristics but also influence bioactivity. Ultimately, metal ion-doped PEM have the potential to promote adipogenic and osteogenic differentiation.

The doping of metal ions into PEMs was expected to result in complex formation between metal ions and functional groups of polyelectrolytes, primarily involving all O and N groups, including hydroxyl groups, which are integral to the complex formation. In both the Chi/Alg and Chi/HA systems, the highest concentrations of metal ions were detected for Fe^{3+} and Ca^{2+}, followed by Cu^{2+} and Co^{2+} as measured by Inductively Coupled Plasma Mass Spectrometry (ICP-MS). In the system involving metal ions and polysaccharides like Alg and HA, the nitrogen in amino groups and the oxygen-containing functional groups (carboxylic groups) in Alg and HA are the Lewis bases, whereas the metal ions belong to different categories of Lewis acids. The Ca^{2+} and Fe^{3+} ions represent strong acids, while cobalt and copper exhibit intermediate strengths [250]. This interaction forms coordination complexes where the metal ions are coordinated by the Lewis basic sites on the polysaccharides such as the oxygen atoms in carboxylic groups, as well as nitrogen atoms in amino groups, influencing their incorporation efficiency into multilayer systems. This interpretation increases the quantity of metal ions found in both Chi/Alg and Chi/HA systems, which corresponds to the previous finding of higher binding affinity for iron compared to cobalt and copper ions [251]. Conversely, Co^{2+} and Cu^{2+} are softer acids, forming weaker bonds [249]. The increased quantity of metal ions incorporated into Alg-PEMs compared to HA-PEMs is probably related to the higher charge density, the structural conformation of alginate that favours metal ion binding (such as the "egg-box" model), and the higher affinity of alginate's carboxylate groups for metal ions [96]. Alginate's ability to form more stable and tightly bound complexes makes it more effective in incorporating metal ions than hyaluronic acid as seen in the MS-ICP studies. Additionally,

HA tends to form more flexible, hydrated structures, which may not trap metal ions as effectively as alginate. The flexibility of HA might lead to weaker or more transient metal ion interactions within HA- PEMs.

FTIR spectroscopy revealed that metal ions interact with specific functional groups (hydroxyl, carboxylic, and amino groups) of polysaccharides. The spectra showed characteristic peaks for both pure materials and the multilayers, with slight shifts and changes in intensity upon metal ion doping. The broadening and intensity changes in the peaks (e.g., O-H and N-H stretching at 3335 cm^{-1}), which are caused by the hydroxyl, carboxylic, and amine groups present in the PEM and suggest that metal ions influence the hydrogen bonding network within the multilayers. Similarly, the band at 1600 cm^{-1} exhibited a slight shift to a higher wavenumber (redshift) or lower wavenumber (blue shift), signifying interaction between the carboxylic group (COO-) of Alg and the metal ions, as reported previously [252]. The signal at 1538 cm^{-1} attributed to chitosan amino groups reacting with the alginate carboxylate groups [241], broadened after the additional of metal ions to multilayers. This broadening suggests coordination with the carboxyl group of Alg, protecting them from interaction with the amine group of Chi. The slight shifts in the C-O glycosidic bond peaks (1100 cm^{-1} and 1030 cm^{-1}) for Ca^{2+}, Co^{2+}, and Cu^{2+} suggested that this effect stems from a coordination of the ions with neighboring mannuronate and guluronate units [97, 253]. This indicates that these metal ions alter the polysaccharide backbone structure, which could impact the mechanical and chemical properties of the multilayers. The interaction between metal ions and the functional groups of chitosan (Chi) and hyaluronic acid (HA) in the [Chi/HA] multilayers was also investigated. The spectra revealed distinctive features: The multilayers [Chi/HA] displayed characteristic bands including O–H and N–H stretching at 3275 cm^{-1} that shifts to 3300cm^{-1} , carbonyl bands at 1608 and 1730 cm^{-1}. In $[Chi/HA]_{100}$ multilayers, new bands appeared at 1317 cm^{-1}, indicative of C-O and C-N amide II stretches, alongside saccharide unit vibrations between 1200 and 900 cm^{-1}. Upon doping with metal ions, slight spectral shifts were observed: Co^{2+} and Ca^{2+} induced a redshift in the amide II band to 1605 cm^{-1}, while Fe^{3+} and Cu^{2+} shifted it to 1608 cm^{-1}. The carboxylic group stretch of HA showed moderate changes, with Co^{2+} and Cu^{2+} inducing shifts to 1406 cm^{-1} and Ca^{2+} and Fe^{3+} to 1410 cm^{-1}. The bands associated with metal ions at 1070 cm^{-1} exhibited lower intensities and slight shifts towards higher wavenumbers in the spectra of Co^{2+} and Fe^{3+} doped multilayers. These findings indicate that metal ions, particularly Fe^{3+} and Ca^{2+}, significantly alter the vibrational characteristics of [Chi/HA] multilayers observed in FTIR spectra. Generally, small changes observed in the FTIR spectra, within the range of approximately ~5 to 10 cm^{-1}, indicate the involvement of oxygen (hydroxyl and carboxyl groups) in complex formation. Contrary to the prior expectations, there is no observable interaction of nitrogen (amine group) with metal ions in the studied PEM

multilayers. Hence, it was concluded that the interaction between amine groups and metal ions is not strong enough in competition to the carboxylic groups, suggesting that the amine groups do not effectively interact with metal ions. Consequently, it was determined that metal ions cannot cross-link Alg or HA and Chi by bridging oxygen and nitrogen atoms. Therefore, the term "doping" PEM with metal ions was employed instead of "cross-linking" to accurately describe the nature of the interaction. These spectroscopic changes reflect the complexation and interaction of metal ions with the functional groups of Chi and Alg or HA within the multilayer structure, suggesting potential implications for their biomedical applications.

The surface wettability of the various multilayer systems was determined by measuring the water contact angle using the sessile drop technique to evaluate the effect of the metal ions on this physical property since protein adsorption, cell adhesion, and growth are influenced by wetting properties. The study showed significant results by investigating the influence of metal ion doping on the surface wettability of both [Chi/Alg] and [Chi/HA] multilayers. Particularly, doping with a high concentration of Fe^{3+} ions significantly increases WCA typically above 70°, indicating a shift towards a more hydrophobic surface. However, upon doping with Ca^{2+}, Co^{2+}, and Cu^{2+} ions, the WCA was not within the reported range of moderately wettable surfaces, typically around 40°to 70° [33, 47]. This finding highlights the strong influence of Fe^{3+} ions in reducing surface hydrophilicity, potentially altering surface properties. It was also noted that there was a notable increase in the water contact angle (WCA) of [Chi/Alg] compared to [Chi/HA] multilayers, namely 82° and 73°, respectively. The possible reason could be that alginate (Alg) has a higher charge density than hyaluronic acid (HA). Fe^{3+} ions effectively screen carboxylic groups in PEMs due to their high charge density. The dominance of screened carboxylic groups reduces their hydrophilicity and accessibility [254], making amino groups more prominent. Consequently, the hydrophilicity of the PEM decreases. In contrast, other metal ions, present at lower concentrations and exhibiting weaker interactions (as confirmed by MS-ICP and FTIR results respectively), are unlikely to significantly impact the wettability of PEMs, with any changes expected to be minimal or moderate at most. These complexes can rearrange or expose additional hydrophilic sites on the surface, improving the ability of the multilayers to interact with water.

The surface charge density i.e. zeta potential, significantly influences protein adsorption, cell adhesion, and fate such as adhesion and proliferation [45]. Some authors propose that the zeta potential value of PEMs not only reflects the charge distribution of the outermost (terminal) layer but also the composition of layers beneath due to the existence of a swollen, conductive surface layer, which contrasts with WCA measurements, where wettability is primarily controlled by the terminal (outermost) layer composition[255]. Polycations, such as

chitosan, are assumed to increase the surface charge towards a positive value under acidic conditions, while polyanions, such as alginate, decrease the surface charge towards a negative value at basic pH levels. The study on zeta potential measurements of [Chi/Alg] polyelectrolyte multilayers (PEM), both plain and doped with high concentrations of metal ions, provides insights into how metal ion doping influences surface charge characteristics. In conclusion, metal ion doping significantly influences the surface charge properties of [Chi/Alg] PEM, particularly enhancing positive charges under acidic conditions. This finding highlights the potential of Ca^{2+} and Fe^{3+} ions to modulate surface charge dynamics, which could impact interactions with biological molecules and cells. The negligible differences observed at physiological pH (7.4) indicated that these metal ion-doped PEMs maintain biocompatibility in biological contexts. Further, the plain [Chi/HA] multilayers, with HA as the outermost layer, exhibited relatively stable negative zeta potentials at physiological pH. When doped with Co^{2+} and Cu^{2+}, the multilayers showed no significant deviation from the plain multilayers, consistent with their low uptake levels as measured by ICP-MS. In contrast, doping with Ca^{2+} and Fe^{3+} resulted in a notable increase in positive zeta potential at highly acidic conditions, indicating enhanced positive surface charge. In a low-pH (acidic) the dominance of protonated amino groups results in high potential values (e.g., zeta potential) due to the electrostatic interactions and surface charge, while Increasing pH leads to the deprotonation of carboxylic groups (but also amino groups pf CHI) that dominate then in the basic region. In the acidic region, the amino groups of Chi dominate due to their protonation results in high potential values due to the electrostatic interactions and surface charge. As the pH increases, deprotonation of both the carboxylic groups oh HA and the amino groups of Chi occurs. In the basic region, the carboxylic groups dominate due to their higher deprotonation levels. Consequently, differences in the basic range are minimal, as the high quantity of deprotonated carboxylic groups. The point of zero charge (PZC) for Co^{2+} and Cu^{2+} doped multilayers aligned closely with the plain multilayers at pH 4.2, while Fe^{3+} and Ca^{2+} doped multilayers showed a slight shift towards higher pH values (4.6 and 5.8, respectively), suggesting a shift towards more positive potentials. These findings underscore the influence of metal ions on surface charge characteristics, which could impact interactions with biological environments and applications in biomedical settings. In conclusion, surfaces with higher positive zeta potential might attract more water molecules (lower WCA), making them more hydrophilic, while surfaces with negative zeta potential might repel water (higher WCA), making them more hydrophobic. Metal ion doping can alter both the zeta potential and wettability of surfaces. Doping with positively charged metal ions (like Fe^{3+}) can increase the Coulomb interaction with carboxylic groups of Alg and HA, which lead to screening their negative charges leading to a dominance of amino groups of Chi at acidic pH, potentially making it more hydrophobic.

The comprehensive findings from atomic force microscopy (AFM) and nanoindentation studies provide an in-depth characterization of [Chi/Alg] and [Chi/HA] polyelectrolyte multilayers (PEMs) doped with various metal ions. AFM measurements, performed in a hydrated state, revealed that both plain and metal ions-doped PEMs exhibit granular surface morphologies. The granular structure of [Chi/Alg] and [Chi/HA] multilayers related to the process of film formation [247, 256]. The surface topography of plain [Chi/Alg] PEMs showed small granular structures with a roughness value of approximately 3.4 nm. However, surface roughness varied significantly with the incorporation of different metal ions. [Chi/Alg] doping with Ca^{2+} and Co^{2+} led to a smoother surface, decreasing roughness compared to the plain [Chi/Alg] and [Chi/HA] PEMs, In contrast surface topography of the plain [Chi/HA] multilayer and metal ions-doped PEMs had a granular surface morphology with slight changes to increase in roughness when Co^{2+} and Cu^{2+} were utilized. Notably, Fe^{3+}-doped PEMs exhibited significantly rougher surface compared to other metal ions and plain PEM, this highlights the increased presence of Fe^{3+} ions in both systems and their pronounced influence on the PEM structure. Overall, the surface roughness of all polyelectrolyte multilayers (PEMs), which are on a nanometer scale, can be regarded as smooth in comparison to the size of cells. This suggests that the surface roughness is unlikely to have a significant impact on cell attachment.

Additionally, nanoindentation studies offered insights into the mechanical properties of these multilayers. The plain [Chi/Alg] and [Chi/HA] PEMs had the highest elastic modulus, indicating superior stiffness compared to PEMs doped with metal ions. However elastic modulus metal ions-doped PEMs presented results contradicting our initial expectation, where we assumed that the addition of the metal ions to PEMs would improve the elastic modulus by coordination complex between neighboring polyelectrolyte chains of Chi and HA that corresponds to observe in PEM made of alginate and chitosan. The Alg-based PEMs and treatment with metal ions presented a lower modulus compared to HA-based PEMs; this could be related to the thickness as observed in a previous study; the modulus and hardness of the film decrease sharply with an increase in thickness [257]. Another explanation for the higher modulus in ultrathin films is related to strain energy density, which tends to be greater in thinner samples compared to thicker ones. If the strain remains consistent across all thicknesses, the thinner sample experiences a greater stress. This increased stress in turn leads to a higher modulus in the thinner sample. This phenomenon is particularly noticeable when the film thickness reaches nanometer scales [257].

5.2 Biological studies on serum protein adsorption, cell adhesion, and proliferation

Adhesive proteins are required to promote cell adhesion and proliferation on polyelectrolyte multilayers (PEMs), hence serum protein adsorption is an important measure of a material's

ability to support cell attachment and growth [31]. The capacity of [Chi/Alg] and [Chi/HA] PEMs to bind proteins was assessed using a conventional bicinchoninic acid (BCA) test, with 10% Fetal Bovine Serum (FBS) serving as the model protein combination. The study demonstrated that [Chi/Alg] multilayers doped with metal ions had considerably greater protein adsorption than plain [Chi/Alg]. This shows that the presence of metal ions increases the protein-binding ability of PEMs. Interestingly, the type and quantity of metal ions had no significant effect on the amount of protein adsorption. Despite the greater concentration of Fe^{3+} ions in the PEM of both systems, as assessed by Inductively Coupled Plasma Mass Spectrometry (ICP-MS) experiments, protein adsorption levels were slightly higher comparing to other metal ion-doped PEMs. The increased adsorption for Fe^{3+} doped PEMs is linked to its lower wettability (more hydrophobic surfaces tend to adsorb more proteins) [258] . This implies that certain metal ions such as Cu^{2+} can considerably improve the protein-binding ability of [Chi/HA] PEMs. The enhanced protein adsorption on metal ion-doped PEMs could be due to the interaction between metal ions and proteins, which might facilitate the binding of proteins to the PEM surface [239]. In contrast, [Chi/HA] PEMs doped with Ca^{2+} and Co^{2+} exhibited no significant change in protein adsorption when compared to plain [Chi/HA]. This suggests that not all metal ions have an identical effect on the protein-binding ability of [Chi/HA] PEMs. Furthermore, bovine serum albumin, which makes up most of FBS, has an affinity for bivalent cations like Ca^{2+}, Cu^{2+}, and Co^{2+}, which may account for enhanced protein adsorption despite different metal ion concentrations in the PEM [259]. The capability of PEMs multilayers doped with metal ions of both systems to bind to serum protein was in line with wetting properties and had a similar effect except for the Ca^{2+} doped [Chi/Alg]. The increased serum protein adsorption was found on Ca^{2+} doped [Chi/Alg] compared to Ca^{2+} doped [Chi/HA], which can relate to a softer surface lets the proteins keep their natural conformation, making it easier for them to adsorb on the surface [260]. Lower adsorption of serum protein observed on plain [Chi/Alg] than plain [Chi/HA] might be associated with high wettability, where the hydrophilicity surface adsorbs fewer proteins. On the other hand, the increase in the adsorption of serum proteins by the Cu^{2+} doped PEMs of both systems was not expected, but that corresponds with the results of the cells adhesion study in the next section, where high effects indicate the presence of adhesion protein on the substrate. The increased protein adsorption observed in metal ion-doped systems indicates enhanced bioactivity, although the specific composition of the adsorbed protein layer might differ depending on the metal ion. This difference in composition can affect subsequent interactions with cells. For example, the predominant adsorption of serum albumin might passivate the surface, while fibronectin and vitronectin binding could enhance cell interactions [33, 45].

The study investigated the adhesion and spreading of embryonic fibroblasts (C3H10T1/2) on plain and metal ion-doped multilayers was performed after 4h by the quantification of cell count and area, including visualization of actin filaments, vinculin in focal adhesions and nuclei. The cell counts significantly decreased with increasing concentrations of Cu^{2+} in both systems. However, there were no significant differences in cell count for PEMs doped with Ca^{2+} and Fe^{3+} compared to plain [Chi/HA]. Both systems exhibit increased cell spreading with Fe^{3+} and Cu^{2+} doping, but [Chi/HA] is more responsive to lower concentrations. Interestingly, at low Fe^{3+} concentrations (5mM), a more extensive cell area was observed. Both systems show minimal impact with Ca^{2+} and Co^{2+}, but their overall responses depend on the specific metal ion and concentration used. Different metal ions can interact differently with polyelectrolytes and proteins. The promoting effect of Fe^{3+} might have a specific coordination complex with protein functional groups that enhance adsorption and subsequent supports cell adhesion and spreading. Additionally, the strong effect of iron ions is particularly consistent with the findings of previous studies, which demonstrated that Fe^{3+} doped alginate films specifically enhanced the binding of fibronectin and vitronectin, enhancing cell attachment. In contrast, alginate films doped with Ca^{2+} did not demonstrate this advantageous effect [131]. As high concentrations of copper can cause cytotoxic effects thus, maintaining the proper ion concentration is crucial [261]. Nevertheless, Cu^{2+} plays an important role in activating focal adhesion and actin cytoskeleton pathways; this is especially advantageous for cell-doped alginate films since they selectively increase focal adhesion binding [261]. Despite this, cell adhesion also depends on substrate stiffness; a softer surface may inhibit cell adhesion and spread [122, 262]. However, decreases in elastic moduli after metal ions doping in PEM were demonstrated as unrelated because they are still very high in a range that supports cell adhesion and spreading fibronectin and vitronectin, which enhances cell attachment.

Furthermore, the enhanced vinculin expression and actin filament organization in cells seeded on Fe^{3+}-doped [Chi/HA] suggest that Fe^{3+} ions may facilitate stronger focal adhesion and cytoskeletal interactions, promoting cell spreading. In contrast, higher concentrations of Ca^{2+} and Co^{2+} ions might disrupt these processes, leading to reduced cell size and vinculin expression. Also, the increased nuclear staining of CD44 in cells on Co^{2+} and Cu^{2+}-doped [Chi/HA] indicated that these metal ions may influence the signaling pathways mediated by CD44, enhancing cell adhesion and spreading. Previous studies have demonstrated that the nuclear translocation of CD44 is associated with the activation of the transcription factor STAT3, which binds to the cyclin D1 promoter, thereby promoting cell proliferation [263]. Likewise, the study was conducted on the adhesion of embryonic fibroblasts (C3H10T1/2) on plain and metal ion-doped [Chi/Alg] multilayers, and it was observed that Fe^{3+} and Cu^{2+} may promote cell adhesion and spreading by enhancing interactions between the metal ions and

the polyelectrolytes and proteins, facilitating the formation of focal adhesions and actin filament organization. Fe^{3+} ions, even at low concentrations, create favourable conditions for cell spreading and strong focal adhesions, This is related to an enhanced serum protein adsorption and reduced surface wettability to plain [Chi/Alg] which is related to the binding of attachment factors like vitronectin from serum and ligation of integrins, improving the adhesion and spreading of cells [33, 45, 264]. Furthermore, the lack of significant effects on cell count and weak expression of focal adhesions at lower concentrations suggest that Ca^{2+} and Co^{2+} may not interact as strongly with the polyelectrolytes and proteins to enhance cell adhesion. However, higher concentrations slightly improve cell spreading, possibly due to increased ionic interactions that facilitate moderate focal adhesion formation. Moreover, the multilayers containing Fe^{3+} at low concentrations exhibited the highest cell spreading and longitudinal distribution of actin filaments with well-expressed vinculin-positive focal adhesions due to several possible reasons related to the unique biochemical interactions between iron ions, the polyelectrolytes, and the cells. Iron ions are essential for several cellular functions. These activities can boost cellular activity and encourage widespread cell spreading and adhesion. The presence of iron may promote cell metabolism, resulting in enhanced actin filament organization and focal adhesion production [265]. In addition, Fe^{3+} ions have a high propensity for attaching to numerous functional groups in proteins, including carboxylate and phosphates [13]. This strong binding can stabilize the protein complexes involved in cell adhesion and spreading, facilitating the creation of focal adhesions and ordered actin filaments. The unique coordination complex of Fe^{3+} might result in stronger and more stable interactions with polyelectrolytes and cell surface proteins [265]. Fe^{3+} might influence the activation of focal adhesion kinase (FAK), a critical protein in the formation of focal adhesions and actin organization [130, 264]. Enhanced FAK activation can lead to better focal adhesion formation and cytoskeletal arrangement, contributing to the observed cellular behaviours. Cu^{2+} has a strong affinity for various protein functional groups, which can stabilize focal adhesions and promote the organization of actin filaments. The coordination complex of Cu^{2+} with proteins might differ from that of Fe^{3+}, leading to variations in cell morphology and focal adhesion patterns [261]. Overall, Fe^{3+} and Cu^{2+} distinct bioactivity, biochemical and mechanical interactions with [Chi/Alg] multilayers and cells lead to reported variations in cell spreading, actin filament structure, and focal adhesion formation.

The study investigated cell proliferation and morphology on plain [Chi/Alg], [Chi/HA] and metal ion-doped PEM. The QBlue assay quantified viable cells after 24 and 72 hours, showing varying effects of metal ions on cell growth. Cells on plain multilayers [Chi/HA] exhibited increased metabolic activity and formed confluent layers after 24 hours. The promoting effect of metal ions in PEM significantly increased cell adhesion and proliferation when HA as

polyanion, which may be due to the stimulation of CD44 clustering and the organization of cytoskeletal structures [266]. In both systems of results, the presence of metal ions in PEM influences cell growth. This influence varies depending on the metal ion concentration and the specific ion used. Both studies observed changes in cell behaviour over time 24 and 72 h. Initially observed effects (such as inhibition or promotion of cell growth) may evolve into different outcomes over longer incubation periods. Both studies highlight the concentration-dependent effects of metal ions. For instance, lower concentrations of Co^{2+} initially inhibit cell growth, while higher concentrations promote cell aggregation followed by increased spreading. Similarly, Cu^{2+} and Fe^{3+} show varying effects based on concentration, affecting cell proliferation and morphology. Results concerning the growth of C3H10T1/2 cells on multilayers doped with Cu^{2+} and Fe^{3+} are in good agreement with the cell adhesion studies since these metal ions are likely to target inside the cell by integrin-mediated signaling pathways such as Focal Adhesion Kinase (FAK), where integrin engagement activates FAK, which then initiates signaling cascades involved in cell adhesion, and proliferation [130, 267]. Metal ions could modulate FAK activation and downstream signaling. The findings related to the growth of C3H10T1/2 cells on multilayers treated with Cu^{2+} and Fe^{3+} align well with adhesion studies, where cell spreading is closely associated with integrin ligation and subsequent signal transduction processes, both of which play crucial roles in cellular attachment and proliferation [76, 268]. In addition, the changes in physical properties of multilayers, the interaction between function group of polycation (Chi) and polyanions (HA, Alg), along with the specific bioactivity of metal ions, was expected to influence cell behaviour [202, 269, 270].

5.3 Cell differentiation

The effect of PEMs multilayers doped with the highest concentration of metal ions on adipogenic and osteogenic differentiation of the multipotent mouse cell line C3H10T1/2 cells was studied.

5.3.1 Adipogenic differentiation of C3H10/T1/2 cells

Histochemistry staining of lipid vacuoles using Oil red O in cells cultured with dexamethasone as an adipogenic induction medium (positive control) demonstrated enhanced formation of neutral lipids in the cytoplasm. Dexamethasone activates glucocorticoid receptors, leading to the expression of genes critical for adipogenesis, such as PPAR ɣ (peroxisome proliferator-activated receptor gamma) and C/EBPα (CCAAT/enhancer binding protein alpha) [185, 271]. Increased in perilipin expression was indicative of enhanced lipid storage and intracellular lipids content [238]. Furthermore, the high expression of Glut4 demonstrated that the cells could respond to insulin [237]. In contrast, the plain [Chi/Alg] and [Chi/HA] multilayers did not

support adipogenesis. While the plain [Chi/HA] multilayers did not promote lipid accumulation in the cells, they exhibited weak expression of perilipin and GLUT4, consistent with previous studies suggesting that HA may promote adipogenic differentiation in soft tissue engineering scaffolds [272]. The enhanced differentiation in [Chi/HA] multilayer, evidenced by larger lipid vacuoles stained with Oil Red and a stronger adipogenic marker expression, was pronounced when doped with Cu^{2+} and Fe^{3+}, in comparison to [Chi/Alg] doped with the same ions. Multilayers doped with Fe^{3+} and Cu^{2+} of both systems significantly promoted adipogenic differentiation, as demonstrated by lipid vacuoles formation and increased perilipin and GLUT4 expression. This effect may be attributed to ability of Fe^{3+} and Cu^{2+} ions to interact with cellular signaling pathways that regulate adipogenesis. These ions likely activate transcription factors and signaling cascades, enhancing differentiation from preadipocytes into adipocytes. Specifically, PPARγ and C/EBPα, essential transcription factors for adipocyte differentiation and lipid accumulation, are upregulated by Fe^{3+} and Cu^{2+} [185, 273].

Also, the presence of Fe^{3+} ions within multilayers influences the surface properties of PEMs, such as surface charge, and wettability, which affect cell adhesion, spreading, and differentiation. For instance, positively charged surfaces, observed in Fe^{3+} doped PEMs with zeta potential, and enhanced cell adhesion and vinculin-positive focal adhesions compared to the plain PEMs. Moreover, reduced hydrophilicity caused by Fe^{3+} doping, as indicated by increased water contact angle (WCA), facilitate the attachment by decreasing hydration forces [258, 274]. Further, metal ions such as Cu^{2+} and Fe^{3+} may affect cellular metabolism, promoting lipid accumulation and the formation of lipid vacuoles characteristic of mature adipocytes. This effect is observable through increased Oil Red O staining, indicating higher lipid content in cells cultured on these doped multilayers. Fe^{3+} and Cu^{2+} ions also modulate gene expression related to adipogenesis, including the upregulation of perilipin and GLUT4. These proteins are involved in lipid metabolism and glucose uptake, respectively, essential for adipocyte function. Cells can absorb copper ions via the ATP7A transporter protein, promoting the differentiation of MSCs into the adipogenic lineage. The significant expression of GLUT4 and perilipin accompanies this process [275]. According to a previous study, where iron-related genes such as IRP1 play a critical role in adipocyte physiology [276]. Therefore, the finding that Fe^{3+} doping of multilayers promoted adipogenesis indicated an effect of Fe^{3+} ions bound to these PEM. Interestingly, finding was that cells seeded on Ca^{2+} doped PEMs enhanced the adipogenic differentiation because calcium can regulate and stimulate adipogenic differentiation via (PPAR γ) receptor and (cAMP) pathways [205, 206]. Overall, in both PEM systems, the presence of metal ions (Fe^{3+}, Cu^{2+}, and Ca^{2+}) promotes adipogenic differentiation. This is evidenced by the formation of lipid vacuoles stained with Oil Red and the increased expression of adipogenic markers (perilipin and GLUT4). By contrast, Co^{2+}

doped with PEMs of both systems showed no significant support for adipogenesis, as evidenced by weak or absent staining for lipid vacuoles and adipogenic markers. These findings correspond with reports that Co^{2+} inhibits adipogenesis and suppresses markers like PPARγ [277]. Perilipin and GLUT4 are consistently expressed in cells cultured on Fe^{3+}, Cu^{2+}, and sometimes Ca^{2+} doped multilayers, indicating robust adipogenic differentiation. This expression pattern is localized to lipid droplets and throughout the cytoplasm, characteristic of mature adipocytes. The bioactivity of Fe^{3+} and Cu^{2+} ions appears to play a critical role in promoting adipogenic differentiation across both studies. These ions likely interact with cellular signaling pathways and surface properties of the multilayers to enhance adipocyte maturation and function. Interestingly, Fe^{3+} and Cu^{2+} doped multilayers show adipogenic marker expression comparable to cells cultured in specific adipogenic differentiation media. This suggests that these metal ions effectively mimic or enhance adipogenic differentiation signals normally provided by specialized culture conditions. Studies on adipogenic differentiation of C3H10T1/2 fibroblasts indicate that effect of metal ions doping with PEMs multilayers cannot be attributed simply changes in physical surface properties, which influence cellular attachment and spreading. Instead, the presence of specific metal ions, such as Cu^{2+} and Fe^{3+}, appears to play a more direct role in guiding cellular fate. More specifically, findings suggest that C3H10T1/2 fibroblasts exhibit a more spread-out phenotype on Cu^{2+}- and Fe^{3+}-doped PEMs. In line with the study by McBeath et al., which showed that increased cell spreading tends to osteogenic differentiation, while a round phenotype of cells promotes adipogenesis in MSCs [243]. In this study, C3H10T1/2 fibroblasts displayed rounder cell phenotypes resulting from Ca^{2+} doping on [Chi/Alg] multilayers promoted differentiation toward the adipogenic lineage, while Fe^{3+} and Cu^{2+} doping multilayers induced more spread-out phenotypes promote to adipogenic differentiation. This suggests that the release or presentation of metal ions by the multilayers plays a key role in directing cell differentiation [270, 278]. Although the low quantities of metal ions (Ca^{2+}, Cu^{2+} and Fe^{3+}) present in the multilayers are evidently bioactive and impactful. Their effects include enhancing lipid accumulation, modulating gene expression, and influencing cellular metabolism. This bioactivity highlights their critical role in adipogenic differentiation, even at low concentrations.

5.3.2 Osteogenic differentiation of C3H10T1/2 cells

To see the effect of PEMs multilayers doped with metal ions on osteogenic differentiation of C3H10T1/2 cells. The positive control of cells treated with osteogenic media (OM) supplements dexamethasone, ascorbic acid (Asc), and ß glycerophosphate to stimulate osteogenic differentiation. Dexamethasone activates the expression of Runx2 which acts as transcription factor for procollagen genes, particularly type I collagen, which is the most

abundant collagen in bone matrix [279]. Asc is important for osteogenic differentiation because it is a cofactor for enzymes that hydroxylates the amino acids such as proline and lysine in pro-collagen, which is required for the formation of the helical structure of the collagen I into the ECM for bone structure [279]. β-Glycerophosphate is a phosphate source required for mineralization [280]. Moreover, dexamethasone (Dex), in combination with ascorbic acid (Asc) and ß-glycerophosphate (β-Gly), regulates the osteogenesis of stem cells with mineralization in vitro [280]. Cells treated with osteogenic media (OM) containing the aforementioned supplements exhibited a significant upregulation in the gene expression of all four markers, demonstrating robust osteogenic differentiation in the positive control group. The osteogenic differentiation of C3H10T1/2 cells cultured in basal medium (BM) (negative control) on either plain PEMs or PEMs doped with metal ions was assessed by analyzing the expression of key osteogenic markers, such as ALP (alkaline phosphatase), noggin, osterix, and Runx2, through qRT-PCR at day 14 post-differentiation.

This study explored the effects of metal ion doping on [Chi/Alg] and [Chi/HA] PEMs, focusing on their ability to promote osteogenic differentiation of C3H10T1/2 cells. The results highlighted significant differences in the performance of these systems, influenced by the composition of the PEMs and the type of metal ions incorporated. Interestingly, when C3H10T1/2 cells were cultured on metal ions-doped [Chi/Alg] PEMs in BM, an increase in the expression of osteogenic markers was observed compared to cells on plain [Chi/Alg] PEMs. This suggests that the metal ions within the PEMs play an important role in promoting differentiation, even in the absence of osteogenic media. Among the metal ions, Fe^{3+}-doped [Chi/ALg] notably enhanced the expression of ALP and Noggin, which are critical markers for early osteogenic differentiation. Fe^{3+} also enhanced a significantly higher expression of Osterix, a transcription factor essential for bone formation, surpassing even the positive control treated with osteogenic media. Similarly, Cu^{2+}-doped PEMs showed a marked increase in the expression of ALP, noggin, and Osterix compare to plain [Chi/Alg], further supporting the idea that these ions can effectively promote osteogenesis. Co^{2+}-doped [Chi/Alg] demonstrated a substantial increase in Runx2 expression, a key transcription factor involved in osteoblast differentiation and bone development. It is also interesting to observe that multilayers of plain [Chi/HA] showed lower markers expression than plain [Chi/Alg] and negative control, which corresponds with previous studies that demonstrated that HA promoted chondrogenic differentiation because of the partially mimicking ECM of bone and cartilage [281, 282], while and Alg enhanced osteogenic MSC differentiation [283]. However, [Chi/HA] doped with Co^{2+}, Cu^{2+} and Fe^{3+}, cells cells exhibited significantly higher expression of key osteogenic markers ALP**,** noggin**,** Runx2**,** and Osterix compared to cells on plain [Chi/HA]. Interestingly, Fe^{3+} doping in [Chi/HA] led to expression levels of ALP, noggin and osterix that surpassed those of

cells cultured in osteogenic media (OM). Metal ions such as Fe^{3+}, Cu^{2+}, and Co^{2+} are known to directly influence signaling pathways involved in osteogenic differentiation such as MAPK pathways [284] . Their interaction with HA-dominant PEMs may enhance these effects more significantly than with Alg. In addition, the result exhibited that multilayers [Chi/HA] doped with metal ions were higher expression markers compared to [Chi/Alg] doped with metal ions, which could be related to HA can bind to a variety of cell surface receptors named hyaladherins, such as CD44 and RHAMM [266] . CD44 proteins are involved in a diversity of cellular functions, including growth and differentiation into osteogenic or chondrogenic pathway [266, 285]. The expression of ALP is an early bone marker protein and an essential enzyme for the mineralization of the extracellular matrix, promoting the formation of hydroxyapatite crystals in the bone matrix [286]. The metal ion-doped [Chi/Alg] showed weak ALP expression compared to the metal ion-doped [Chi/HA]. This lack of ALP gene translation can be influenced by modifications such as phosphorylation, proteolysis of essential elements of the translational machinery, and specific trans-acting factors such as RNA-binding proteins and miRNA [287]. On the other hand, noggin may block BMP signalling to promote the maturation of osteoblastic cells, but it may not block BMP action to induce cells into osteoblastic pathways at a competent stage. In addition, noggin may have a beneficial function in membranous bone formation [288], which could be a reason for increasing the expression of Noggin in metal ions-doped PEMs multilayers of both systems. Another crucial transcription factor is osterix, which regulates gene expression when pre-osteoblasts differentiate into osteocytes in the final stage [289]. Compared to positive control, the osterix expression marker was significantly higher when Fe^{3+} was used in both systems [Chi/Alg] and [Chi/HA]. We assume the cells enable complete osteogenesis compared to the negative and positive controls. Runx2 is a zinc finger transcription factor that is essential in osteoblast and osteoclast differentiation as well as bone remodeling, which could, on one side, explain the reason behind the lower expression of Runx2 in cells grown on [Chi/HA]-Fe^{3+} compared to positive control. Furthermore, Runx2 triggers the expression of major bone matrix genes during the early stages of osteoblast differentiation. It promotes the production of proteins such as osteocalcin (OSC), collagen I and osterix [290, 291]. Moreover, the increase in Runx2 expression observed when Co^{2+} was used is probably due to the cobalt can induce molecular responses to low oxygen (hypoxia) through changing some genes such as (HIF-1a) and (VEGF) [292]. The qRT-PCR shows that increased expression levels varied depending on the type of metal ions and the systems. The study also investigated calcium phosphate deposition after three weeks of post-differentiation through Alizarin red staining, which specifically interacts with hydroxyapatite to identify mineralized extracellular matrix (ECM). This staining revealed the formation of mineralized nodules on cells grown on Cu^{2+} and Fe^{3+}-doped PEMs of both

systems, even in the absence of inducing osteogenic media, suggesting that these metal ions effectively promote mineralization. Interestingly, Fe^{3+} doped multilayer PEMs showed stronger positive staining of mineralized matrix formation. Co^{2+}-doped PEMs of both syatems also showed enhanced staining, further confirming the role of metal ions in accelerating osteogenic differentiation and mineralized matrix formation. In contrast, plain [Chi/Alg] PEMs exhibited only faint staining, highlighting the critical role of metal ions, while plain [Chi/HA] PEMs exhibited an absence of mineralization.

Further analysis of osteogenic differentiation was conducted via immunofluorescence staining for collagen I (Col I) and osteocalcin (OCN), both crucial markers of bone formation. After three weeks of C3H10T1/2 fibroblasts cells incubation in both OM and BM, positive staining was observed, particularly in cells cultured with metal ions-doped PEMs. The cells grown on Fe^{3+}-doped PEMs of both systems displayed strong expression of Col I, with an organized fibrillary structure, and higher levels of osteocalcin, indicating enhanced matrix formation and osteoblast activity. Cu^{2+}-doped PEMs of [Chi/Alg] and [Chi/HA] also promoted significant expression of Col I and OCN, suggesting strong osteogenic potential. In contrast, cells grown on plain [Chi/Alg] PEMs exhibited slightly staining, indicate reduced osteogenic differentiation and matrix development. However, cells cultured in basal medium (BM) and on the plain [Chi/HA] multilayers failed to form osteoinductive proteins like Col I and could not favour the differentiation of C3H10T1/2 into osteogenic lineage. The osteogenic differentiation exhibited by strong standing when cells grown in (OM) (positive control).

These findings collectively demonstrate that PEMs treatment with metal ions, particularly Fe^{3+} and Cu^{2+}, significantly enhances osteogenic differentiation of C3H10T1/2 cells, as evidenced by increased expression of key osteogenic markers, mineralization, and matrix formation. The ability of these metal ions to promote osteogenesis, even without the use of additional osteogenic supplements, highlights their potential for use in bone regeneration. In consideration, iron is the free-bound ion component of the procollagen proline hydroxylase and the procollagen lysine hydroxylase, hence both enzymes affect the hydroxylation of proline and lysine remains in the stability of collagen [223]. Moreover, Wang and colleagues reported the positive effect of iron oxide nanoparticles (IONPs) on the osteogenic differentiation of human BMSCs in vitro [284]. The doping multilayers with Co^{2+} led to a diminished proliferation rate, as confirmed by the results of the cell proliferation study using (Q blue) while enhancing the ability of C3H10T1/2 cells to differentiate into the osteogenic lineage. Where the Co^{2+} led to increased HIF-1α and VEGF mRNA expression, hence both molecules play an important role in regulating angiogenic-osteogenic coupling [204, 292]. Also, the copper stimulates the collagen fiber deposition of osteogenic cell differentiation, which corresponding with study showing that copper stimulates the osteogenic differentiation

of MSCs [293]. Overall, the study on the osteogenic differentiation of multipotent C3H10T1/2 fibroblasts revealed that the influence of doping PEMs with metal ions on the cell's fate could not fully explained by alterations in the surface's physical properties, despite their role in the attachments and spreading of C3H10T1/2 fibroblasts. Cell spreading promotes the deposition of the osteogenic matrix during bone formation. These variations in cell shape are driven by changes in the expression of integrins, cadherins, and cytoskeletal proteins [243, 294]. McBeath et al. demonstrated that cell spreading increases osteoblast differentiation in preosteoblastic progenitor cells. Previous results revealed a significant increase in cell spreading within the PEM system [Chi/Alg] and [Chi/HA]-doped with metal ions, particularly Fe^{3+}. In these cases, it is noteworthy that the differentiation process is influenced not only by the presence of metal ions but also by the observed spreading phenotypes of cells. These results confirmed the protein production of osteogenic proteins at later stages but also supported that the release from or presentation of metal ions by multilayers can induce osteogenic differentiation. The latter was proven when looking at Alizarin red staining of the mineralized matrix, which was more pronounced in cells cultured on PEMs doped with metal ions than in plain PEMs. The qRT-PCR results correspond closely with the observations from CLSM images of immunostaining. Altogether, this confirms that the osteogenic markers expressed in cells grown on PEMs exposed to metal ions, especially Fe^{3+} were efficiently translated into proteins and were accompanied by real osteoblast development, though the quantities of metal ions are very low, obviously bioactive. Overall, Fe^{3+} and Cu^{2+} ions assist in promoting differentiation processes i.e., adipogenic and osteogenic differentiation. These ions enhance the expression of specific markers (osteogenic markers like ALP, noggin, osterix, and Runx2; and adipogenic markers like perilipin and GLUT4) and promote the formation of characteristic structures (mineralized nodules and lipid vacuoles) in their respective differentiation pathways. This suggests that Fe^{3+} and Cu^{2+} ions are crucial in modulating cellular signaling pathways and surface properties to support the differentiation and maturation of cells in both osteogenic and adipogenic contexts.

Conclusion and outlook

Polyelectrolyte multilayers (PEMs) with metal ions offers a promising approach to guiding stem cell differentiation on implants surfaces and tissue engineering, with potential applications in regenerating tissues such as bone, cartilage. This study contributes to the development of functional nanostructured materials with specific bioactivity for tissue engineering and regenerative medicine applications. The aim of the present PhD work was to investigate the effects of doping PEMs multilayers with metal ions on the surface properties of the PEMs and the biological processes such as protein adsorption, cell adhesion, proliferation and differentiation. PEMs multilayers fabricated using the layer-by-layer (LbL) technique, employing chitosan (Chi) as polycation and either alginate (Alg) or hyaluronic acid (HA) as polyanion. ICP-MS analysis confirmed the successful incorporation of Ca^{2+}, Co^{2+}, Cu^{2+}, and Fe^{3+} into [Chi/Alg] and [Chi/ HA] multilayers. Notably, Ca^{2+} and Fe^{3+} exhibited strong ionic interaction with the carboxyl group of Alg and HA, whereas Co^{2+} and Cu^{2+} were incorporated in lower amounts, particularly in [Chi/ HA] multilayers. This finding suggests that the metal ions primarily bind to the functional groups in pendant fashion, implying that there is no significant crosslinking of polyelectrolytes within the multilayers but instead doping of the system with metal ions. Furthermore, this study demonstrated that different metal ions, in terms of both type and concentration, had only a slight impact on the surface properties of PEMs, except for Fe^{3+}, which significantly reduced surface wettability. Variations in polyelectrolyte type and metal ions significantly influenced the cellular behavior of C3H10T1/2 cells, including adhesion, proliferation, and differentiation. These effects were primarily dependent on the type of metal ion rather than its concentration or the changes in physical properties. For instance, even small amounts of Cu^{2+} doped PEMs of both systems significantly enhanced cell adhesion and proliferation. In terms of differentiation, metal ions played a crucial role in directing lineage commitment. Although, $Ca^{2+}$was present in large amount of in [Chi/Alg] multilayers, but did not strongly induce adipogenic differentiation as expected. However, this study demonstrates that doping PEM with Cu^{2+} and Fe^{3+}, can be used to promote adipogenic differentiation of C3H10T1/2 cells. Conversely, even small amount of Co^{2+} in PEMs multilayers of both systems promoted osteogenic differentiation. The significant effects of these trace amounts suggest a strong interaction between the cells and the metal ions bound to the polysaccharides in the PEM multilayers. Interestingly, Co^{2+}, Cu^{2+}, and Fe^{3+} doped [Chi/Alg] and [Chi/ HA] multilayers promoted osteogenic differentiation in the absence of an induction medium. The differentiation process was primarily influenced more by bioactivity of metal ions and PEM composition rather than the changes in the multilayers' physical properties. Importantly, [Chi/HA] PEMs exhibited superior osteogenic potential compared to [Chi/Alg],

likely due to hyaluronic acid’s interaction with CD44 and RHAMM receptors, which enhance osteoblast differentiation. Overall, the thin and soft PEM of alginate/hyaluronic and chitosan enriched with metal ions can control stem cells' adhesion, proliferation, and differentiation. These results provided new insights that may be of interest for future studies, suggesting the potential to use of this type of surface coating, without the addition of cytokines to develop bioactive implant materials. Such materials could find application in tissue engineering to support healing and regenerative medicine, particularly in processes like bone regeneration.

References

[1] A.J. Salgado, O.P. Coutinho, R.L. Reis, Bone tissue engineering: state of the art and future trends, Macromolecular bioscience 4(8) (2004) 743-765.

[2] F.J. O'brien, Biomaterials & scaffolds for tissue engineering, Materials today 14(3) (2011) 88-95.

[3] B.D. Ratner, A.S. Hoffman, F.J. Schoen, J.E. Lemons, Biomaterials science: an introduction to materials in medicine, MRS Bull 31 (2006) 59.

[4] E. Eisenbarth, Biomaterials for tissue engineering, Advanced Engineering Materials 9(12) (2007) 1051-1060.

[5] T.J. Keane, S.F. Badylak, Biomaterials for tissue engineering applications, Seminars in pediatric surgery, Elsevier, 2014, pp. 112-118.

[6] S. Bauer, P. Schmuki, K. Von Der Mark, J. Park, Engineering biocompatible implant surfaces: Part I: Materials and surfaces, Progress in Materials Science 58(3) (2013) 261-326.

[7] H. Qu, H. Fu, Z. Han, Y. Sun, Biomaterials for bone tissue engineering scaffolds: A review, RSC advances 9(45) (2019) 26252-26262.

[8] M. Abbasian, B. Massoumi, R. Mohammad-Rezaei, H. Samadian, M. Jaymand, Scaffolding polymeric biomaterials: Are naturally occurring biological macromolecules more appropriate for tissue engineering?, International journal of biological macromolecules 134 (2019) 673-694.

[9] A.H. Rouchi, M. Mahdavi-Mazdeh, Regenerative medicine in organ and tissue transplantation: shortly and practically achievable?, International journal of organ transplantation medicine 6(3) (2015) 93.

[10] M.S.B. Reddy, D. Ponnamma, R. Choudhary, K.K. Sadasivuni, A comparative review of natural and synthetic biopolymer composite scaffolds, Polymers 13(7) (2021) 1105.

[11] A. Bharadwaz, A.C. Jayasuriya, Recent trends in the application of widely used natural and synthetic polymer nanocomposites in bone tissue regeneration, Materials Science and Engineering: C 110 (2020) 110698.

[12] R.L. Reis, N.M. Neves, J.F. Mano, M.E. Gomes, A.P. Marques, H.S. Azevedo, Natural-based polymers for biomedical applications, Elsevier2008.

[13] T.E. Kruger, A.H. Miller, J. Wang, Collagen scaffolds in bone sialoprotein-mediated bone regeneration, The Scientific World Journal 2013 (2013).

[14] B.A. Harley, L.J. Gibson, In vivo and in vitro applications of collagen-GAG scaffolds, Chemical Engineering Journal 137(1) (2008) 102-121.

[15] Y. Liang, K.L. Kiick, Heparin-functionalized polymeric biomaterials in tissue engineering and drug delivery applications, Acta biomaterialia 10(4) (2014) 1588-1600.

[16] E. Tognana, A. Borrione, C. De Luca, A. Pavesio, Hyalograft® C: hyaluronan-based scaffolds in tissue-engineered cartilage, Cells Tissues Organs 186(2) (2007) 97-103.
[17] A. Köwitsch, G. Zhou, T. Groth, Medical application of glycosaminoglycans: a review, Journal of tissue engineering and regenerative medicine 12(1) (2018) e23-e41.
[18] S. Ruppert, T. Hawn, A. Arrigoni, T. Wight, P. Bollyky, Tissue integrity signals communicated by high-molecular weight hyaluronan and the resolution of inflammation, Immunologic research 58 (2014) 186-192.
[19] K.R. Taylor, R.L. Gallo, Glycosaminoglycans and their proteoglycans: host-associated molecular patterns for initiation and modulation of inflammation, The FASEB Journal 20(1) (2006) 9-22.
[20] N.S. Gandhi, R.L. Mancera, The structure of glycosaminoglycans and their interactions with proteins, Chemical biology & drug design 72(6) (2008) 455-482.
[21] G.F. Muschler, C. Nakamoto, L.G. Griffith, Engineering principles of clinical cell-based tissue engineering, JBJS 86(7) (2004) 1541-1558.
[22] D.S. Katti, S. Lakshmi, R. Langer, C. Laurencin, Toxicity, biodegradation and elimination of polyanhydrides, Advanced drug delivery reviews 54(7) (2002) 933-961.
[23] T. Sharkawi, F. Cornhill, A. Lafont, P. Sabaria, M. Vert, Intravascular bioresorbable polymeric stents: a potential alternative to current drug eluting metal stents, Journal of pharmaceutical sciences 96(11) (2007) 2829-2837.
[24] E.J. Hollick, D.J. Spalton, P.G. Ursell, M.V. Pande, Biocompatibility of poly (methyl methacrylate), silicone, and AcrySof intraocular lenses: randomized comparison of the cellular reaction on the anterior lens surface, Journal of Cataract & Refractive Surgery 24(3) (1998) 361-366.
[25] E.J. Hollick, D.J. Spalton, P.G. Ursell, M.V. Pande, S.A. Barman, J.F. Boyce, K. Tilling, The effect of polymethylmethacrylate, silicone, and polyacrylic intraocular lenses on posterior capsular opacification 3 years after cataract surgery, Ophthalmology 106(1) (1999) 49-55.
[26] T.H. Barker, The role of ECM proteins and protein fragments in guiding cell behavior in regenerative medicine, Biomaterials 32(18) (2011) 4211-4214.
[27] J.H. Collier, T. Segura, Evolving the use of peptides as components of biomaterials, Biomaterials 32(18) (2011) 4198-4204.
[28] S.L. Bellis, Advantages of RGD peptides for directing cell association with biomaterials, Biomaterials 32(18) (2011) 4205-4210.
[29] H. Shin, S. Jo, A.G. Mikos, Biomimetic materials for tissue engineering, Biomaterials 24(24) (2003) 4353-4364.
[30] T. Groth, Z.-M. Liu, Q. Gu, K. Kirchhof, D. Peschel, A. Barry, Development of bioactive surface coatings for tissue engineering applications, Biomedicine & Pharmacotherapy 8(62) (2008) 488-489.

[31] T. Groth, G. Altankov, A. Kostadinova, N. Krasteva, W. Albrecht, D. Paul, Altered vitronectin receptor (αv integrin) function in fibroblasts adhering on hydrophobic glass, Journal of Biomedical Materials Research: An Official Journal of The Society for Biomaterials, The Japanese Society for Biomaterials, and The Australian Society for Biomaterials 44(3) (1999) 341-351.

[32] T. Groth, K. Klosz, E. Campbell, R. New, B. Hall, H. Goering, Protein adsorption, lymphocyte adhesion and platelet adhesion/activation on polyurethane ureas is related to hard segment content and composition, Journal of Biomaterials Science, Polymer Edition 6(6) (1995) 497-510.

[33] N. Faucheux, R. Schweiss, K. Lützow, C. Werner, T. Groth, Self-assembled monolayers with different terminating groups as model substrates for cell adhesion studies, Biomaterials 25(14) (2004) 2721-2730.

[34] T. Groth, Z.-M. Liu, M. Niepel, D. Peschel, K. Kirchhof, G. Altankov, N. Faucheux, Chemical and physical modifications of biomaterial surfaces to control adhesion of cells, Advances in regenerative medicine: role of nanotechnology, and engineering principles, Springer2010, pp. 253-284.

[35] M.M. Stevens, J.H. George, Exploring and engineering the cell surface interface, Science 310(5751) (2005) 1135-1138.

[36] K. Kirchhof, K. Hristova, N. Krasteva, G. Altankov, T. Groth, Multilayer coatings on biomaterials for control of MG-63 osteoblast adhesion and growth, Journal of Materials Science: Materials in Medicine 20 (2009) 897-907.

[37] M.S. Niepel, D. Peschel, X. Sisquella, J.A. Planell, T. Groth, pH-dependent modulation of fibroblast adhesion on multilayers composed of poly (ethylene imine) and heparin, Biomaterials 30(28) (2009) 4939-4947.

[38] S. Ricard-Blum, The collagen family, Cold Spring Harbor perspectives in biology 3(1) (2011) a004978.

[39] M. Weber, H. Steinle, S. Golombek, L. Hann, C. Schlensak, H.P. Wendel, M. Avci-Adali, Blood-contacting biomaterials: in vitro evaluation of the hemocompatibility, Frontiers in bioengineering and biotechnology 6 (2018) 99.

[40] L. Vroman, A. Adams, G. Fischer, P. Munoz, Interaction of high molecular weight kininogen, factor XII, and fibrinogen in plasma at interfaces, (1980).

[41] M.M. Markiewski, B. Nilsson, K.N. Ekdahl, T.E. Mollnes, J.D. Lambris, Complement and coagulation: strangers or partners in crime?, Trends in immunology 28(4) (2007) 184-192.

[42] L. Tang, J.W. Eaton, Fibrin (ogen) mediates acute inflammatory responses to biomaterials, The Journal of experimental medicine 178(6) (1993) 2147-2156.

[43] C.R. Jenney, J.M. Anderson, Adsorbed IgG: a potent adhesive substrate for human macrophages, Journal of Biomedical Materials Research: An Official Journal of The Society

for Biomaterials, The Japanese Society for Biomaterials, and The Australian Society for Biomaterials and the Korean Society for Biomaterials 50(3) (2000) 281-290.
[44] M. Morra, Biochemical modification of titanium surfaces: peptides and ECM proteins, Eur Cell Mater 12(1) (2006) 15.
[45] G. Altankov, K. Richau, T. Groth, The role of surface zeta potential and substratum chemistry for regulation of dermal fibroblasts interaction, Materialwissenschaft und Werkstofftechnik: Entwicklung, Fertigung, Prüfung, Eigenschaften und Anwendungen technischer Werkstoffe 34(12) (2003) 1120-1128.
[46] M. Lundqvist, I. Sethson, B.-H. Jonsson, Protein adsorption onto silica nanoparticles: conformational changes depend on the particles' curvature and the protein stability, Langmuir 20(24) (2004) 10639-10647.
[47] E.A. Vogler, Structure and reactivity of water at biomaterial surfaces, Advances in colloid and interface science 74(1-3) (1998) 69-117.
[48] R. Tzoneva, M. Heuchel, T. Groth, G. Altankov, W. Albrecht, D. Paul, Fibrinogen adsorption and platelet interactions on polymer membranes, Journal of Biomaterials Science, Polymer Edition 13(9) (2002) 1033-1050.
[49] S.P. Mitra, Protein adsorption on biomaterial surfaces: Subsequent conformational and biological consequences–A review, J Surf Sci Technol 36(1–2) (2020) 7-38.
[50] M. Ma, R.M. Hill, Superhydrophobic surfaces, Current opinion in colloid & interface science 11(4) (2006) 193-202.
[51] Y. Tamada, Y. Ikada, Fibroblast growth on polymer surfaces and biosynthesis of collagen, Journal of biomedical materials research 28(7) (1994) 783-789.
[52] W. Norde, J. Lyklema, Why proteins prefer interfaces, Journal of Biomaterials Science, Polymer Edition 2(3) (1991) 183-202.
[53] P. Bongrand, C. Capo, R. Depieds, Physics of cell adhesion, Progress in surface Science 12(3) (1982) 217-285.
[54] N. Aggarwal, Modulating cell behaviour through biomimetic multilayers of natural and semi-synthetic glycosaminoglycans, Halle (Saale), Universitäts-und Landesbibliothek Sachsen-Anhalt, Diss., 2014, 2014.
[55] F. Gentile, L. Tirinato, E. Battista, F. Causa, C. Liberale, E.M. di Fabrizio, P. Decuzzi, Cells preferentially grow on rough substrates, Biomaterials 31(28) (2010) 7205-7212.
[56] M.S. Niepel, B.K. Ekambaram, C.E. Schmelzer, T. Groth, Polyelectrolyte multilayers of poly (l-lysine) and hyaluronic acid on nanostructured surfaces affect stem cell response, Nanoscale 11(6) (2019) 2878-2891.
[57] G. Ladam, P. Schaaf, F.J. Cuisinier, G. Decher, J.-C. Voegel, Protein adsorption onto auto-assembled polyelectrolyte films, Langmuir 17(3) (2001) 878-882.

[58] M. Müller, T. Rieser, P.L. Dubin, K. Lunkwitz, Selective interaction between proteins and the outermost surface of polyelectrolyte multilayers: influence of the polyanion type, pH and salt, Macromolecular rapid communications 22(6) (2001) 390-395.
[59] C.R. Wittmer, J.A. Phelps, W.M. Saltzman, P.R. Van Tassel, Fibronectin terminated multilayer films: protein adsorption and cell attachment studies, Biomaterials 28(5) (2007) 851-860.
[60] I. Boraschi-Diaz, J. Wang, J.S. Mort, S.V. Komarova, Collagen type I as a ligand for receptor-mediated signaling, Frontiers in Physics 5 (2017) 12.
[61] M. Zhao, G. Altankov, U. Grabiec, M. Bennett, M. Salmeron-Sanchez, F. Dehghani, T. Groth, Molecular composition of GAG-collagen I multilayers affects remodeling of terminal layers and osteogenic differentiation of adipose-derived stem cells, Acta Biomaterialia 41 (2016) 86-99.
[62] B.D. Ratner, A.S. Hoffman, F.J. Schoen, J.E. Lemons, Biomaterials science: an introduction to materials in medicine, Elsevier2004.
[63] K.S. Ødegaard, J. Torgersen, C.W. Elverum, Structural and biomedical properties of common additively manufactured biomaterials: A concise review, Metals 10(12) (2020) 1677.
[64] J.M. Anderson, Biological responses to materials, Annual review of materials research 31(1) (2001) 81-110.
[65] D.S. Salloum, J.B. Schlenoff, Protein adsorption modalities on polyelectrolyte multilayers, Biomacromolecules 5(3) (2004) 1089-1096.
[66] F. Grinnell, M. Feld, Fibronectin adsorption on hydrophilic and hydrophobic surfaces detected by antibody binding and analyzed during cell adhesion in serum-containing medium, Journal of Biological Chemistry 257(9) (1982) 4888-4893.
[67] T. Boudou, T. Crouzier, K. Ren, G. Blin, C. Picart, Multiple functionalities of polyelectrolyte multilayer films: new biomedical applications, Advanced materials 22(4) (2010) 441-467.
[68] R. Langer, VacantiJP: Tissue engineering, Science 260(5110) (1993) 920-926.
[69] V. Gribova, R. Auzely-Velty, C. Picart, Polyelectrolyte multilayer assemblies on materials surfaces: from cell adhesion to tissue engineering, Chemistry of Materials 24(5) (2012) 854-869.
[70] D. Klee, Z. Ademovic, A. Bosserhoff, H. Hoecker, G. Maziolis, H.-J. Erli, Surface modification of poly (vinylidenefluoride) to improve the osteoblast adhesion, Biomaterials 24(21) (2003) 3663-3670.
[71] A. Vonarbourg, C. Passirani, P. Saulnier, J.-P. Benoit, Parameters influencing the stealthiness of colloidal drug delivery systems, Biomaterials 27(24) (2006) 4356-4373.
[72] L. Bačáková, K. Walachová, V. Švorcˇík, V. Hnatowicz, Adhesion and proliferation of rat vascular smooth muscle cells (VSMC) on polyethylene implanted with O+ and C+ ions, Journal of Biomaterials Science, Polymer Edition 12(7) (2001) 817-834.

[73] B. Seifert, G. Mihanetzis, T. Groth, W. Albrecht, K. Richau, Y. Missirlis, D. Paul, G. Von Sengbusch, Polyetherimide: A new membrane-forming polymer for biomedical applications, Artificial organs 26(2) (2002) 189-199.

[74] B. Zhao, W.J. Brittain, Polymer brushes: surface-immobilized macromolecules, Progress in Polymer Science 25(5) (2000) 677-710.

[75] A.J. García, Surface modification of biomaterials, Foundations of Regenerative Medicine: Clinical and Therapeutic Applications (2009) 368-378.

[76] R.O. Hynes, The extracellular matrix: not just pretty fibrils, Science 326(5957) (2009) 1216-1219.

[77] C. Mas-Moruno, Surface functionalization of biomaterials for bone tissue regeneration and repair, Peptides and proteins as biomaterials for tissue regeneration and repair, Elsevier2018, pp. 73-100.

[78] M. Morra, Biomolecular modification of implant surfaces, Expert review of medical devices 4(3) (2007) 361-372.

[79] R. Iler, Multilayers of colloidal particles, Journal of colloid and interface science 21(6) (1966) 569-594.

[80] G. Decher, J.D. Hong, J. Schmitt, Buildup of ultrathin multilayer films by a self-assembly process: III. Consecutively alternating adsorption of anionic and cationic polyelectrolytes on charged surfaces, Thin solid films 210 (1992) 831-835.

[81] J. Borges, J.F. Mano, Molecular interactions driving the layer-by-layer assembly of multilayers, Chemical reviews 114(18) (2014) 8883-8942.

[82] H. Zhu, J. Ji, J. Shen, Biomacromolecules electrostatic self-assembly on 3-dimensional tissue engineering scaffold, Biomacromolecules 5(5) (2004) 1933-1939.

[83] J.B. Schlenoff, H. Ly, M. Li, Charge and mass balance in polyelectrolyte multilayers, Journal of the American Chemical Society 120(30) (1998) 7626-7634.

[84] T. Groth, A. Lendlein, Layer-by-layer deposition of polyelectrolytes—a versatile tool for the in vivo repair of blood vessels, Angewandte Chemie International Edition 43(8) (2004) 926-928.

[85] J.F. Quinn, A.P. Johnston, G.K. Such, A.N. Zelikin, F. Caruso, Next generation, sequentially assembled ultrathin films: beyond electrostatics, Chemical Society Reviews 36(5) (2007) 707-718.

[86] J.B. Schlenoff, S.T. Dubas, Mechanism of polyelectrolyte multilayer growth: charge overcompensation and distribution, Macromolecules 34(3) (2001) 592-598.

[87] J. Lyklema, L. Deschênes, The first step in layer-by-layer deposition: Electrostatics and/or non-electrostatics?, Advances in colloid and interface science 168(1-2) (2011) 135-148.

[88] S.L. Clark, P.T. Hammond, The role of secondary interactions in selective electrostatic multilayer deposition, Langmuir 16(26) (2000) 10206-10214.

[89] S. Boddohi, C.E. Killingsworth, M.J. Kipper, Polyelectrolyte multilayer assembly as a function of pH and ionic strength using the polysaccharides chitosan and heparin, Biomacromolecules 9(7) (2008) 2021-2028.

[90] L. Richert, Y. Arntz, P. Schaaf, J.-C. Voegel, C. Picart, pH dependent growth of poly (L-lysine)/poly (L-glutamic) acid multilayer films and their cell adhesion properties, Surface Science 570(1-2) (2004) 13-29.

[91] L. Richert, P. Lavalle, E. Payan, X.Z. Shu, G.D. Prestwich, J.-F. Stoltz, P. Schaaf, J.-C. Voegel, C. Picart, Layer by layer buildup of polysaccharide films: physical chemistry and cellular adhesion aspects, Langmuir 20(2) (2004) 448-458.

[92] R. Steitz, W. Jaeger, R.v. Klitzing, Influence of charge density and ionic strength on the multilayer formation of strong polyelectrolytes, Langmuir 17(15) (2001) 4471-4474.

[93] M. Schönhoff, Layered polyelectrolyte complexes: physics of formation and molecular properties, Journal of Physics: Condensed Matter 15(49) (2003) R1781.

[94] M. Gopinadhan, O. Ivanova, H. Ahrens, J.-U. Günther, R. Steitz, C.A. Helm, The influence of secondary interactions during the formation of polyelectrolyte multilayers: Layer thickness, bound water and layer interpenetration, The Journal of Physical Chemistry B 111(29) (2007) 8426-8434.

[95] A. Mentbayeva, A. Ospanova, Z. Tashmuhambetova, V. Sokolova, S. Sukhishvili, Polymer–metal complexes in polyelectrolyte multilayer films as catalysts for oxidation of toluene, Langmuir 28(32) (2012) 11948-11955.

[96] P. Agulhon, V. Markova, M. Robitzer, F.o. Quignard, T. Mineva, Structure of alginate gels: interaction of diuronate units with divalent cations from density functional calculations, Biomacromolecules 13(6) (2012) 1899-1907.

[97] J. Qu, Q. Hu, K. Shen, K. Zhang, Y. Li, H. Li, Q. Zhang, J. Wang, W. Quan, The preparation and characterization of chitosan rods modified with Fe3+ by a chelation mechanism, Carbohydrate research 346(6) (2011) 822-827.

[98] X. Huang, A.B. Schubert, J.D. Chrisman, N.S. Zacharia, Formation and tunable disassembly of polyelectrolyte–Cu2+ layer-by-layer complex film, Langmuir 29(42) (2013) 12959-12968.

[99] R.R. Costa, J.F. Mano, Polyelectrolyte multilayered assemblies in biomedical technologies, Chemical Society Reviews 43(10) (2014) 3453-3479.

[100] A. Nishiguchi, H. Yoshida, M. Matsusaki, M. Akashi, Rapid construction of three-dimensional multilayered tissues with endothelial tube networks by the cell-accumulation technique, Advanced Materials 23(31) (2011) 3506-3510.

[101] M. Matsusaki, K. Kadowaki, Y. Nakahara, M. Akashi, Fabrication of cellular multilayers with nanometer-sized extracellular matrix films, Angewandte Chemie International Edition 46(25) (2007) 4689-4692.

[102] M. Keeney, X. Jiang, M. Yamane, M. Lee, S. Goodman, F. Yang, Nanocoating for biomolecule delivery using layer-by-layer self-assembly, Journal of Materials Chemistry B 3(45) (2015) 8757-8770.

[103] Z. Tang, Y. Wang, P. Podsiadlo, N.A. Kotov, Biomedical applications of layer-by-layer assembly: from biomimetics to tissue engineering, Advanced materials 18(24) (2006) 3203-3224.

[104] S. Zankovych, M. Diefenbeck, J. Bossert, T. Mückley, C. Schrader, J. Schmidt, H. Schubert, S. Bischoff, M. Faucon, U. Finger, The effect of polyelectrolyte multilayer coated titanium alloy surfaces on implant anchorage in rats, Acta Biomaterialia 9(1) (2013) 4926-4934.

[105] P.T. Hammond, Form and function in multilayer assembly: New applications at the nanoscale, Advanced Materials 16(15) (2004) 1271-1293.

[106] N. Aggarwal, N. Altgärde, S. Svedhem, K. Zhang, S. Fischer, T. Groth, Effect of molecular composition of heparin and cellulose sulfate on multilayer formation and cell response, Langmuir 29(45) (2013) 13853-13864.

[107] M. Zhao, L. Li, C. Zhou, F. Heyroth, B. Fuhrmann, K. Maeder, T. Groth, Improved stability and cell response by intrinsic cross-linking of multilayers from collagen I and oxidized glycosaminoglycans, Biomacromolecules 15(11) (2014) 4272-4280.

[108] K. Kirchhof, K. Hristova, N. Krasteva, G. Altankov, T. Groth, Multilayer coatings on biomaterials for control of MG-63 osteoblast adhesion and growth, Journal of Materials Science: Materials in Medicine 20(4) (2009) 897-907.

[109] I. Antoniac, Biologically responsive biomaterials for tissue engineering, Springer Science & Business Media2012.

[110] S.F. Badylak, D.O. Freytes, T.W. Gilbert, Extracellular matrix as a biological scaffold material: Structure and function, Acta biomaterialia 5(1) (2009) 1-13.

[111] E.Y. Egawa, K. Kato, M. Hiraoka, T. Nakaji-Hirabayashi, H. Iwata, Enhanced proliferation of neural stem cells in a collagen hydrogel incorporating engineered epidermal growth factor, Biomaterials 32(21) (2011) 4737-4743.

[112] T.J. Levingstone, A. Matsiko, G.R. Dickson, F.J. O'Brien, J.P. Gleeson, A biomimetic multi-layered collagen-based scaffold for osteochondral repair, Acta biomaterialia 10(5) (2014) 1996-2004.

[113] M. Schnabelrauch, D. Scharnweber, J. Schiller, Sulfated glycosaminoglycans as promising artificial extracellular matrix components to improve the regeneration of tissues, Current medicinal chemistry 20(20) (2013) 2501-2523.

[114] R. Pankov, K.M. Yamada, Fibronectin at a glance, Journal of cell science 115(20) (2002) 3861-3863.

[115] A. Mansour, M.A. Mezour, Z. Badran, F. Tamimi, Extracellular matrices for bone regeneration: a literature review, Tissue Engineering Part A 23(23-24) (2017) 1436-1451.
[116] R. Anouz, A. Repanas, E. Schwarz, T. Groth, Novel Surface Coatings Using Oxidized Glycosaminoglycans as Delivery Systems of Bone Morphogenetic Protein 2 (BMP-2) for Bone Regeneration, Macromolecular bioscience 18(11) (2018) 1800283.
[117] T. Katagiri, A. Yamaguchi, M. Komaki, E. Abe, N. Takahashi, T. Ikeda, V. Rosen, J.M. Wozney, A. Fujisawa-Sehara, T. Suda, Bone morphogenetic protein-2 converts the differentiation pathway of C2C12 myoblasts into the osteoblast lineage, The Journal of cell biology 127(6) (1994) 1755-1766.
[118] J. Raphel, M. Holodniy, S.B. Goodman, S.C. Heilshorn, Multifunctional coatings to simultaneously promote osseointegration and prevent infection of orthopaedic implants, Biomaterials 84 (2016) 301-314.
[119] F. Gong, T. Groth, C. Tu, M. Zhao, X. Huang, J. Chu, Crosstalk between macrophages and mesenchymal stem cells regulated by biomaterials and its role in bone regeneration, Advances in Materials Science and Engineering 2021 (2021) 1-21.
[120] A. Aravamudhan, D. M Ramos, J. Nip, A. Subramanian, R. James, M. D Harmon, X. Yu, S. G Kumbar, Osteoinductive small molecules: growth factor alternatives for bone tissue engineering, Current pharmaceutical design 19(19) (2013) 3420-3428.
[121] K. Ren, T. Crouzier, C. Roy, C. Picart, Polyelectrolyte multilayer films of controlled stiffness modulate myoblast cell differentiation, Advanced functional materials 18(9) (2008) 1378-1389.
[122] L. Richert, F. Boulmedais, P. Lavalle, J. Mutterer, E. Ferreux, G. Decher, P. Schaaf, J.-C. Voegel, C. Picart, Improvement of stability and cell adhesion properties of polyelectrolyte multilayer films by chemical cross-linking, Biomacromolecules 5(2) (2004) 284-294.
[123] H. Chen, W. Ouyang, B. Lawuyi, S. Prakash, Genipin cross-linked alginate-chitosan microcapsules: membrane characterization and optimization of cross-linking reaction, Biomacromolecules 7(7) (2006) 2091-2098.
[124] G. Apte, A. Repanas, C. Willems, A. Mujtaba, C.E. Schmelzer, A. Raichur, F. Syrowatka, T. Groth, Effect of Different Crosslinking Strategies on Physical Properties and Biocompatibility of Freestanding Multilayer Films Made of Alginate and Chitosan, Macromolecular Bioscience 19(11) (2019) 1900181.
[125] C. Chaubaroux, E. Vrana, C. Debry, P. Schaaf, B. Senger, J.-C. Voegel, Y. Haikel, C. Ringwald, J. Hemmerlé, P. Lavalle, Collagen-based fibrillar multilayer films cross-linked by a natural agent, Biomacromolecules 13(7) (2012) 2128-2135.
[126] J.M. Silva, S.G. Caridade, R.R. Costa, N.M. Alves, T. Groth, C. Picart, R.L. Reis, J.F. Mano, pH responsiveness of multilayered films and membranes made of polysaccharides, Langmuir 31(41) (2015) 11318-11328.

[127] A.L. Hillberg, C.A. Holmes, M. Tabrizian, Effect of genipin cross-linking on the cellular adhesion properties of layer-by-layer assembled polyelectrolyte films, Biomaterials 30(27) (2009) 4463-4470.
[128] W.-P. Voo, C.-W. Ooi, A. Islam, B.-T. Tey, E.-S. Chan, Calcium alginate hydrogel beads with high stiffness and extended dissolution behaviour, European Polymer Journal 75 (2016) 343-353.
[129] J.M. Silva, S.G. Caridade, R.L. Reis, J.F. Mano, Polysaccharide-based freestanding multilayered membranes exhibiting reversible switchable properties, Soft Matter 12(4) (2016) 1200-1209.
[130] I. Machida-Sano, Y. Matsuda, H. Namiki, In vitro adhesion of human dermal fibroblasts on iron cross-linked alginate films, Biomedical Materials 4(2) (2009) 025008.
[131] I. Machida-Sano, S. Ogawa, H. Ueda, Y. Kimura, N. Satoh, H. Namiki, Effects of composition of iron-cross-linked alginate hydrogels for cultivation of human dermal fibroblasts, International journal of biomaterials 2012 (2012).
[132] K.C. Krogman, K.F. Lyon, P.T. Hammond, Metal ion reactive thin films using spray electrostatic LbL assembly, The Journal of Physical Chemistry B 112(46) (2008) 14453-14460.
[133] M. Cao, J. Wang, Y. Wang, Surface patterns induced by Cu2+ ions on BPEI/PAA layer-by-layer assembly, Langmuir 23(6) (2007) 3142-3149.
[134] M.S. Hasnain, A.K. Nayak, Natural polysaccharides in drug delivery and biomedical applications, Academic Press2019.
[135] J. Liu, S. Willför, C. Xu, A review of bioactive plant polysaccharides: Biological activities, functionalization, and biomedical applications, Bioactive Carbohydrates and Dietary Fibre 5(1) (2015) 31-61.
[136] G. Orive, E. Santos, J. Pedraz, R. Hernández, Application of cell encapsulation for controlled delivery of biological therapeutics, Advanced Drug Delivery Reviews 67 (2014) 3-14.
[137] Z. Shariatinia, Pharmaceutical applications of natural polysaccharides, Natural polysaccharides in drug delivery and biomedical applications, Elsevier2019, pp. 15-57.
[138] F. Wurm, B. Rietzler, T. Pham, T. Bechtold, Multivalent ions as reactive crosslinkers for biopolymers—a review, Molecules 25(8) (2020) 1840.
[139] V. Zargar, M. Asghari, A. Dashti, A review on chitin and chitosan polymers: structure, chemistry, solubility, derivatives, and applications, ChemBioEng reviews 2(3) (2015) 204-226.
[140] K. Mazeau, S. Pérez, M. Rinaudo, Predicted influence of N-acetyl group content on the conformational extension of chitin and chitosan chains, (2000).

[141] M. Rinaudo, M. Milas, P. Le Dung, Characterization of chitosan. Influence of ionic strength and degree of acetylation on chain expansion, International journal of biological macromolecules 15(5) (1993) 281-285.
[142] J. Lizardi-Mendoza, W.M.A. Monal, F.M.G. Valencia, Chemical characteristics and functional properties of chitosan, Chitosan in the preservation of agricultural commodities, Elsevier2016, pp. 3-31.
[143] X. Wang, Y. Du, L. Fan, H. Liu, Y. Hu, Chitosan-metal complexes as antimicrobial agent: Synthesis, characterization and Structure-activity study, Polymer Bulletin 55(1) (2005) 105-113.
[144] S. Kim, Competitive biological activities of chitosan and its derivatives: antimicrobial, antioxidant, anticancer, and anti-inflammatory activities, International journal of polymer science 2018 (2018).
[145] J.R. Rodríguez-Núñez, J. López-Cervantes, D.I. Sánchez-Machado, B. Ramírez-Wong, P. Torres-Chavez, M.O. Cortez-Rocha, Antimicrobial activity of chitosan-based films against Salmonella typhimurium and Staphylococcus aureus, International journal of food science & technology 47(10) (2012) 2127-2133.
[146] Y. Liu, Y. Cai, X. Jiang, J. Wu, X. Le, Molecular interactions, characterization and antimicrobial activity of curcumin–chitosan blend films, Food Hydrocolloids 52 (2016) 564-572.
[147] Y. Qin, Alginate fibres: an overview of the production processes and applications in wound management, Polymer international 57(2) (2008) 171-180.
[148] M.N. Pacho, V.E. Manzano, N.B. D'Accorso, Synthesis of micro-and nanoparticles of alginate and chitosan for controlled release of drugs, Natural Polysaccharides in Drug Delivery and Biomedical Applications, Elsevier2019, pp. 363-398.
[149] H.V. Sæther, H.K. Holme, G. Maurstad, O. Smidsrød, B.T. Stokke, Polyelectrolyte complex formation using alginate and chitosan, Carbohydrate Polymers 74(4) (2008) 813-821.
[150] C. Peniche, W. Argüelles-Monal, Chitosan based polyelectrolyte complexes, Macromolecular Symposia, Wiley Online Library, 2001, pp. 103-116.
[151] J. Liu, Y. Fu, C. Xiao, Formation of multilayer through layer-by-layer assembly of starch-based polyanion with divalent metal ion, Carbohydrate polymers 203 (2019) 409-414.
[152] M. Muhammad, C. Willems, J. Rodríguez-Fernández, G. Gallego-Ferrer, T. Groth, Synthesis and characterization of oxidized polysaccharides for in situ forming hydrogels, Biomolecules 10(8) (2020) 1185.
[153] K.Y. Lee, DJM (2012). Alginate: properties and biomedical applications, Prog. Polym. Sci 37 106-126.
[154] E. Papakonstantinou, M. Roth, G. Karakiulakis, Hyaluronic acid: A key molecule in skin aging, Dermato-endocrinology 4(3) (2012) 253-258.

[155] J. Necas, L. Bartosikova, P. Brauner, J. Kolar, Hyaluronic acid (hyaluronan): a review, Veterinarni medicina 53(8) (2008) 397-411.
[156] L. Nagy, S. Yamashita, T. Yamaguchi, P. Sipos, H. Wakita, M. Nomura, The local structures of Cu (II) and Zn (II) complexes of hyaluronate, Journal of inorganic biochemistry 72(1-2) (1998) 49-55.
[157] R.A. Muzzarelli, F. Greco, A. Busilacchi, V. Sollazzo, A. Gigante, Chitosan, hyaluronan and chondroitin sulfate in tissue engineering for cartilage regeneration: a review, Carbohydrate polymers 89(3) (2012) 723-739.
[158] M. Holmes, M. Bayliss, H. Muir, Hyaluronic acid in human articular cartilage. Age-related changes in content and size, Biochemical Journal 250(2) (1988) 435-441.
[159] R. Stern, A.A. Asari, K.N. Sugahara, Hyaluronan fragments: an information-rich system, European journal of cell biology 85(8) (2006) 699-715.
[160] B. Toole, Hyaluronan and its binding proteins, the hyaladherins, Current opinion in cell biology 2(5) (1990) 839-844.
[161] P. Teder, R.W. Vandivier, D. Jiang, J. Liang, L. Cohn, E. Puré, P.M. Henson, P.W. Noble, Resolution of lung inflammation by CD44, Science 296(5565) (2002) 155-158.
[162] A.J. Day, C.A. de la Motte, Hyaluronan cross-linking: a protective mechanism in inflammation?, TRENDS in Immunology 26(12) (2005) 637-643.
[163] A. Fakhari, C. Berkland, Applications and emerging trends of hyaluronic acid in tissue engineering, as a dermal filler and in osteoarthritis treatment, Acta biomaterialia 9(7) (2013) 7081-7092.
[164] N.W. Marion, J.J. Mao, Mesenchymal stem cells and tissue engineering, Methods in enzymology 420 (2006) 339-361.
[165] S. Singh, A. Srivastava, V. Kumar, A. Pandey, D. Kumar, C. Rajpurohit, V. Khanna, S. Yadav, A. Pant, Stem cells in neurotoxicology/developmental neurotoxicology: current scenario and future prospects, Molecular neurobiology 53 (2016) 6938-6949.
[166] M.R. Alison, R. Poulsom, S. Forbes, N.A. Wright, An introduction to stem cells, The Journal of Pathology: A Journal of the Pathological Society of Great Britain and Ireland 197(4) (2002) 419-423.
[167] A. Friedenstein, R. Chailakhjan, K. Lalykina, The development of fibroblast colonies in monolayer cultures of guinea-pig bone marrow and spleen cells, Cell Proliferation 3(4) (1970) 393-403.
[168] M. Alkhalil, A. Smajilagic, A. Redzic, Human dental pulp mesenchymal stem cells isolation and osteoblast differentiation, Med Glas (Zenica) 12(1) (2015) 27-32.
[169] E. Alizadeh, N. Zarghami, M.B. Eslaminejad, A. Akbarzadeh, A. Barzegar, S.A. Mohammadi, The effect of dimethyl sulfoxide on hepatic differentiation of mesenchymal stem cells, Artificial cells, nanomedicine, and biotechnology 44(1) (2016) 157-164.

[170] L.d.S. Meirelles, P.C. Chagastelles, N.B. Nardi, Mesenchymal stem cells reside in virtually all post-natal organs and tissues, Journal of cell science 119(11) (2006) 2204-2213.
[171] P.S. In't Anker, S.A. Scherjon, C. Kleijburg-van der Keur, G.M. de Groot-Swings, F.H. Claas, W.E. Fibbe, H.H. Kanhai, Isolation of mesenchymal stem cells of fetal or maternal origin from human placenta, Stem cells 22(7) (2004) 1338-1345.
[172] M.F. Pittenger, A.M. Mackay, S.C. Beck, R.K. Jaiswal, R. Douglas, J.D. Mosca, M.A. Moorman, D.W. Simonetti, S. Craig, D.R. Marshak, Multilineage potential of adult human mesenchymal stem cells, science 284(5411) (1999) 143-147.
[173] D.P. Kavanagh, J. Robinson, N. Kalia, Mesenchymal stem cell priming: fine-tuning adhesion and function, Stem cell reviews and reports 10(4) (2014) 587-599.
[174] K. Le Blanc, C. Tammik, K. Rosendahl, E. Zetterberg, O. Ringdén, HLA expression and immunologic propertiesof differentiated and undifferentiated mesenchymal stem cells, Experimental hematology 31(10) (2003) 890-896.
[175] M. Kassem, M. Kristiansen, B.M. Abdallah, Mesenchymal stem cells: cell biology and potential use in therapy, Basic & clinical pharmacology & toxicology 95(5) (2004) 209-214.
[176] H. Rippon, A. Bishop, Embryonic stem cells, Cell proliferation 37(1) (2004) 23-34.
[177] D. Noël, F. Djouad, C. Jorgense, Regenerative medicine through mesenchymal stem cells for bone and cartilage repair, Current opinion in investigational drugs (London, England: 2000) 3(7) (2002) 1000-1004.
[178] F.P. Barry, J.M. Murphy, Mesenchymal stem cells: clinical applications and biological characterization, The international journal of biochemistry & cell biology 36(4) (2004) 568-584.
[179] A.I. Caplan, Adult mesenchymal stem cells for tissue engineering versus regenerative medicine, Journal of cellular physiology 213(2) (2007) 341-347.
[180] S. Chen, M. Lewallen, T. Xie, Adhesion in the stem cell niche: biological roles and regulation, Development 140(2) (2013) 255-265.
[181] P.S. Mathieu, E.G. Loboa, Cytoskeletal and focal adhesion influences on mesenchymal stem cell shape, mechanical properties, and differentiation down osteogenic, adipogenic, and chondrogenic pathways, Tissue Engineering Part B: Reviews 18(6) (2012) 436-444.
[182] G. Abagnale, A. Sechi, M. Steger, Q. Zhou, C.-C. Kuo, G. Aydin, C. Schalla, G. Müller-Newen, M. Zenke, I.G. Costa, Surface topography guides morphology and spatial patterning of induced pluripotent stem cell colonies, Stem cell reports 9(2) (2017) 654-666.
[183] A.J. Steward, D.J. Kelly, Mechanical regulation of mesenchymal stem cell differentiation, Journal of anatomy 227(6) (2015) 717-731.
[184] P.R. Baraniak, T.C. McDevitt, Stem cell paracrine actions and tissue regeneration, Regenerative medicine 5(1) (2010) 121-143.
[185] Z. Cao, R.M. Umek, S.L. McKnight, Regulated expression of three C/EBP isoforms during adipose conversion of 3T3-L1 cells, Genes & development 5(9) (1991) 1538-1552.

[186] Y. Xiao, V. Peperzak, L. van Rijn, J. Borst, J.D. de Bruijn, Dexamethasone treatment during the expansion phase maintains stemness of bone marrow mesenchymal stem cells, Journal of tissue engineering and regenerative medicine 4(5) (2010) 374-386.
[187] M. Coelho, M. Fernandes, Human bone cell cultures in biocompatibility testing. Part II: effect of ascorbic acid, β-glycerophosphate and dexamethasone on osteoblastic differentiation, Biomaterials 21(11) (2000) 1095-1102.
[188] B.E. Grottkau, Y. Lin, Osteogenesis of adipose-derived stem cells, Bone research 1(1) (2013) 133-145.
[189] A. Infante, C.I. Rodríguez, Osteogenesis and aging: lessons from mesenchymal stem cells, Stem cell research & therapy 9(1) (2018) 1-7.
[190] T. Komori, Regulation of osteoblast differentiation by transcription factors, Journal of cellular biochemistry 99(5) (2006) 1233-1239.
[191] J. Tanjaya, P. Ha, Y. Zhang, C. Wang, Y. Shah, E. Berthiaume, H.C. Pan, J. Shi, J. Kwak, B. Wu, Genetic and pharmacologic suppression of PPARγ enhances NELL-1-stimulated bone regeneration, Biomaterials 287 (2022) 121609.
[192] E. Jang, H. Jeong, J. Kang, N. Kim, M. Kim, S. Choi, S. Yoo, J. Hong, M. Bae, E. Hwang, TM-25659 enhances osteogenic differentiation and suppresses adipogenic differentiation by modulating the transcriptional co-activator TAZ, British journal of pharmacology 165(5) (2012) 1584-1594.
[193] Y. Zhang, G. Marsboom, P.T. Toth, J. Rehman, Mitochondrial respiration regulates adipogenic differentiation of human mesenchymal stem cells, PloS one 8(10) (2013) e77077.
[194] F. Atashi, A. Modarressi, M.S. Pepper, The role of reactive oxygen species in mesenchymal stem cell adipogenic and osteogenic differentiation: a review, Stem cells and development 24(10) (2015) 1150-1163.
[195] J. Wei, J. Shimazu, M.P. Makinistoglu, A. Maurizi, D. Kajimura, H. Zong, T. Takarada, T. Iezaki, J.E. Pessin, E. Hinoi, Glucose uptake and Runx2 synergize to orchestrate osteoblast differentiation and bone formation, Cell 161(7) (2015) 1576-1591.
[196] K.V. Tormos, E. Anso, R.B. Hamanaka, J. Eisenbart, J. Joseph, B. Kalyanaraman, N.S. Chandel, Mitochondrial complex III ROS regulate adipocyte differentiation, Cell metabolism 14(4) (2011) 537-544.
[197] M. Valorani, E. Montelatici, A. Germani, A. Biddle, D. D'Alessandro, R. Strollo, M. Patrizi, L. Lazzari, E. Nye, W. Otto, Pre-culturing human adipose tissue mesenchymal stem cells under hypoxia increases their adipogenic and osteogenic differentiation potentials, Cell proliferation 45(3) (2012) 225-238.
[198] Q. Chen, P. Shou, C. Zheng, M. Jiang, G. Cao, Q. Yang, J. Cao, N. Xie, T. Velletri, X. Zhang, Fate decision of mesenchymal stem cells: adipocytes or osteoblasts?, Cell Death & Differentiation 23(7) (2016) 1128-1139.

[199] K.P. Carter, A.M. Young, A.E. Palmer, Fluorescent sensors for measuring metal ions in living systems, Chemical reviews 114(8) (2014) 4564-4601.
[200] G. Crisponi, V.M. Nurchi, Metal ion toxicity, Encyclopedia of Inorganic and Bioinorganic Chemistry (2011) 1-14.
[201] Z. Chen, W. Zhang, M. Wang, L.J. Backman, J. Chen, Effects of zinc, magnesium, and iron ions on bone tissue engineering, ACS Biomaterials Science & Engineering 8(6) (2022) 2321-2335.
[202] K. Glenske, P. Donkiewicz, A. Köwitsch, N. Milosevic-Oljaca, P. Rider, S. Rofall, J. Franke, O. Jung, R. Smeets, R. Schnettler, Applications of metals for bone regeneration, International journal of molecular sciences 19(3) (2018) 826.
[203] J.W. Erdman Jr, I.A. Macdonald, S.H. Zeisel, Present knowledge in nutrition, John Wiley & Sons2012.
[204] K. Peters, S. Staehlke, H. Rebl, A. Jonitz-Heincke, O. Hahn, Impact of Metal Ions on Cellular Functions: A Focus on Mesenchymal Stem/Stromal Cell Differentiation, International Journal of Molecular Sciences 25(18) (2024) 10127.
[205] H. Shi, Y.-D. HALVORSEN, P.N. ELLIS, W.O. WILKISON, M.B. ZEMEL, Role of intracellular calcium in human adipocyte differentiation, Physiological genomics 3(2) (2000) 75-82.
[206] K. Borkowski, K. Wrzesinski, A. Rogowska-Wrzesinska, K. Audouze, J. Bakke, R.K. Petersen, F.G. Haj, L. Madsen, K. Kristiansen, Proteomic analysis of cAMP-mediated signaling during differentiation of 3 T3-L1 preadipocytes, Biochimica et Biophysica Acta (BBA)-Proteins and Proteomics 1844(12) (2014) 2096-2107.
[207] J. Ye, W. Ai, F. Zhang, X. Zhu, G. Shu, L. Wang, P. Gao, Q. Xi, Y. Zhang, Q. Jiang, Enhanced proliferation of porcine bone marrow mesenchymal stem cells induced by extracellular calcium is associated with the activation of the calcium-sensing receptor and ERK signaling pathway, Stem cells international 2016 (2016).
[208] E.M. Brown, R.J. MacLeod, Extracellular calcium sensing and extracellular calcium signaling, Physiological reviews 81(1) (2001) 239-297.
[209] A.M. Barradas, H.A. Fernandes, N. Groen, Y.C. Chai, J. Schrooten, J. Van de Peppel, J.P. Van Leeuwen, C.A. Van Blitterswijk, J. De Boer, A calcium-induced signaling cascade leading to osteogenic differentiation of human bone marrow-derived mesenchymal stromal cells, Biomaterials 33(11) (2012) 3205-3215.
[210] M. Kobayashi, S. Shimizu, Cobalt proteins, European Journal of Biochemistry 261(1) (1999) 1-9.
[211] S. Okamoto, L.D. Eltis, The biological occurrence and trafficking of cobalt, Metallomics 3(10) (2011) 963-970.

[212] Q. Shi, X. Luo, Z. Huang, A.C. Midgley, B. Wang, R. Liu, D. Zhi, T. Wei, X. Zhou, M. Qiao, Cobalt-mediated multi-functional dressings promote bacteria-infected wound healing, Acta Biomaterialia 86 (2019) 465-479.
[213] W. Fan, R. Crawford, Y. Xiao, Enhancing in vivo vascularized bone formation by cobalt chloride-treated bone marrow stromal cells in a tissue engineered periosteum model, Biomaterials 31(13) (2010) 3580-3589.
[214] T. Tanaka, I. Kojima, T. Ohse, J.R. Ingelfinger, S. Adler, T. Fujita, M. Nangaku, Cobalt promotes angiogenesis via hypoxia-inducible factor and protects tubulointerstitium in the remnant kidney model, Laboratory investigation 85(10) (2005) 1292-1307.
[215] E. Quinlan, S. Partap, M.M. Azevedo, G. Jell, M.M. Stevens, F.J. O'Brien, Hypoxia-mimicking bioactive glass/collagen glycosaminoglycan composite scaffolds to enhance angiogenesis and bone repair, Biomaterials 52 (2015) 358-366.
[216] J. Kwak, S.J. Choi, W. Oh, Y.S. Yang, H.B. Jeon, E.S. Jeon, Cobalt chloride enhances the anti-inflammatory potency of human umbilical cord blood-derived mesenchymal stem cells through the ERK-HIF-1α-MicroRNA-146a-mediated signaling pathway, Stem cells international 2018 (2018).
[217] M. Ziche, J. Jones, P.M. Gullino, Role of prostaglandin E1 and copper in angiogenesis, Journal of the National Cancer Institute 69(2) (1982) 475-482.
[218] G. Borkow, Using copper to improve the well-being of the skin, Current chemical biology 8(2) (2014) 89-102.
[219] L. Matos, A. Gouveia, H. Almeida, Copper ability to induce premature senescence in human fibroblasts, Age 34(4) (2012) 783-794.
[220] C. Gérard, L.-J. Bordeleau, J. Barralet, C.J. Doillon, The stimulation of angiogenesis and collagen deposition by copper, Biomaterials 31(5) (2010) 824-831.
[221] B.R. Stern, Essentiality and toxicity in copper health risk assessment: overview, update and regulatory considerations, Journal of Toxicology and Environmental Health, Part A 73(2-3) (2010) 114-127.
[222] W.E. Winter, L.A. Bazydlo, N.S. Harris, The molecular biology of human iron metabolism, Laboratory medicine 45(2) (2014) 92-102.
[223] L. Aravind, E.V. Koonin, The DNA-repair protein AlkB, EGL-9, and leprecan define new families of 2-oxoglutarate-and iron-dependent dioxygenases, Genome biology 2(3) (2001) 1-8.
[224] S. Bose, D. Banerjee, S. Robertson, S. Vahabzadeh, Enhanced in vivo bone and blood vessel formation by iron oxide and silica doped 3D printed tricalcium phosphate scaffolds, Annals of biomedical engineering 46(9) (2018) 1241-1253.

[225] S. Vahabzadeh, S. Bose, Effects of iron on physical and mechanical properties, and osteoblast cell interaction in β-tricalcium phosphate, Annals of biomedical engineering 45(3) (2017) 819-828.

[226] K.S. Houschyar, C. Tapking, M.R. Borrelli, D. Popp, D. Duscher, Z.N. Maan, M.P. Chelliah, J. Li, K. Harati, C. Wallner, Wnt pathway in bone repair and regeneration–what do we know so far, Frontiers in cell and developmental biology 6 (2019) 170.

[227] J.-A. Kim, H.-K. Choi, T.-M. Kim, S.-H. Leem, I.-H. Oh, Regulation of mesenchymal stromal cells through fine tuning of canonical Wnt signaling, Stem cell research 14(3) (2015) 356-368.

[228] G.W. Gale, H. Cui, K.A. Reinhardt, Aqueous cleaning and surface conditioning processes, Handbook of silicon wafer cleaning technology, Elsevier2018, pp. 185-252.

[229] A. Denuziere, D. Ferrier, O. Damour, A. Domard, Chitosan–chondroitin sulfate and chitosan–hyaluronate polyelectrolyte complexes: biological properties, Biomaterials 19(14) (1998) 1275-1285.

[230] R. Schasfoort, Surface Plasmon Resonance Instruments, Handbook of Surface Plasmon Resonance (2017) 60-105.

[231] J. De Feijter, d.J. Benjamins, F. Veer, Ellipsometry as a tool to study the adsorption behavior of synthetic and biopolymers at the air–water interface, Biopolymers: Original Research on Biomolecules 17(7) (1978) 1759-1772.

[232] T.J. Halthur, U.M. Elofsson, Multilayers of charged polypeptides as studied by in situ ellipsometry and quartz crystal microbalance with dissipation, Langmuir 20(5) (2004) 1739-1745.

[233] P. Gould, Smart, clean surfaces, Materials Today 6(11) (2003) 44-48.

[234] S. Honary, F. Zahir, Effect of zeta potential on the properties of nano-drug delivery systems-a review (Part 1), Tropical Journal of Pharmaceutical Research 12(2) (2013) 255-264.

[235] J.E. Sader, J.W. Chon, P. Mulvaney, Calibration of rectangular atomic force microscope cantilevers, Review of scientific instruments 70(10) (1999) 3967-3969.

[236] A. Renger, Johnson, KL, Contact Mechanics. Cambridge etc., Cambridge University Press 1985. XII, 452 pp.,£ 17.50 P/B. ISBN 0521347963, Wiley Online Library, 1989.

[237] H. Yamamoto, S. Kurebayashi, T. Hirose, H. Kouhara, S. Kasayama, Reduced IRS-2 and GLUT4 expression in PPARγ2-induced adipocytes derived from C/EBPβ and C/EBPδ-deficient mouse embryonic fibroblasts, Journal of Cell Science 115(18) (2002) 3601-3607.

[238] S. Dinescu, B. Galateanu, A. Lungu, E. Radu, S. Nae, H. Iovu, M. Costache, Perilipin expression reveals adipogenic potential of hADSCs inside superporous polymeric cellular delivery systems, BioMed Research International 2014 (2014).

[239] T. Crouzier, T. Boudou, C. Picart, Polysaccharide-based polyelectrolyte multilayers, Current Opinion in Colloid & Interface Science 15(6) (2010) 417-426.
[240] G. Cardenas, S.P. Miranda, FTIR and TGA studies of chitosan composite films, Journal of the Chilean Chemical Society 49(4) (2004) 291-295.
[241] G. Lawrie, I. Keen, B. Drew, A. Chandler-Temple, L. Rintoul, P. Fredericks, L. Grøndahl, Interactions between alginate and chitosan biopolymers characterized using FTIR and XPS, Biomacromolecules 8(8) (2007) 2533-2541.
[242] J.G. Steele, G. Johnson, P.A. Underwood, Role of serum vitronectin and fibronectin in adhesion of fibroblasts following seeding onto tissue culture polystyrene, Journal of biomedical materials research 26(7) (1992) 861-884.
[243] R. McBeath, D.M. Pirone, C.M. Nelson, K. Bhadriraju, C.S. Chen, Cell shape, cytoskeletal tension, and RhoA regulate stem cell lineage commitment, Developmental cell 6(4) (2004) 483-495.
[244] G. Zhou, M.S. Niepel, S. Saretia, T. Groth, Reducing the inflammatory responses of biomaterials by surface modification with glycosaminoglycan multilayers, Journal of Biomedical Materials Research Part A 104(2) (2016) 493-502.
[245] G.G. Lima, J.B. Rocha Neto, H.F.d. Carvalho, M.M. Beppu, Control of Surface Properties of Hyaluronan/Chitosan Multilayered Coatings for Tumor Cell Capture, Polysaccharides 2(2) (2021) 387-399.
[246] E.J. Lee, E. Kang, S.-W. Kang, K.M. Huh, Thermo-irreversible glycol chitosan/hyaluronic acid blend hydrogel for injectable tissue engineering, Carbohydrate polymers 244 (2020) 116432.
[247] P. Kujawa, P. Moraille, J. Sanchez, A. Badia, F.M. Winnik, Effect of molecular weight on the exponential growth and morphology of hyaluronan/chitosan multilayers: A surface plasmon resonance spectroscopy and atomic force microscopy investigation, Journal of the American Chemical Society 127(25) (2005) 9224-9234.
[248] J. Campbell, A.S. Vikulina, Layer-by-layer assemblies of biopolymers: Build-up, mechanical stability and molecular dynamics, Polymers 12(9) (2020) 1949.
[249] R.G. Pearson, Hard and soft acids and bases, Journal of the American Chemical society 85(22) (1963) 3533-3539.
[250] R.G. Pearson, Acids and Bases: Hard acids prefer to associate with hard bases, and soft acids prefer to associate with soft bases, Science 151(3707) (1966) 172-177.
[251] Y. Idota, Y. Kogure, T. Kato, K. Yano, H. Arakawa, C. Miyajima, F. Kasahara, T. Ogihara, Relationship between physical parameters of various metal ions and binding affinity for alginate, Biological and Pharmaceutical Bulletin 39(11) (2016) 1893-1896.

[252] H. Chi, L. Cao, J. Wang, Synthesis of cross-linked copolymers of the (3-(2-pyridyl) acrylic acid)–copper (ii) complex in supercritical carbon dioxide for the catalytic oxidation of benzyl alcohol, RSC advances 6(6) (2016) 4434-4441.

[253] L. Gritsch, C. Lovell, W.H. Goldmann, A.R. Boccaccini, Fabrication and characterization of copper (II)-chitosan complexes as antibiotic-free antibacterial biomaterial, Carbohydrate polymers 179 (2018) 370-378.

[254] D.M. Roquero, A. Othman, A. Melman, E. Katz, Iron (III)-cross-linked alginate hydrogels: A critical review, Materials Advances 3(4) (2022) 1849-1873.

[255] R. Zimmermann, O. Birkert, G. Gauglitz, C. Werner, Electrosurface phenomena at polymer films for biosensor applications, Chemphyschem: a European Journal of Chemical Physics and Physical Chemistry 4(5) (2003) 509-514.

[256] W. Yuan, H. Dong, C.M. Li, X. Cui, L. Yu, Z. Lu, Q. Zhou, pH-controlled construction of chitosan/alginate multilayer film: characterization and application for antibody immobilization, Langmuir 23(26) (2007) 13046-13052.

[257] J. Wang, F. Shi, T. Nieh, B. Zhao, M. Brongo, S. Qu, T. Rosenmayer, Thickness dependence of elastic modulus and hardness of on-wafer low-k ultrathin polytetrafluoroethylene films, Scripta materialia 42(7) (2000) 687-694.

[258] P.T. Kühn, The effect of wettability and stiffness on stem cell behavior at bioinerfaces, (2016).

[259] G. Rabbani, S.N. Ahn, Structure, enzymatic activities, glycation and therapeutic potential of human serum albumin: A natural cargo, International journal of biological macromolecules 123 (2019) 979-990.

[260] K. Fromell, Y. Yang, K. Nilsson Ekdahl, B. Nilsson, M. Berglin, H. Elwing, Absence of conformational change in complement factor 3 and factor XII adsorbed to acrylate polymers is related to a high degree of polymer backbone flexibility, Biointerphases 12(2) (2017) 02D417.

[261] Y. Lu, L. Li, Y. Zhu, X. Wang, M. Li, Z. Lin, X. Hu, Y. Zhang, Q. Yin, H. Xia, Multifunctional copper-containing carboxymethyl chitosan/alginate scaffolds for eradicating clinical bacterial infection and promoting bone formation, ACS applied materials & interfaces 10(1) (2018) 127-138.

[262] D. Discher, Matrix elasticity directs stem cell lineage—Soluble factors that limit osteogenesis, Bone (44) (2009) S205-S206.

[263] J.-L. Lee, M.-J. Wang, J.-Y. Chen, Acetylation and activation of STAT3 mediated by nuclear translocation of CD44, The Journal of cell biology 185(6) (2009) 949.

[264] R.O. Hynes, Integrins: bidirectional, allosteric signaling machines, cell 110(6) (2002) 673-687.

[265] D.J. Rinauro, F. Chiti, M. Vendruscolo, R. Limbocker, Misfolded protein oligomers: mechanisms of formation, cytotoxic effects, and pharmacological approaches against protein misfolding diseases, Molecular Neurodegeneration 19(1) (2024) 20.
[266] M. Kisiel, M.M. Martino, M. Ventura, J.A. Hubbell, J. Hilborn, D.A. Ossipov, Improving the osteogenic potential of BMP-2 with hyaluronic acid hydrogel modified with integrin-specific fibronectin fragment, Biomaterials 34(3) (2013) 704-712.
[267] I. Burghardt, F. Lüthen, C. Prinz, B. Kreikemeyer, C. Zietz, H.-G. Neumann, J. Rychly, A dual function of copper in designing regenerative implants, Biomaterials 44 (2015) 36-44.
[268] A.E. Aplin, R. Juliano, Integrin and cytoskeletal regulation of growth factor signaling to the MAP kinase pathway, Journal of Cell Science 112(5) (1999) 695-706.
[269] A.J. Bird, Cellular sensing and transport of metal ions: implications in micronutrient homeostasis, The Journal of nutritional biochemistry 26(11) (2015) 1103-1115.
[270] V. Mourino, J.P. Cattalini, A.R. Boccaccini, Metallic ions as therapeutic agents in tissue engineering scaffolds: an overview of their biological applications and strategies for new developments, Journal of the Royal Society Interface 9(68) (2012) 401-419.
[271] M.A. Scott, V.T. Nguyen, B. Levi, A.W. James, Current methods of adipogenic differentiation of mesenchymal stem cells, Stem cells and development 20(10) (2011) 1793-1804.
[272] Y. Zhu, I.L. Kruglikov, Y. Akgul, P.E. Scherer, Hyaluronan in adipogenesis, adipose tissue physiology and systemic metabolism, Matrix Biology 78 (2019) 284-291.
[273] E. Hu, P. Tontonoz, B.M. Spiegelman, Transdifferentiation of myoblasts by the adipogenic transcription factors PPAR gamma and C/EBP alpha, Proceedings of the national academy of sciences 92(21) (1995) 9856-9860.
[274] T. Groth, Z.-M. Liu, M. Niepel, D. Peschel, K. Kirchhof, G. Altankov, N. Faucheux, Chemical and physical modifications of biomaterial surfaces to control adhesion of cells, Advances in Regenerative Medicine: Role of Nanotechnology, and Engineering Principles: Role of Nanotechnology, and Engineering Principles, Springer, 2010, pp. 253-284.
[275] J.P. Rodríguez, S. Ríos, M. Gonzalez, Modulation of the proliferation and differentiation of human mesenchymal stem cells by copper, Journal of cellular biochemistry 85(1) (2002) 92-100.
[276] M. Festa, G. Ricciardelli, G. Mele, C. Pietropaolo, A. Ruffo, A. Colonna, Overexpression of H ferritin and up-regulation of iron regulatory protein genes during differentiation of 3T3-L1 pre-adipocytes, Journal of Biological Chemistry 275(47) (2000) 36708-36712.
[277] H.I. Yoo, Y.H. Moon, M.S. Kim, Effects of CoCl2 on multi-lineage differentiation of C3H/10T1/2 mesenchymal stem cells, The Korean Journal of Physiology & Pharmacology: Official Journal of the Korean Physiological Society and the Korean Society of Pharmacology 20(1) (2016) 53.

[278] D.M. Vasconcelos, S.G. Santos, M. Lamghari, M.A. Barbosa, The two faces of metal ions: From implants rejection to tissue repair/regeneration, Biomaterials 84 (2016) 262-275.
[279] A. Tabassum, Effect of dexamethasone on the growth and differentiation of osteoblast-like cells derived from the human alveolar bone, Journal of Taibah University Medical Sciences 17(4) (2022) 707-714.
[280] F. Langenbach, J. Handschel, Effects of dexamethasone, ascorbic acid and β-glycerophosphate on the osteogenic differentiation of stem cells in vitro, Stem cell research & therapy 4(5) (2013) 1-7.
[281] L. Gao, R. McBeath, C.S. Chen, Stem cell shape regulates a chondrogenic versus myogenic fate through Rac1 and N-cadherin, Stem cells 28(3) (2010) 564-572.
[282] C.M. Murphy, A. Matsiko, M.G. Haugh, J.P. Gleeson, F.J. O'Brien, Mesenchymal stem cell fate is regulated by the composition and mechanical properties of collagen–glycosaminoglycan scaffolds, Journal of the mechanical behavior of biomedical materials 11 (2012) 53-62.
[283] M. Westhrin, M. Xie, M.Ø. Olderøy, P. Sikorski, B.L. Strand, T. Standal, Osteogenic differentiation of human mesenchymal stem cells in mineralized alginate matrices, PloS one 10(3) (2015) e0120374.
[284] Q. Wang, B. Chen, M. Cao, J. Sun, H. Wu, P. Zhao, J. Xing, Y. Yang, X. Zhang, M. Ji, Response of MAPK pathway to iron oxide nanoparticles in vitro treatment promotes osteogenic differentiation of hBMSCs, Biomaterials 86 (2016) 11-20.
[285] H. Ponta, L. Sherman, P.A. Herrlich, CD44: from adhesion molecules to signalling regulators, Nature reviews Molecular cell biology 4(1) (2003) 33-45.
[286] R. Marom, I. Shur, R. Solomon, D. Benayahu, Characterization of adhesion and differentiation markers of osteogenic marrow stromal cells, Journal of cellular physiology 202(1) (2005) 41-48.
[287] R. de Sousa Abreu, L.O. Penalva, E.M. Marcotte, C. Vogel, Global signatures of protein and mRNA expression levels, Molecular BioSystems 5(12) (2009) 1512-1526.
[288] A. Nifuji, O. Kellermann, M. Noda, Noggin inhibits chondrogenic but not osteogenic differentiation in mesodermal stem cell line C1 and skeletal cells, Endocrinology 145(7) (2004) 3434-3442.
[289] K.M. Sinha, X. Zhou, Genetic and molecular control of osterix in skeletal formation, Journal of cellular biochemistry 114(5) (2013) 975-984.
[290] T. Komori, Regulation of osteoblast differentiation by Runx2, Osteoimmunology: Interactions of the Immune and skeletal systems II, Springer, 2010, pp. 43-49.
[291] A. Cheng, P.G. Genever, SOX9 determines RUNX2 transactivity by directing intracellular degradation, Journal of Bone and Mineral Research 25(12) (2010) 2680-2689.

[292] H.I. Yoo, Y.H. Moon, M.S. Kim, Effects of CoCl2 on multi-lineage differentiation of C3H/10T1/2 mesenchymal stem cells, The Korean Journal of Physiology & Pharmacology 20(1) (2016) 53-62.

[293] J.P. Rodríguez, S. Rios, M. Gonzalez, Modulation of the proliferation and differentiation of human mesenchymal stem cells by copper, Journal of cellular biochemistry 85(1) (2002) 92-100.

[294] B.M. Gumbiner, Cell adhesion: the molecular basis of tissue architecture and morphogenesis, Cell 84(3) (1996) 345-357.

List of tables and figures

Tables

Figures

Acknowledgement

This PhD has been a challenging and truly a life-changing experience for me. During this time, have been fortunate to receive the support and help of many individuals, both academically and personally, without whom this thesis would not have been possible. I would like to express my deepest gratitude to all of them in this acknowledgment.

First, I would like to express my heartfelt gratitude to my advisor and first reviewer, Prof. Dr Thomas Groth, for giving me the opportunity to work in his group and covering the lab expenses that make this study possible. He was always encouraging me to reach the set goals of my PhD. Further, I want to extend my thanks for his concern and advice, which helped me overcome all the obstacles I faced, not only on the professional front but also on the family front.

I would like to extend my sincere thanks to all reviewers for investing the time to read my thesis**.**

Also, I would like to express my gratitude to all my previous and current colleagues at the Biomedical Materials Group for their cooperation, support and familiar atmosphere, which has always kept me motivated, focused and balanced.

I am extremely grateful to Mrs Marlis Porobin for performing the zeta potential measurements, buffer preparation, good cooperation and a friendly atmosphere.

Special thanks go to my mother for her supplication, wishes, moral support, and encouragement during the all PhD period.

I would like to express my deepest gratitude to my husband Hassan, who always stood behind my goals and me. He always trusted me and made me believe I would pass my studies successfully. Further, he always endorsed and encouraged me to go on. Moreover, he took care of our children when I was absent to perform experiments that took a long time, more than 10h during the writing period, which was a hard time for all of us.

Finally, I want to thank my children for their unwavering support and encouragement throughout my PhD journey. Their love, understanding, and patience have been a constant source of motivation for me, and I am grateful for their presence in my life.

“I would like to thank Allah (God) for giving me strength, peace of mind and good health to complete my thesis work. Without His blessings and mercy; this achievement would not have been possible

List of publications

1. H. Kindi, M. Menzel, A. Heilmann, C. E. Schmelzer, M. Herzberg, B. Fuhrmann, et al., "Effect of metal ions on the physical properties of multilayers from hyaluronan and chitosan, and the adhesion, growth and adipogenic differentiation of multipotent mouse fibroblasts," Soft Matter, vol. 17, pp. 8394-8410, 2021.

2. H. Kindi, C. Willems, M. Zhao, M. Menzel, C. E. Schmelzer, M. Herzberg, et al., "Metal Ion Doping of Alginate-Based Surface Coatings Induces Adipogenesis of Stem Cells," ACS Biomaterials Science & Engineering, vol. 8, pp. 4327-4340, 2022.

3. H.Kindi, Thomas Groth, C. Husteden, C.Wölk “Polysaccharide-based multilayers as reservoir for metal ions programming osteogenic stem cell differentiation”, Glycoscience & Therapy 2 (2026) 100020

Conferences

1. Oral peresentation: Thomas Groth & Husnia Kindi, Effect of doping metal ions on Polyelectrolyte multilayers properties, adhesion and spreading and adipogenic differentiation of multipotent mouse fibroblast"; Congress of Tissue Engineering Society **2022** in Manchester.
2. Poster: Husnia Kindi, Matthias Menzel, Christian Schmelzer, Thomas Groth, Cross-linking of multilayer systems from alginate and chitosan with metal ions effects on adhesion, proliferation and adipogenic differentiation of multipotent mouse fibroblasts, TERMIS Congress **2021** in Krakow, Poland
3. Poster: Husnia Kindi, Tobias Hedtke, Andreas Heilmann, Thomas Groth, Development of ternary multilayer systems from polysaccharides and transition metal ions for tissue engineering applications, *the European Society for Artificial Organs (ESAO) winter school, 26th –29th February **2020**, Lutherstadt Wittenberg/Germany.*

4. Poster: Husnia Kindi, Thomas Groth, Cross-linking of multilayer systems from alginate and chitosan with metal ions – effects on adhesion and proliferation of multipotent mouse fibroblasts, *Congress of the European Society for Artificial Organs (ESAO), 3rd –7th September **2019,** Hannover/Germany.*

5. Poster: Husnia Kindi, Marcus Niepel, Alexander Köwitsch, Matthias Menzel, Bodo Fuhrmann, Thomas Groth, Effect of Metal ions on Multilayer Properties and Cell

Response, *the 23r^{d}* (*CRS)* local Chapter meeting, *7th-9th March* ***2019, "****Leipzig/Germany.*

Appendix

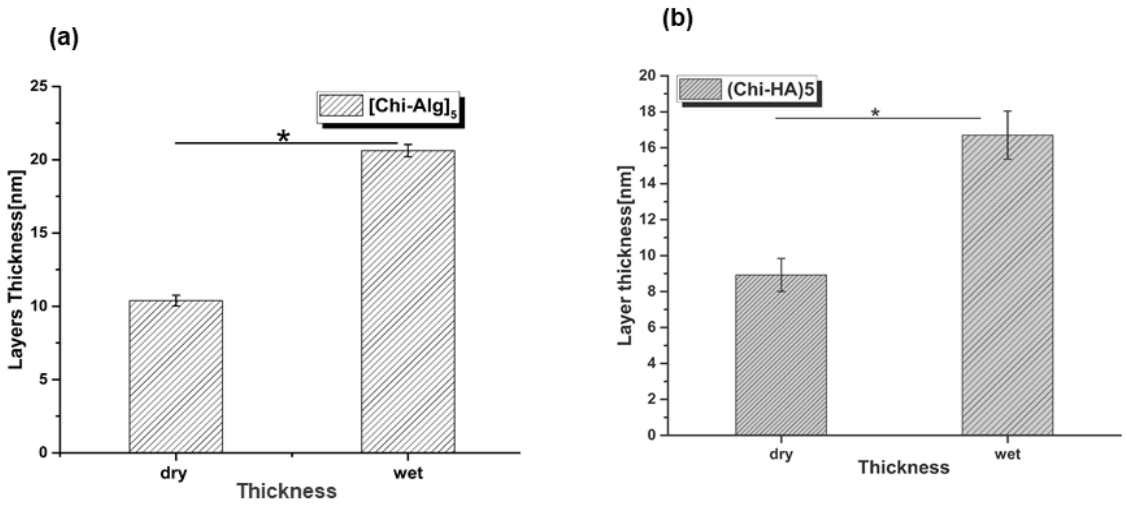

Figure A. 1: Calculated dry and wet thicknesses studied by ellipsometry (In and ex) situ conditions **(a)** plain [Chi/Alg], **(b)** [Chi/HA]. Results represent means ± SD, and thickness measurements were performed two times for each sample.

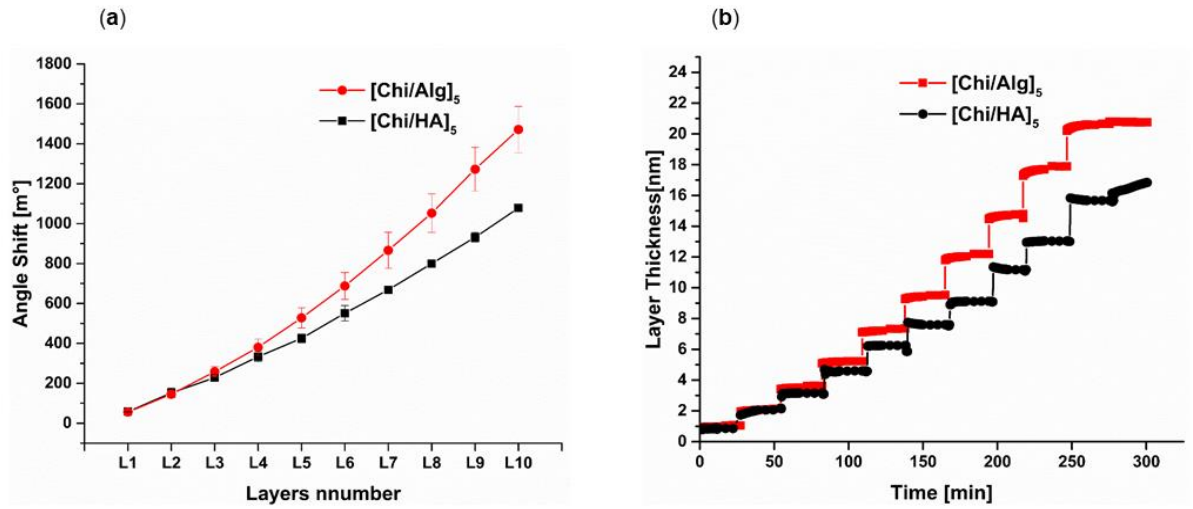

Figure A. 2: (a) Layer growth of PEM systems of [Chi/Alg] and [Chi/HA] by surface plasmon resonance (SPR). Odd layer numbers correspond to polycation (Chi) coating, and even layer numbers correspond to polyanion (Alg / HA). Results represent means ± SD, n = 3. **(b)** In situ measurement of PEMs thickness of [Chi/Alg] and [Chi/HA] by ellipsometry in wet conditions. Results represent means ± SD, n = 3.

1. Cell Cytotoxicity

For the investigation on cells toxicity, cells were cultured in 96 well plates at a density of 5 × 10^4 cellsmL^{-1} in EBM supplemented with 10% FBS and 1% pen/strep and incubated at 37 °C in a humidified 5% CO_2/95 % air atmosphere with different (concentration and type) metal ions for 24 h and 72 h. The non-toxic QBlue® assay was used to measure the metabolic activity of C3H10T1/2 cells. After gently aspirating the old medium, 200 µL of pre-warmed EBM containing the QBlue reagent (ratio 1:10) were added to each well. The samples were again incubated at 37 °C for 3 h, and 100 µL of supernatant from each well was transferred to a 96-well black plate. After that, the fluorescence intensities were determined at (an excitation wavelength of 544 nm and an emission wavelength of 590 nm) (BMGLABTECH, Fluostar OPTIMA, Offenburg, Germany) by using a fluorescence plate reader.

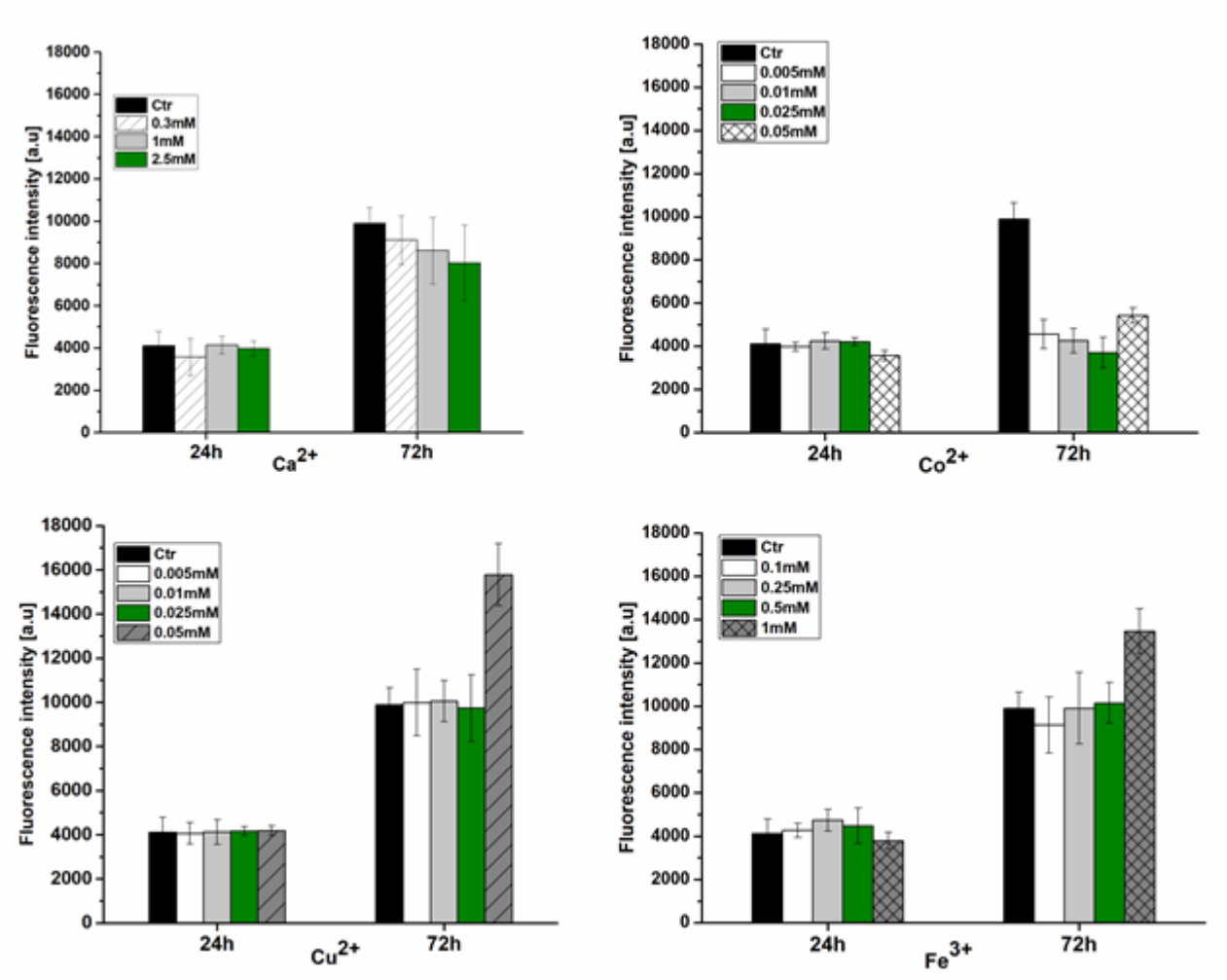

Figure A. 3:C3H10T1/2 cells plated on 96 well plates for 24h. The cells were incubated with EBSM medium and 10%FBS with different (types and concentrations) of metal ions. The QBlue assay was used to determine cell toxicity after 24 and 72 h of culture. Results are means ± SD of two independent experiments.

Based on the results presented in **Figure A.3**, the reduced quantity of cells on multilayers cross-linked with metal ions appears not solely due to toxic effects. The study found that micromolar concentrations of Co^{2+} ions (5 µM) had no cytotoxic effect after 24 h but inhibited further proliferation of cells in this concentration range up to 50 µM. On the other hand, Cu^{2+} did not show any cytotoxicity or growth inhibition compared to the control at the same concentration range. Moreover, calcium and iron ions in the 2.5 mM range showed no signs of cytotoxicity or growth-inhibiting effects on C3H10T1/2 cells. **Figure A.3** also showed that the impact of metal ions (Ca^{2+}, Co^{2+}, Cu^{2+} and Fe^{3+}) on cell proliferation strongly depends on their extracellular concentrations. For example, metal ions in the range of <2.5 mM, 0.05 mM, 0.05 mM, and 1 mM, respectively, were found to promote proliferation. Generally, metal ions at specific concentrations may inhibit cell proliferation. The effects of metal ions on cell proliferation are not solely due to cytotoxicity or growth-inhibiting effects. Other factors, such as the concentration of the metal ions and the specific metal ion used, also play a role.

Curriculum vitae

Personal data

Name:	Husnia Muftah Kindi
Nationality	Libyan
Academic degree	**M.Eng. (Master of Engineering)**

Experience

April/023 - present	Freiwilligen-Agentur Halle-Saalkreis e.V.
07-10/2022	Research assistant at biomedical materials group Martin Luther University Halle-Wittenberg
10/2018-07/2019	Job at Martin Luther University as an assistant scientist in pharmacology and biomaterials.
10/2009-05/2012	Master course Biomedical Engineering at Anhalt University of Applied Science & Martin Luther University Halle-Wittenberg
03/2003-10/2007	Teacher of Physics seconder school at Jamila Elzmarlye secondary school.

Education

04/2015-10/2022	PhD student in the group of Prof. Dr. rer. nat. habil. Thomas Groth, Institute of Pharmacy, Martin-Luther-University Halle-Wittenberg. **Title:** Development of ternary multilayer systems from polysaccharides and transition metal ions for tissue engineering applications.
09/2009-07/2012	Master student Martin Luther University in Halle- Wittenberg and Hochschule Anhalt.
10/2010-05/2012	Master thesis at Biomedical Materials Group, Martin Luther University in Halle- Wittenberg.

Topic: Mechanical properties and cytocompatibility of polysaccharide-based hydrogels.

1999 - 2002 Physic student at Tripoli University.

Fellowships

Martin Luther University Halle-Wittenberg for female PhD students.

Statutory declaration

I herewith declare that I have authored this thesis independently, that I have not used other than the declared sources/ resources, and that I have explicitly marked all material that has been quoted either literally or by content from the used sources.

Hiermit erkläre ich an Eides statt, dass ich die vorliegende Arbeit selbstständig verfasst, andere als die angegebenen Quellen/ Hilfsmittel nicht benutzt, und die von den benutzten Quellen wörtlich und inhaltlich entnommenen Stellen als solche kenntlich gemacht habe.

Halle (Saale), 23.04. 2025

Husnia Kindi